การสังเคราะห์และการประยุกต์ของโครงสร้างระดับไมโคร/นาโนเมตรของโลหะเงินที่ถูกควบคุม
สัณฐานวิทยา

นายหาญชนะ เกตมาลา

วิทยานิพนธ์นี้เป็นส่วนหนึ่งของการศึกษาตามหลักสูตรปริญญาวิทยาศาสตรดุษฎีบัณฑิต
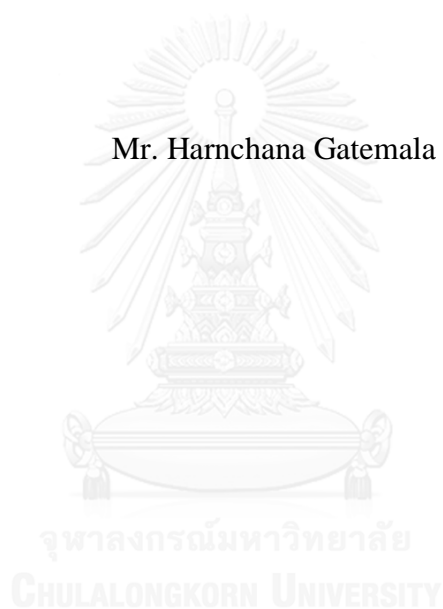สาขาวิชาเคมี ภาควิชาเคมี
คณะวิทยาศาสตร์ จุฬาลงกรณ์มหาวิทยาลัย
ปีการศึกษา 2558
ลิขสิทธิ์ของจุฬาลงกรณ์มหาวิทยาลัย

SYNTHESIS AND APPLICATIONS OF MORPHOLOGICALLY CONTROLLED
SILVER MICRO/NANOSTRUCTURES

Mr. Harnchana Gatemala

A Dissertation Submitted in Partial Fulfillment of the Requirements
for the Degree of Doctor of Philosophy Program in Chemistry
Department of Chemistry
Faculty of Science
Chulalongkorn University
Academic Year 2015

Thesis Title	SYNTHESIS AND APPLICATIONS OF MORPHOLOGICALLY CONTROLLED SILVER MICRO/NANOSTRUCTURES
By	Mr. Harnchana Gatemala
Field of Study	Chemistry
Thesis Advisor	Professor Sanong Ekgasit, Ph.D.
Thesis Co-Advisor	Associate Professor Chuchaat Thammacharoen

Accepted by the Faculty of Science, Chulalongkorn University in Partial Fulfillment of the Requirements for the Doctoral Degree

....Dean of the Faculty of Science
(Associate Professor Polkit Sangvanich, Ph.D.)

THESIS COMMITTEE

....Chairman
(Associate Professor Vudhichai Parasuk, Ph.D.)

....Thesis Advisor
(Professor Sanong Ekgasit, Ph.D.)

....Thesis Co-Advisor
(Associate Professor Chuchaat Thammacharoen)

....Examiner
(Associate Professor Voravee Hoven, Ph.D.)

....Examiner
(Sakulsuk Unarunotai, Ph.D.)

....External Examiner
(Assistant Professor Suttinun Phongtamrug, Ph.D.)

หาญชนะ เกตมาลา : การสังเคราะห์และการประยุกต์ของโครงสร้างระดับไมโคร/นาโน เมตรของโลหะเงินที่ถูกควบคุมสัณฐานวิทยา (SYNTHESIS AND APPLICATIONS OF MORPHOLOGICALLY CONTROLLED SILVER MICRO/NANOSTRUCTURES) อ.ที่ปรึกษาวิทยานิพนธ์หลัก: ศ. ดร. สนอง เอก สิทธิ์, อ.ที่ปรึกษาวิทยานิพนธ์ร่วม: รศ. ชูชาติ ธรรมเจริญ, หน้า.

ในงานวิจัยนี้ได้พัฒนากระบวนการทางเคมีเพื่อควบคุมสัณฐานวิทยาของโลหะเงินใน ระดับไมโครเมตรและนาโนเมตรที่แตกต่างกันทั้งหมด 3 กระบวนการ ซึ่งในแต่ละกระบวนการได้ มีการศึกษาเชิงลึกของกลไกการโตของผลึก ผลการวิจัยพบว่า ในระบบแรกซึ่งเป็นการสังเคราะห์ อนุภาคแบบแผ่นบางในระดับไมโครเมตรและนาโนเมตรของโลหะเงินโดยการรีดิวซ์ด้วย ไฮโดรเจนเปอร์ออกไซด์ภายใต้สิ่งแวดล้อมที่กัดกร่อน ไอออนของคลอไรด์มีความสำคัญต่อการ สร้างสิ่งแวดล้อมที่มีการกัดกร่อนที่สามารถทำลายโครงสร้างเริ่มต้นแบบซิงเกิลคลิสตัล (single crystal) และมัลติพลิทวิน (multiply twinned) ในขณะที่โครงสร้างเริ่มต้นแบบแผ่นไม่ได้รับ ผลกระทบใดๆ ในระบบที่สองเป็นการสังเคราะห์แบบควบคุมสัณฐานวิทยาของซิลเวอร์คลอไรด์ ด้วยกระบวนการเหนี่ยวนำให้ตกผลึกด้วยการเติมไอออนของคลอไรด์ในไอออนเชิงซ้อนซิลเวอร์ แอมมีน ($[Ag(NH_3)_2]^+$) การศึกษากระบวนการโตพบว่า โครงสร้างในกลุ่มแปดกิ่งพัฒนามาจาก โครงสร้างเริ่มต้นแบบลูกบาศก์ภายใต้สิ่งแวดล้อมที่มีไอออนของคลอไรด์มาก ส่วนโครงสร้างใน กลุ่มหกกิ่งพัฒนามาจากโครงสร้างเริ่มต้นแบบทรงเหลี่ยมแปดหน้าภายใต้สิ่งแวดล้อมที่มี แอมโมเนียมาก กระบวนการที่สามเป็นการสังเคราะห์โครงสร้างที่มีความเป็นรูพรุนในระดับนาโน เมตรของโลหะเงินด้วยกระบวนการกัลวานิกของซิลเวอร์คลอไรด์ จากการศึกษากระบวนการโต พบว่า กระบวนการที่เกิดพร้อมกันสองกระบวนการ คือ การกัดกร่อนและการรีดิวซ์ย้อนกลับของ โครงสร้างโลหะเงินที่มีขนาดใหญ่สามารถทำให้ได้โครงสร้างที่มีขนาดเล็กลง จากการค้นพบใน งานวิจัยทั้งหมด สามารถนำไปประยุกต์ใช้กับการพัฒนากระบวนการนำกลับของโลหะเงินจากของ เสียอุตสาหกรรมและของเสียจากห้องปฏิบัติการเคมี โดยการเปลี่ยนซิลเวอร์คลอไรด์ให้เป็นอนุภาค โลหะเงินในระดับไมโครเมตรที่มีความบริสุทธิ์สูง (>99.99%) ซึ่งผลิตภัณฑ์ที่ได้จากกระบวนการ นำกลับสามารถใช้เป็นวัตถุดิบของการผลิตเครื่องประดับเงินได้โดยไม่ต้องผ่านกระบวนการทำให้ บริสุทธิ์เพิ่มเติม

ภาควิชา	เคมี	ลายมือชื่อนิสิต	....
สาขาวิชา	เคมี	ลายมือชื่อ อ.ที่ปรึกษาหลัก	....
ปีการศึกษา	2558	ลายมือชื่อ อ.ที่ปรึกษาร่วม	....

5472902723 : MAJOR CHEMISTRY

KEYWORDS: MORPHOLOGY CONTROLLED SYNTHESIS / SILVER MICRO/NANOSTRUCTURES / SILVER MICROPLATES / NANOPOROUS SILVER MICROSTRUCTURES / SILVER CHLORIDE MICROSTRUCTURES / SILVER RECOVERY

HARNCHANA GATEMALA: SYNTHESIS AND APPLICATIONS OF MORPHOLOGICALLY CONTROLLED SILVER MICRO/NANOSTRUCTURES. ADVISOR: PROF. SANONG EKGASIT, Ph.D., CO-ADVISOR: ASSOC. PROF. CHUCHAAT THAMMACHAROEN, pp.

In this work, three morphologically controlled synthesis protocols of silver micro/nanostructures using chemical approach were developed. The detailed growth mechanisms were extensively studied. The first work was the morphology controlled synthesis of silver micro/nanoplates under an etching environment using hydrogen peroxide (H_2O_2) as a reducing agent. The results revealed that chloride ions (Cl^-) were essential for creating etching environment capable of selective dissolution of single crystal and multiply twinned crystal, while leaving plate structures unaffected. The second work was the morphology controlled synthesis of silver chloride (AgCl) microstructures *via* a precipitation of silver ammine complex ($[Ag(NH_3)_2]^+$) by an addition of Cl^-. The growth mechanism suggested that the eight-pod family grew from the cubic seeds in Cl^--rich environment while the six-pod family grew from an octahedral seeds in an NH_4OH-rich environment. The third work was the morphology controlled synthesis of nanoporous silver microstructures *via* galvanic replacement of AgCl microstructures. The concerting reaction between oxidative etching of nanoporous silver microstructures and re-deposition of Ag atoms converts large silver structures to small structures. The research findings enabled a development of a large scale silver recovery protocol from industry and laboratory wastes by converting AgCl precipitates into highly pure silver microstructures (>99.99%). The recovered products could be directly employed as a raw material for silver jewelry applications.

Department:	Chemistry	Student's Signature	
Field of Study:	Chemistry	Advisor's Signature	
Academic Year:	2015	Co-Advisor's Signature	

ACKNOWLEDGEMENTS

CONTENTS

CONTENT

LIST OF TABLES

จุฬาลงกรณ์มหาวิทยาลัย
CHULALONGKORN UNIVERSITY

LIST OF FIGURES

.

LIST OF SYMBOLS

C   : Precursor concentration

C_0 : Equilibrium concentration

σ   : Supersaturation

γ : Interfacial free energy

G   : Free energy

A   : Surface area

{ }   : Crystallographic facet

< >   : Direction

[ ]   : Concentration

E^0_{cell} : Standard cell potential

E^0 : Standard reduction potential

°C   : Degree Celsius

θ   : Incident angle

LIST OF ABBREVIATIONS

XPS   : X-ray photoelectron spectroscopy

EDS   : Energy dispersive X-ray spectroscopy

FTIR   : Fourier transform infrared spectroscopy

XRD   : X-ray diffraction

SEM   : Scanning electron microscope

UV-vis   : UV-visible spectroscopy

SEI   : Secondary electron image

CCD   : Central composite design

CTAB   : Cetyltrimethylammonium bromide

PVP   : Poly(vinyl pyrrolidone)

AgMPs   : Silver microparticles

AgNPs   : Silver nanoparticles

AgClNs   : Silver chloride nanoparticles

AgMPls   : Silver microplates

AgNPls   : Silver nanoplates

AgNSs   : Silver nanospheres

8pAgCl   : Octapod AgCl microstructures

6pAgCl   : Hexapod AgCl microstructures

8x3pAgCl   : Octapod AgCl microstructures with 3 small pods at the tip of

                                           primary pods

6x4pAgCl   : Hexapod AgCl microstructures with 4 small pods at the tip of

                                           primary pods

np-AgMSs   : Nanoporous silver microstructures

np-6pAgMSs   : Nanoporous hexapod microstructures

np-8pAgMSs   : Nanoporous octapod microstructures

np-OhAgMSs   : Nanoporous octahedral microstructures

L-AA   : L-ascorbic acid

MO   : Methyl orange

MB   : Methylene blue

CHAPTER I

INTRODUCTION

1.1 GROWTH MECHANISM OF METAL MICRO/NANOSTRUCTURES

Morphology-controlled synthesis of functional metal micro/nanostructures has attracted much attention as their physicochemical properties can be tuned by changing morphology (shape, size and composition) [1]. Anisotropic nanostructures such as one-dimensional (1D) nanorods [2, 3], nanowires [4, 5], two-dimensional (2D) nanoplates and nanosheets [6-9], three-dimensional (3D) branched microcrystals [10-13] exhibit potential applications as catalyst, electronic device, sensor, energy storage and medical device materials. To tune the morphology and properties of these materials for particular application, it is important to understand the fundamental of the growth mechanism because the morphology could be designed at the beginning of the fabrication process.

The formation and crystal growth mechanism of metal nanostructures was proposed based on the solution-phase synthesis by LaMer and co-worker in 1950, as shown in Figure 1.1 [14]. This model divided the growth mechanism into three parts. Based on the model, the first part is the generation of atoms which metal precursors are reduced in to zero-valent metal atoms. The next period is nucleation which the atomic concentration is increasing with an increasing of reaction time. Once the concentration reaches supersaturation (σ), which defines as Equation 1.1, the atoms will aggregate into small clusters or fluctuating structures in order to reduce the

Gibb's free energy (G) and surface energy. The fluctuating structures can be changed into seed particles when their sizes become larger.

$$\sigma = \ln(C/C_0) \qquad \text{(Eq. 1.1)}$$

where C is the precursor concentration and C_0 is the equilibrium concentration.
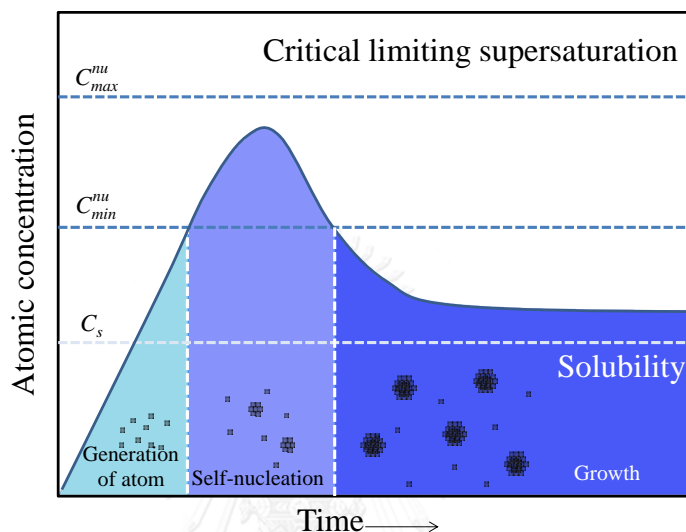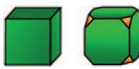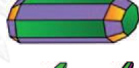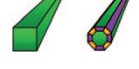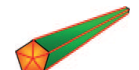
Figure 1.1 Plot of atomic concentration as a function of time demonstrating the generation of atoms, nucleation and growth. Reprinted with permission from Ref [14] and [1]. Copyright 1950 American Chemical Society and 2009 Wiley.

When the atomic concentration is dropped below minimum supersaturation, the nucleation period is terminated and the growth period is introduced. From LaMer model, the parameters which control the morphology of the final products are the seed morphology and the growth process. Seed morphology will dictate the structure of final products as shown in Table 1.1.

In general, the seed morphology may take a form as single crystal, singly-twinned, multiply-twinned, plate with stacking faults or the mixture in the synthesis. The key parameters to control seed morphology are very complicated. Xia and co-

Table 1.1 A summary of different shapes that have been achieved for various metal nanocrystals. The green, orange, and purple colors represent the {100}, {111}, and {110} facets, respectively. Reprinted with permission from Ref [1]. Copyright 2009 Wiley.

Structures	Shapes	Schematic drawing	Metals
single-crystal	perfect/truncated cube[a]		Pd, Ag, Au, Pt, Cu, Rh, Bi, Fe
	perfect/truncated octahedron[a]		Pd, Ag, Au, Pt
	perfect/truncated tetrahedron[a]		Ag, Au, Pt, Rh
	rectangular bar		Pd, Ag, Pt
	octagonal rod		Pd, Au, Fe, Co, Ni
	rectangular or octagonal wire		Pb, In, Sn, Sb, Fe, Co
singly twinned	right bipyramid		Pd, Ag
	beam		Ag
multiply twinned	decahedron[a]		Pd, Ag, Au
	icosahedron[a]		Pd, Au
	five-fold twinned pentagonal rod		Pd, Ag, Au, Cu
	five-fold twinned pentagonal wire		Ag, Au, Cu
plate with stacking faults	triangular/hexagonal plate		Pd, Ag, Au, Cu, Pb, Bi, Co, Ni
	disc		Sn, Co

[a] Platonic solid.

workers suggested that the key parameters to control seed morphology are thermodynamic and kinetic factors [1].

The thermodynamic control is defined that the greatest proportion of the most stable product will be generated. From the consideration of Wulff's theorem [1], the minimization of total surface free energy of a single crystal, the most stable product is the structure which has the lowest surface free energy (γ). The interfacial free energy can be defined as the free energy required for creating a unit area of "new" surface as shown in Equation 1.2

$$\gamma = \left(\frac{\partial G}{\partial A}\right)_{n_i, P, T} \qquad \text{(Eq. 1.2)}$$

where G is the free energy and A is the surface area. For fcc crystal structure, the surface energy decreases in the order $\gamma_{\{111\}} < \gamma_{\{100\}} < \gamma_{\{110\}}$. This result suggested that the structure covered by {111} facets (*i.e.*, octahedral and tetrahedral shape) should be preferentially existed. Nevertheless, both shapes have large surface area compared to a cube of the same volume. Therefore, theses seed particles are formed as truncated octahedrons which covered by {111} and {100} facets. However, the multiply twinned seed which is considered as an assembly of five single crystal seeds can be created [15]. After the completing of assembly process of five tetrahedral units, it will leave a gap of 7.35°. This defected region will increase the total free energy when the decahedral seed is enlarged the size. As a result, the multiply twinned seed is stable only at a relatively small size.

According to thermodynamic control hypothesis, the most stable structure is the single crystal which has the lowest energy and covered by {111} and {100} facets. In principle, a metastable seed can be held by tuning the reaction conditions

before the reaction reaches equilibrium which is called the kinetic control [16]. Under slow atomic generation condition, the singly twinned or multiply twinned seed will prevail over the single crystal seed due to the fact that they can be kept at small size for longer period. Under the very slow reduction, the random hexagonal close packing (rhcp) together with the generation of stacking faults are taken place. This growth mechanism is known as kinetic control. Thus, the kinetic control can be achieved by i) slowing of reduction, ii) using the weak reducing agent (chemical reduction) or sacrificial metal (galvanic replacement), iii) introducing the concerted oxidation/reduction process, or iv) introducing the Ostwald ripening process [1].

1.2 STRUCTURAL CONTROL SYNTHESIS OF METAL NANOSTRUCTURES

The morphology of final product can also be controlled in the growth period. The preferential growth mechanism depends on the nature of materials. The screw dislocation, layer-by-layer and dendritic growth strongly depend on growth rate and supersaturation, as shown in Figure 1.2 [17, 18]. At low growth rate and low supersaturation, which is a very rare case, the screw dislocation growth is preferred. At the moderate growth rate and supersaturation, the layer-by-layer growth which generates the larger structure with the same morphology dominates. At the high growth rate and supersaturation, the dendritic growth which creates the branched structures is preferred.

The morphology of final product can be selectively controlled by an oxidative etching process. In this process, metal atoms are oxidized to ions by an addition of O_2 and ligands (such as Cl^- and Br^-).[2] The structures that withstand the oxidative
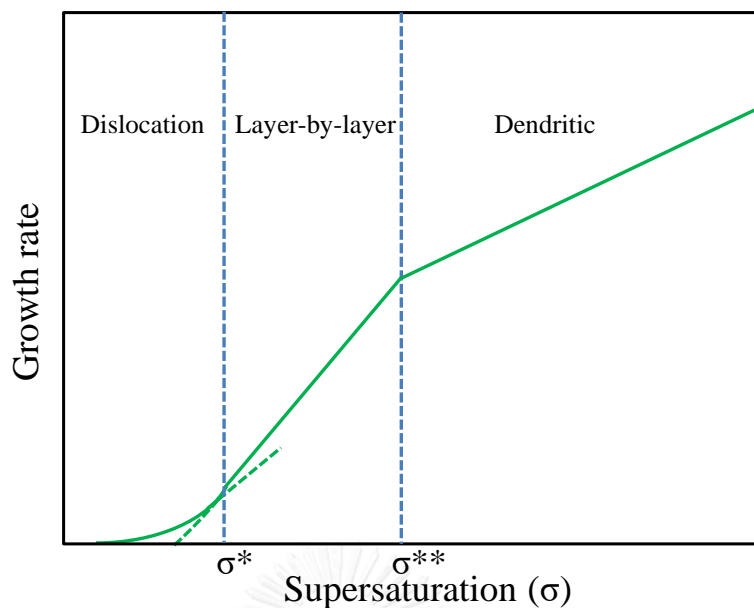
Figure 1.2 Different crystal growth modes as a function of growth rate and supersaturation [17, 18]. Reprinted with permission from Ref [18]. Copyright 2013 American Chemical Society.

environment will grow while the others will be destroyed. The oxidative etching of many noble metals such as Ag, Rh, and Pd have been investigated [2, 19-23].

The surface blocking process to preserve specific facets of metal nanostructures to control the morphology is also well documented. Capping agent selectively protects certain facets while promotes the growth on the non-protected facets [1]. There are many capping agents that use in metal nanostructure synthesis. For example, poly(vinyl pyrrolidone) (PVP) is a polymeric capping agent whose oxygen atoms preferential adsorb on the {100} facets of Ag and Pd [24]. Bromide ion can selectively adsorb on {111} facets of Ag, Au, Pt and Pd [25]. Citrate ions bind most strongly to {111} facets [26, 27]. The mechanism of capping agent on the growth of metal nanostructures is explained in thermodynamic control aspect which

interfacial free energy of bound surface is reduced through chemisorption [1]. They are confirmed by X-ray photoelectron spectroscopy (XPS), energy dispersive X-ray spectroscopy (EDXS), Fourier transform infrared spectroscopy (FTIR), and Raman technique [28-33].

1.3 MORPHOLOGY CONTROLLED SYNTHESIS OF SILVER MICRO/NANOSTRUCTURES

Silver is a precious metal which has attracted much attention as it offers potential applications in various areas such as catalyst, electronic device manufacturing, sensor, and medical device. Various morphology including nanocubes [34], nanoplates [6-8], nanorods [2], nanowires [4, 5], and branched microcrystals [10] of silver were successfully synthesized. The morphology of functional silver micro/nanostructures is dictated by the original seed and growth environment as mentioned above. The single crystal seed grows to cube, octahedron, tetrahedron, and rectangular bar. The singly twinned seed grows to right bipyramid and beam. The multiply twinned seed grows to decahedron, icosahedron and pentagonal rod. The plate with stacking faults seed grows to hexagonal and triangular plate [1, 12, 25]. Like the growth mechanism of other noble metals, the seed selection protocol is crucial for the structural controlled synthesis of silver micro/nanostructures as it dictated the final products. Various etchants have been employed for selective preservation or selective elimination of certain structures. Cl^-/O_2 dissolves singly and multiply twinned seed [2, 35-37], halide ion etches Ag{110} facets [37], NH_4OH/H_2O_2 etches single crystal seed containing Ag{100} facets [38, 39], while H_2O_2 etches all structures with different rate [27]. Subsequently, the survival seeds

further grow to larger structures. The surface blocking process is also practiced for shape-controlled synthesis. Several organic capping agents such as citrate, cetyltrimethylammonium bromide (CTAB), poly(vinyl pyrrolidone) (PVP), and inorganic capping agents such as halide ions, cyanide ion, or thiol were used for selective facet protection while promoting growth in specific facets. Halide ions adsorbed and formed silver halide layer on Ag{111} facet [40-46]. Moreover, the use of different reducing agent (both of chemical reduction and galvanic replacement) has an influent on the morphology of silver micro/nanostructures as it controls the reduction rate.

In this work, we developed chemical synthesis protocols to fabricate silver micro/nanostructures. By controlling the reaction environment and experimental conditions, various silver micro/nanostructures could be selectively prepared. In the first work, we explored a simple, rapid and environmentally friendly protocol for a large scale synthesis of silver microplates from $[Ag(NH_3)_2]^+$ under an oxidative etching environment containing O_2/Cl^-, NH_4OH/H_2O_2, and H_2O_2. The results suggested that the presence of Cl^- is essential for the formation and growth of plate structures as shown in Figure 1.3. The growth mechanism of silver microplates was proposed in Figure 1.4. The silver microplates withstand the oxidative environment due to the selective passivation of Ag{111} basal plane while truncated cubes, icosahedra, and pentagonal rods with Ag{100} envelopes were destroyed. The developed protocol enables an environmental friendly fabrication of highly pure silver microplates and silver microparticles directly from AgCl precipitate.
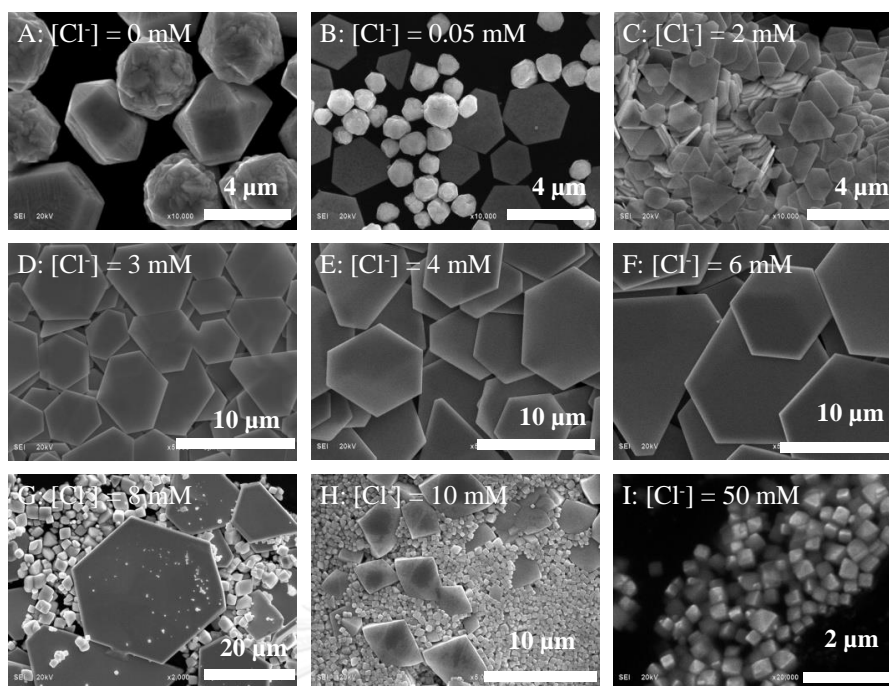
Figure 1.3 Structural control of silver microstructures by an addition of NaCl. Cl⁻ with H_2O_2 and O_2 function as an efficient shape selective agents [47].
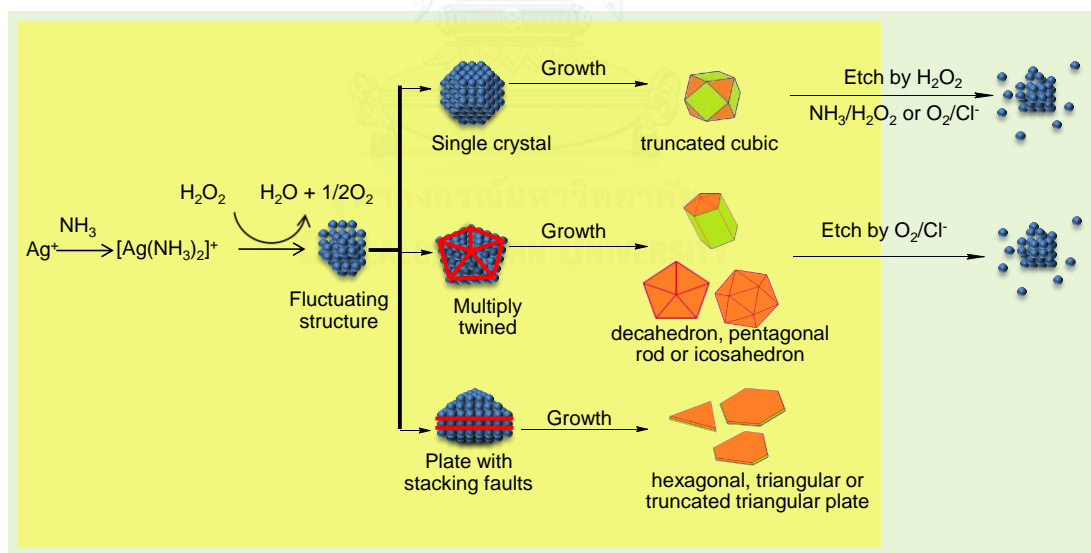
Figure 1.4 Proposed mechanism on the selective formation of AgMPls under an etching environment containing NH_4OH/H_2O_2, H_2O_2, O_2/Cl^-. The green facets indicate Ag{100} while the orange facets indicate Ag{111} [47].

In the second work, we successfully controlled the growth along <100> and <111> directions of AgCl microstructures under a control precipitation from silver ammine complex in an NH_4OH or Cl^- dominated environment. We found that the final microstructures are governed by the original seed morphology and growth environment as shown in Figure 1.5. The growth mechanism was revealed as shown in Figure 1.6. Under a Cl^--dominated environment, octapod family grew from cubic seeds as the growth along <111> directions is favored. On the other hand, hexapod family grew from octahedral seeds under an NH_4OH-dominated environment as NH_4OH preferentially etches AgCl{111} facet while preserving the AgCl{100} facet. The obtained AgCl microstructures could be employed as efficient Ag@AgCl visible-light photocatalysts.

In the third work, we fabricated 3D nanoporous silver microstructures (np-AgMSs) from AgCl templates with precisely controlled grain size and pore size by galvanic replacement approach. The grain size of silver particle could be tuned from 47 nm to 136 nm by varying the concentration NaCl electrolyte. The concerting reactions between the oxidative etching of np-AgMSs (by Cl^- and Cl^-/O_2) and the re-deposition of Ag atoms continuously takes place *via* kinetically controlled mechanism until AgCl microcrystal template is depleted. These processes convert large grains into small grains as shown in Figure 1.7.
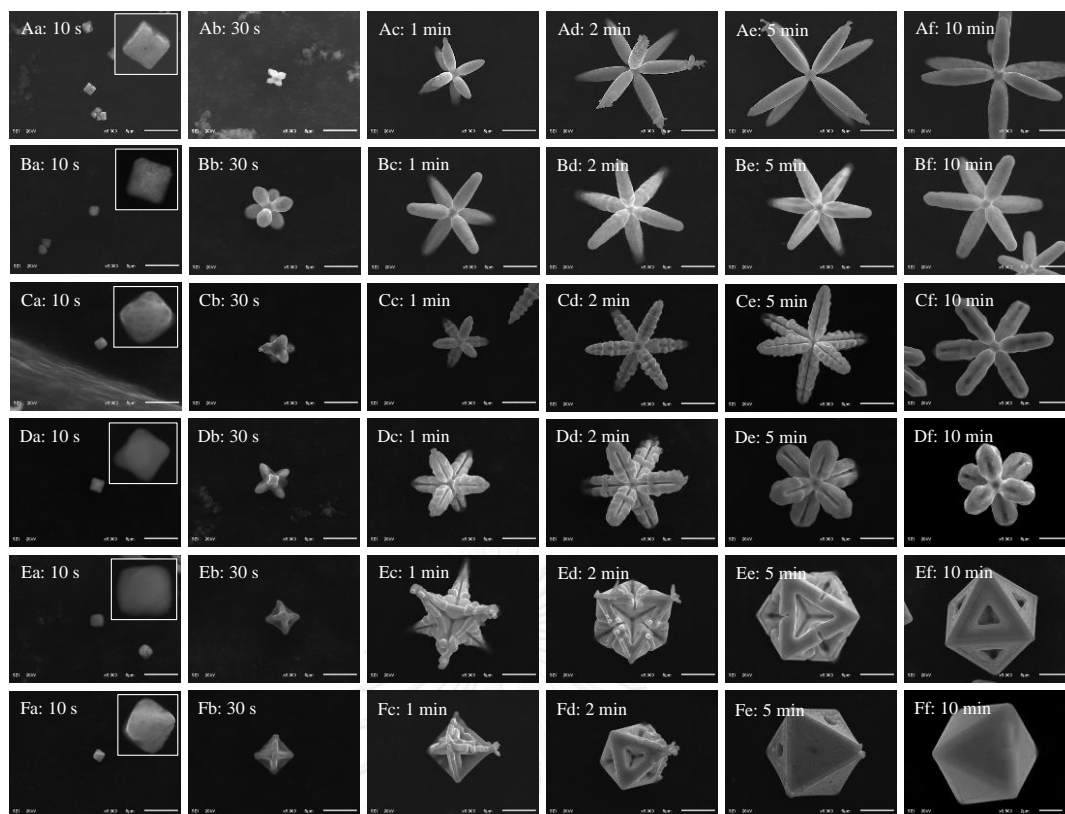
Figure 1.5 Time dependent structural evolution of various AgCl microstructures. Octapod family (octapod AgCl and octapod AgCl with fish bone structure) was grown from cubic seed while hexapod family (hexapod AgCl, hexapod AgCl with 4-blade arrowhead, caged octahedron AgCl, and octahedron) was grown from octahedral seeds. The structural evolution was experimentally observed by time dependent SEM analysis. The evolving micro/nanostructure was selectively separated by flash-drying technique [48].
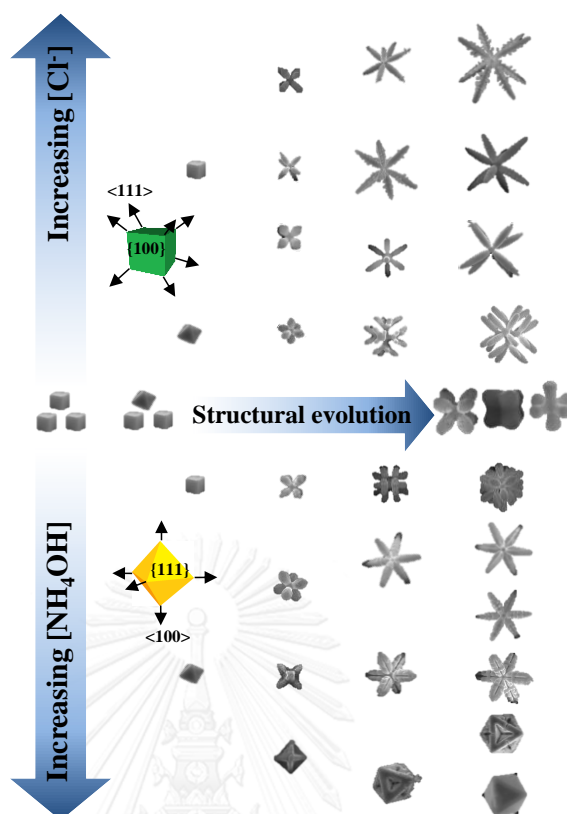
Figure 1.6 Schematic illustration shows seed selectivity and concomitant structural development of 3D AgCl microstructures under the influence of Cl$^-$ and NH$_4$OH [48].
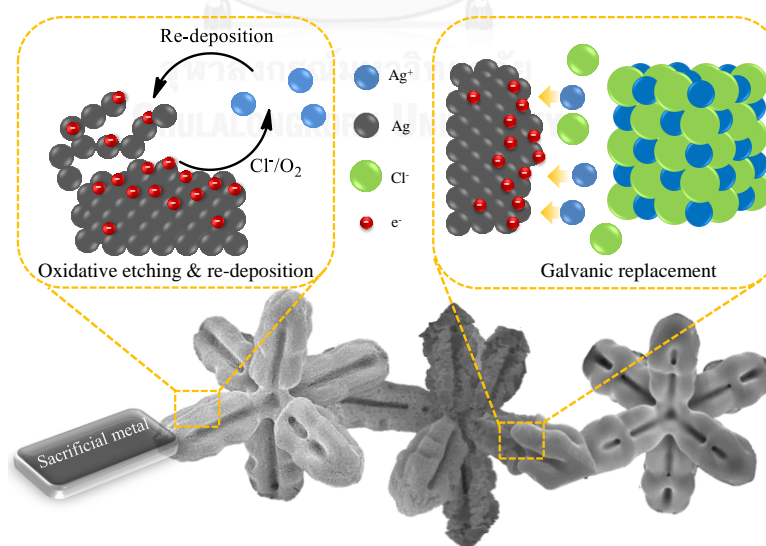
Figure 1.7 Proposed mechanism on the formation of np-AgMSs under the concerting of galvanic replacement and oxidative etching/re-deposition reaction.

To our knowledge, a green silver recovery process from AgCl precipitates using hydrogen peroxide (H_2O_2) as the sole reducing agent was developed. The optimization of recovery conditions (pH, concentration of Ag^+, and the mole ratio of H_2O_2/Ag^+) was investigated using central composite design (CCD) technique. The developed protocol is very economical as tab water can be used as a solvent. Moreover, this process is simple, rapid, highly efficient, and environmentally friendly. It can be used for large scale recovery of silver wastes in the real industrial plants. We successfully performed a pilot scale recovery of silver waste solution with the volume of 50 L. The recovered weight of metallic silver was 715 grams (92% recovery efficiency). In Figure 1.8, the recovered product is highly pure (99.99%) silver microplates or microcrystals (depending on precipitating condition). We have demonstrated that the recovered metallic silver can be used directly as silver clay for the fabrication of silver jewelry.
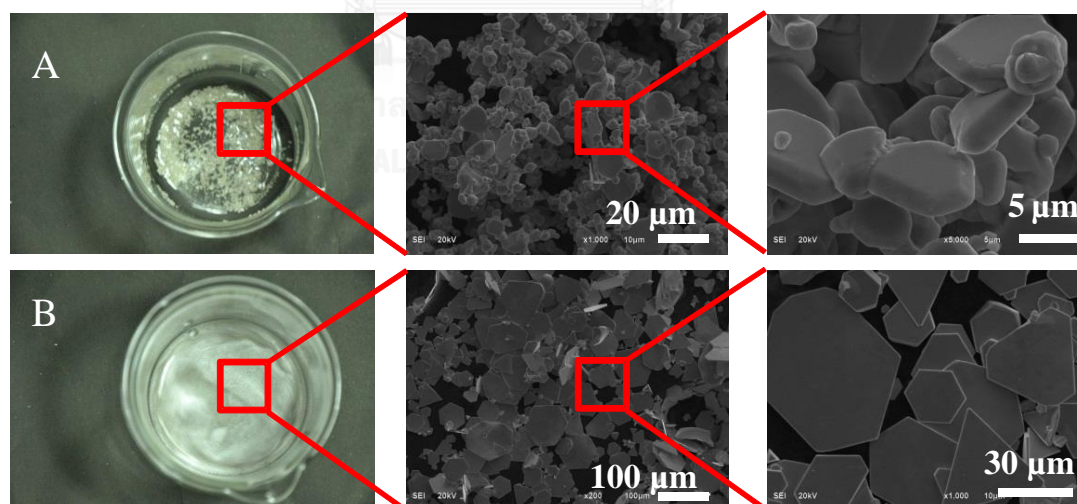
Figure 1.8 Morphologies of silver microstructures. The samples were prepared using the same condition as experimental condition 3 (A) without and (B) with 0.5% w/v PVP.

1.4 OBJECTIVES

1.4.1 To develop a chemical synthetic protocol to control the morphology of silver micro/nanoplates by H_2O_2 reduction of $[Ag(NH_3)_2]^+$ under an extremely oxidative etching environment.

1.4.2 To develop a chemical synthetic protocol to control the morphology of AgCl microstructures by a Cl^--induced precipitation from $[Ag(NH_3)_2]^+$.

1.4.3 To develop an electrodeless technique to control the morphology of nanoporous silver microstructures by galvanic replacement with Zn metal.

1.4.4 To explore the potential application of a chemical synthetic protocol of silver microplates as an environmentally friendly process for silver recovery from industrial and laboratory wastes.

1.4.5 To explore the potential application of recovered silver microstructures as silver clay for hand-made silver jewelry fabrication.

1.4.6 To explore the potential application of AgCl microstructures as an efficient photocatalyst for the decomposition of organic dyes.

1.4.7 To explore the potential application of nanoporous silver microstructures as an efficient catalyst.

1.5 SCOPE OF THIS DISSERTATION

1.5.1 To develop a process for the fabrication of silver micro/nanoplates, AgCl microstructures and nanoporous silver microstructures *via* chemical approach by optimizing the experimental conditions *i.e.*, solution pH, concentration of reactants and electrolyte.

1.5.2 To optimize the experimental conditions for a large scale synthesis and morphological control of silver microstructures.

1.5.3 To characterize morphologies of silver microstructures by scanning electron microscope (SEM), energy dispersive X-ray spectrometer (EDS), X-ray diffraction (XRD), X-ray photoelectron spectra (XPS) and investigate the catalytic activity by UV-visible spectroscopy.

1.5.4 To explore the potential application of the research findings including; recovered silver as silver clay, AgCl microstructures as photocatalysts, nanoporous silver microstructures as catalysts.

1.5.5 To develop an environmentally friendly process for silver recovery from silver-contained wastes.

1.6 BENEFIT OF THIS DISSERTATION

1.6.1 To recover highly pure metallic silver (>99.99%) by the rapid, highly efficient and environmentally friendly process.

1.6.2 Production of silver clay from recovered silver microstructures for silver jewelry application.

1.6.3 To synthesize the morphologically controlled silver micro/nanostructures by highly efficient and environmentally friendly process.

CHAPTER II

RAPID FABRICATION OF SILVER MICROPLATES

UNDER AN OXIDATIVE ETCHING ENVIRONMENT

CONSISTING OF O_2/Cl^-, NH_4OH/H_2O_2, AND H_2O_2

2.1 INTRODUCTION

In the past decade, morphology-controlled synthesis has become an important means for the fabrication of functional materials with desired properties as the nano-enable properties could be efficiently controlled through the size and shape manipulation. Functional micro/nanostructure of silver has attached much attention as it offers potential applications in catalyst, electronic device, sensor, and medical device fabrications. Complex structures including nanocubes [34], nanoplates [6-8], nanorods [2], nanowires [4, 5], and branched microcrystals [10] were successfully synthesized. Reviews on the synthesis and characterization of silver nanoplates have recently been published [1, 49-51]. The plate like nanostructure with large contact area has shown potential application in the fabrication of solar cell with high photocurrent [52].

The morphology of silver micro/nanostructures can be tuned through seed selection and growth process [1, 12, 25]. The morphology of seed particles is crucial for the structural controlled synthesis as it dictates the final products. The single crystal seed grows to cube, octahedron, tetrahedron, and rectangular bar. The singly

twinned seed grows to right bipyramid and beam. The multiply twinned seed grows to decahedron, icosahedron and pentagonal rod. The plate with stacking faults seed grows to hexagonal and triangular plate. Oxidative etching has been employed for selective preservation or selective elimination of certain crystallographic structures. For example, Cl^-/O_2 dissolves singly and multiply twinned seeds [2, 35-37], halide ion etches Ag{110} facets [37], NH_4OH/H_2O_2 etches single crystal seeds containing Ag{100} facets [38, 39], while H_2O_2 etches all silver structures [27]. Surface blocking was also practiced in shape-controlled synthesis. Several organic capping agents such as citrate, cetyltrimethylammonium bromide (CTAB), poly(vinyl pyrrolidone) (PVP) and inorganic capping agents such as halide ions, cyanide ion, and thiol were used for selective protection of certain facets while promoting growth on the non-protected facets [40-46].

The efficient catalytic decomposition of hydrogen peroxide (H_2O_2) by silver metal was well-documented [53-55]. The decomposition of H_2O_2 on silver metal at high concentration is extremely violent with a releasing of intense heat, water vapor, and oxygen gas. H_2O_2 has been employed as an efficient etchant and a seed-selecting agent for the fabrication of silver nanostructures [27, 56-58] Although H_2O_2 is well-known as a strong oxidizing agent, it is an efficient reducing agent under an alkaline condition [10, 58-61]. There are few reports exploiting the reducing capability of H_2O_2 for the fabrication of silver micro/nanostructures. Silver nanosheets and 3D flowerlike silver microstructures were fabricated by H_2O_2 reduction of Ag^+ and $[Ag(NH_3)_2]^+$ [10, 60]. Recently, a direct synthesis of silver microdisk on a plastic substrate by H_2O_2 reduction was demonstrated [61].

This paper reveals a simple yet efficient approach for the production of silver microplates *via* H_2O_2 reduction of $[Ag(NH_3)_2]^+$ complex under an influence of Cl^-. For the first time, we demonstrated a fabrication of silver microplates under an etching environment containing O_2/Cl^-, NH_4OH/H_2O_2, and H_2O_2. Under such environment, the survival of plate structures were promoted by chloride passivation of the dominated $Ag\{111\}$ facets while truncated cubes, icosahedra, and pentagonal rods with $Ag\{100\}$ envelopes were selectively destroyed. This method has several advantages including: (1) simple and rapid as the reaction is completed within 1 h, (2) operated under an ambient condition with high concentration of silver ion, (3) employed environmentally friendly reducing agent without using any capping agent or surfactant, and (4) ease separation of products. We also demonstrated a direct preparation of AgMPs and AgMPls from wasted silver chloride precipitates using the developed protocol.

2.2 EXPERIMENTAL SECTION

2.1.1 Chemicals

Silver nitrate ($AgNO_3$, purity$\geq$99.8%), sodium chloride (NaCl, purity$\geq$99%), nitric acid (HNO_3, 65% w/v), ammonium hydroxide solution (NH_4OH, 25% w/w), and hydrogen peroxide solution (H_2O_2, 30% w/w) were purchased from Merck®. Poly(vinyl pyrrolidone) (PVP, $M_w \approx 360,000$) was purchased from Aldrich. All chemicals were used as received. Deionized (DI) water was used as a solvent. Prior to use, all glassware and magnetic bars were thoroughly cleaned with detergent, rinsed with DI water, rinsed with 6 M nitric acid, and thoroughly rinsed again with DI water.

2.2.2 Reducing capability of H_2O_2

To demonstrate the reducing capability of H_2O_2 under an alkaline condition, silver microparticles (AgMPs) were synthesized from colorless silver ammine complex ($[Ag(NH_3)_2]^+$). Briefly, a clear solution of $[Ag(NH_3)_2]^+$ complex (~pH 10) was prepared by mixing $AgNO_3$ solution (1 M, 1 mL) with an NH_4OH (5.3 M, 1.7 mL) and PVP (5% w/v, 10 mL). The total volume was adjusted to 97.7 mL by DI water. As H_2O_2 (30% w/w, 2.3 mL) was added into the solution, the reduction of the complex to metallic silver could be noticed *via* the evolution of oxygen bubbles with an instant development of light brown silver colloid. The precipitated AgMPs were collected and cleaned with DI water. Under this condition, the concentration of $AgNO_3$, NH_4OH, H_2O_2 and PVP were 0.01 M, 0.09 M, 0.22 M, and 0.5% w/v respectively.

2.2.3 Synthesis of silver microplates (AgMPls)

AgMPls were selectively synthesized *via* the reduction of $[Ag(NH_3)_2]^+$ with a presence of Cl^- using H_2O_2 as a reducing agent. Briefly, a colloid of AgCl nanoparticles (AgClNPs) was prepared by a rapid injection of NaCl solution (0.1 M, 4 mL) into a solution of $AgNO_3$ (1 M, 1 mL) and PVP (5% w/v, 10 mL) under a vigorous stir. A milky white colloid of AgClNPs spontaneously developed. The total volume was adjusted to 96 mL by DI water. The colloid was further stirred for 5 min before an addition of NH_4OH solution (5.3 M, 1.7 mL). The colloid became less opaque due to a partial dissolution of AgClNPs with a formation of a water soluble $[Ag(NH_3)_2]^+$ complex (Equation 2.1). To induce a formation of AgMPls, H_2O_2 solution (30% w/w, 2.3 mL) was quickly injected into the colloid. The milky white colloid briefly turned light brown before becoming sparkling glitter within 2 min due

to the formation of AgMPls. The development of AgMPls and the progress of the reaction could be noticed by an evolution of oxygen bubbles (Equation 2.2) [62]. The colloid became intense glittering as the reaction proceeded while the white AgClNPs were disappeared. The colloid was further stirred for 1 h to ensure a complete reaction. The shiny silver precipitates were collected and washed 5 times with DI water. Under the standard condition, the concentration of NaCl, NH₄OH, H₂O₂, AgNO₃, PVP were 0.004, 0.09, 0.22, 0.01 M, and 0.5% w/v respectively. To investigate the influence of Cl⁻, NH₄OH, H₂O₂, Ag⁺, and PVP on the morphology of AgMPs, their final concentrations were systematically manipulated within the range of 0–50 mM, 0–0.45 M, 0–0.88 M, 5–40 mM, and 0–2% w/v respectively.

$$AgCl + 2NH_4OH \rightleftharpoons \left[Ag(NH_3)_2\right]^+ + Cl^- + 2H_2O \qquad \text{(Eq. 2.1)}$$

$$2[Ag(NH_3)_2]^+ + H_2O_2 \longrightarrow$$
$$2Ag + 4NH_3 + 2H_2O + 1/2O_2 \quad ; E_{cell}^0 = 0.227 \text{ V} \qquad \text{(Eq. 2.2)}$$
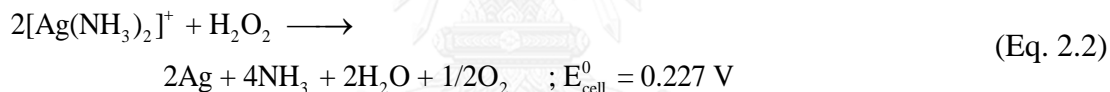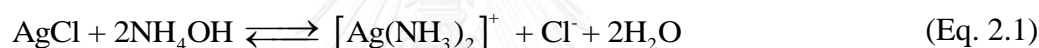
2.2.4 Structural Investigation

Morphology (size and shape) of the AgMPs and AgMPls was recorded by a scanning electron microscope (SEM, JEOL JSM-6510A) operating at 20 kV under a high vacuum mode with a secondary electron image (SEI) detector. A built-in energy dispersive X-ray spectrometer (EDS) was employed for monitoring elemental compositions of the AgMPls. The X-ray diffraction (XRD) patterns were collected by an X-ray diffractometer (Philips PW3710) operated at room temperature with a scanning rate of 0.02 deg/min, using Cu K_α irradiation (40 kV, 30 mA). The diffractograms were recorded in the 30°–80° region with a 0.2° resolution. X-ray photoelectron spectra (XPS) were performed on an AXIS ULTRA (Kratos Analytical, England) using Al K_α X-rays (1486.6 eV) as the exciting source. The charging

calibration was performed by referring the C1s to the binding energy at 285 eV. The XPS data analysis was conducted with standard ESCA-300 software package.

2.3 RESULTS AND DISCUSSION

Figure 2.1 shows an SEM micrograph of the silver microcrystals synthesized by the H_2O_2 reduction of $[Ag(NH_3)_2]^+$ without Cl^-. The microcrystals consisted of truncated cubes, icosahedra, pentagonal rods, hexagonal plates, and irregular particles. According to a detailed structural investigation (Figure 2.2), the irregular-shaped particles were, in fact, the under developed icosahedra. Based on a statistical analysis of 500 particles from non-overlapping SEM micrographs, the as-synthesized AgMPs consisted of 10.4% truncated cubes, 82.1% icosahedra and pentagonal rods, and 7.5% hexagonal plates (Figure 2.3A). The structural distribution confirmed that the multiply twinned crystals were the most thermodynamically favorable structures as they grown into icosahedra and pentagonal rod [2, 25, 63]. The multiply twinned are known to favorably developed at high concentration of gold and silver ions [63]. H_2O_2 is known to etch silver nanoparticle with a selective preservation of Ag{111} facets [27]. NH_3, on the other hand, selectively passivate and prohibit etching of Ag{111} facets [4]. As a result, crystals with dominated Ag{111} facets (*i.e.*, icosahedra) could withstand the oxidative etching of H_2O_2 and NH_4OH.
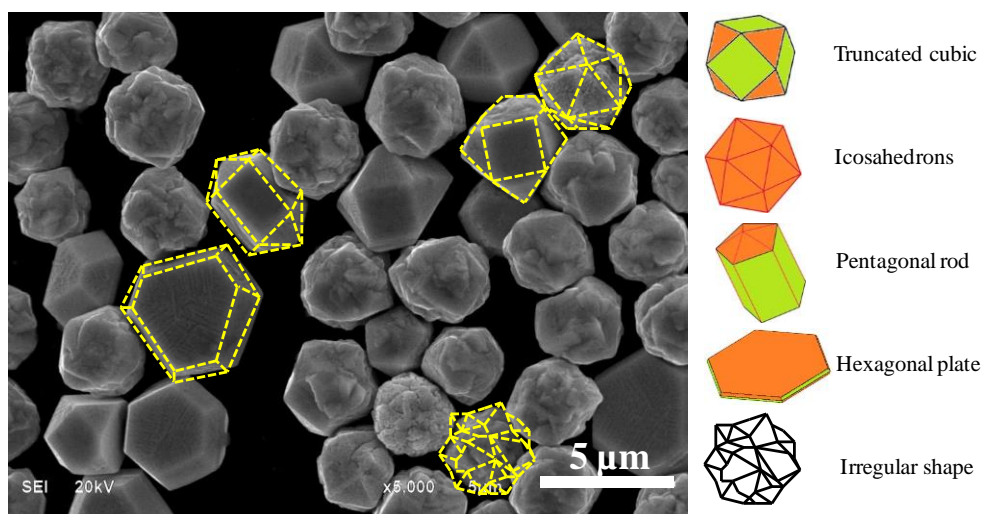
Figure 2.1 An SEM micrograph of AgMPs synthesized by H_2O_2 reduction of $[Ag(NH_3)_2]^+$. The orange and green surfaces indicated {111} and {100} facets, respectively. The experimental condition are $[AgNO_3]$ = 10 mM, $[NH_4OH]$ = 0.09 M, $[H_2O_2]$ = 0.22 M, and [PVP] = 0.5% w/v [47].
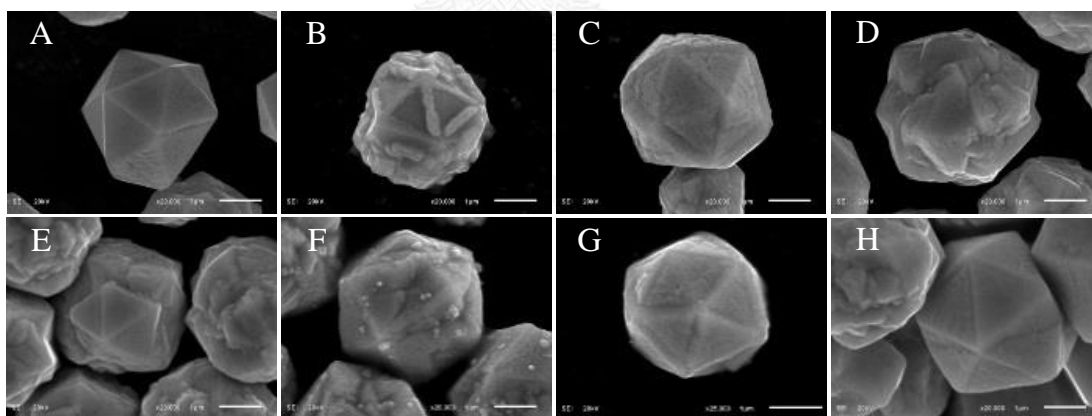
Figure 2.2 SEM micrographs show the structural evolution of icosahedra under H_2O_2-reduction of $[Ag(NH_3)_2]^+$ complex without Cl^-. The irregular shapes of silver microstructures are, in fact, the under devoloped icosahedra. The above SEM micrographs suggest that the structure grows layer-by-layer [47].
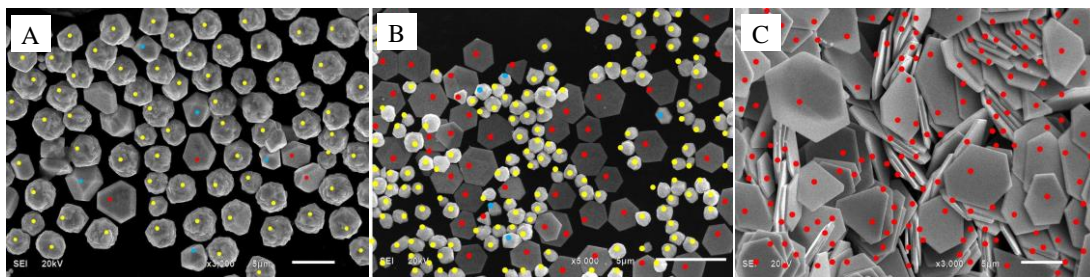
Figure 2.3 SEM micrographs of silver microparticles synthesized with Cl⁻ concentration of: (A) 0 mM, (B) 0.05 mM, and (C) 4 mM. The experimental condition are $[AgNO_3]$ = 10 mM, $[H_2O_2]$ = 220 mM, $[NH_4OH]$ = 90 mM, $[PVP]$ = 0.5% w/v. The number average of the structures were calculated from more than 500 particles of unique SEM micrographs. The colours represent: yellow = multiply twinned particles, blue = single crystal particles, and red = plates [47].

The isolated AgMPs also suggested that PVP plays an important role on facilitating particle growth as well as preventing aggregation. The well-separated particles with uniform size of 3–4 μm suggest a non-overlapping nucleation and growth period enabled by a sufficient stabilization by PVP and surface passivation by NH_3 [4].

Due to the positive electrochemical potentials of Equation 2.2, $[Ag(NH_3)_2]^+$ can be reduced by H_2O_2 [10, 60, 61]. With the presence of NH_4OH, $[Ag(NH_3)_2]^+$ instantaneously forms due to the high complex formation constant of NH_3 with Ag^+ (K_f = 1.6x10⁷) [64]. We hypothesized that $[Ag(NH_3)_2]^+$ functioned as the silver supply for the formation of AgMPs. Under a neutral condition, H_2O_2 efficiently oxidizes silver nanospheres to Ag^+ [65]. However, under an alkaline condition, H_2O_2 does not etch the newly generated seeds with stacking faults while the greater reduction potential compared to the oxidation potential favor the reduction [58]. As a result,

silver seeds with stacking faults survived and grew into micrometer size AgMPs even at a relatively high concentration of H_2O_2 (*i.e.*, in Figure 2.1, $[H_2O_2]/[Ag^+] = 22$).

Selective formation of AgMPls: Since Cl⁻ with dissolved O_2 is known to selectively etch singly and multiply twinned seed [2, 35-37], the reduction of $[Ag(NH_3)_2]^+$ by H_2O_2 under the influence of Cl⁻ was conducted. The addition of Cl⁻ was expected to work synergically with the *in-situ* generated O_2 from H_2O_2 decomposition as an efficient O_2/Cl⁻ etchant. Figure 2.4 shows structural evolution of AgMPs under the influence of Cl⁻. Surprisingly, even at a very low concentration of Cl⁻ (0.05 mM, Figure 2.4B), large icosahedra disappeared with a development of silver nanoplates (AgNPls). According to a statistical calculation of more than 500 particles from non-repeating SEM micrographs (Figure 2.3), the products consist of 2.5% small truncated cubes (average size of 1 μm), 76.4% small icosahedra (average size of 1 μm), and 21.1% microplates (average bisector length of 3 μm). When the concentration of Cl⁻ ion was increased, the AgNPls became larger and thicker (average bisector length of 9 μm and average thickness of 300 nm). The truncated cubes and the icosahedra disappeared as the concentration of Cl⁻ was increased to 4 mM (Figures 2.3, 2.4E, and 2.5). However, when the concentration of Cl⁻ was greater than 10 mM, the AgMPls were not obtained since all $[Ag(NH_3)_2]^+$ was precipitated as AgCl (Figures 2.4H and 2.4I). The solid AgCl is non-soluble in the reaction media due to the low concentration of NH_4OH. The H_2O_2 reduction of solid AgCl to metallic silver cannot be achieved unless more NH_4OH is added in order to generate the water soluble $[Ag(NH_3)_2]^+$. The AgMPls in Figure 2.4E were highly pure silver (99.5%) as confirmed by EDS and XRD data (Figures 2.6 and 2.7A). According to EDS data, a trace amount of chloride indicated a formation of thin AgCl film on the basal planes

[44-46]. The thin AgCl film can be removed by washing with 0.1 M NH$_4$OH solution (Figure 2.6). The XRD data in Figure 2.7B show that the intensity ratios of (111) and (200) peaks increase with an increasing of Cl$^-$ concentration which correspond to the higher number of AgMPls population. The silver nanostructures [52, 66] similar to those in Figures 2.4C–2.4F have been employed for electronic device fabrication and substrate for thin film solar cell. The smooth surface with large contacted area enable a prolong service lifetime in conductive ink and high photocurrent enhancement in thin film solar cells [52].
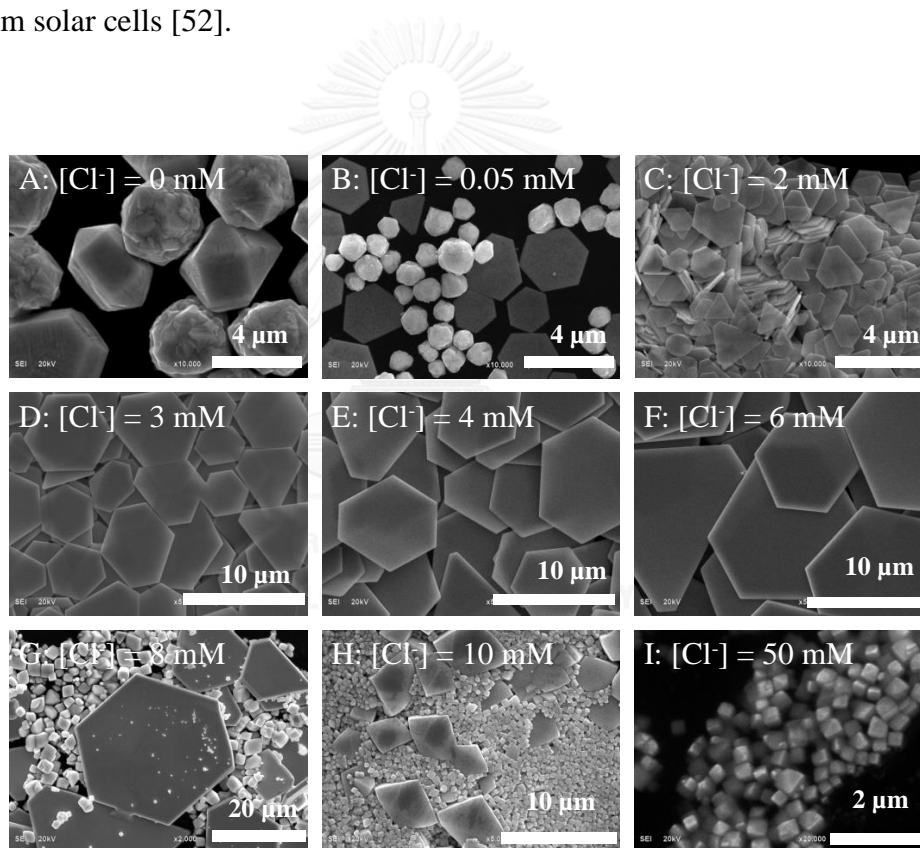
Figure 2.4 SEM micrographs show AgMPls synthesized by H$_2$O$_2$ reduction of [Ag(NH$_3$)$_2$]$^+$ under the influence of [Cl$^-$]: (A) 0, (B) 0.05, (C) 2, (D) 3, (E) 4, (F) 6, (G) 8, (H) 10, and (I) 50 mM. The experimental condition are [AgNO$_3$] = 10 mM, [H$_2$O$_2$] = 220 mM, [NH$_4$OH] = 90 mM, [PVP] = 0.5% w/v. The Cl$^-$ was introduced in the form of NaCl solution before an addition of H$_2$O$_2$ [47].

The selective dissolution of multiply twinned and single crystal particles by O_2/Cl^- [2, 35-37] and NH_4OH/H_2O_2 [38, 39] has been reported. In our case, the O_2 gas was *in-situ* generated by the H_2O_2 oxidation (Equation 2.2), the auto-decomposition of H_2O_2 over silver surface [53], and the auto-decomposition of H_2O_2 under alkaline condition [67]. An addition of Cl^-, thus, induced a formation of O_2/Cl^- etchant which capable of dissolving multiply twinned and single crystals while promoting the survival of AgMPls by Cl^--passivation.
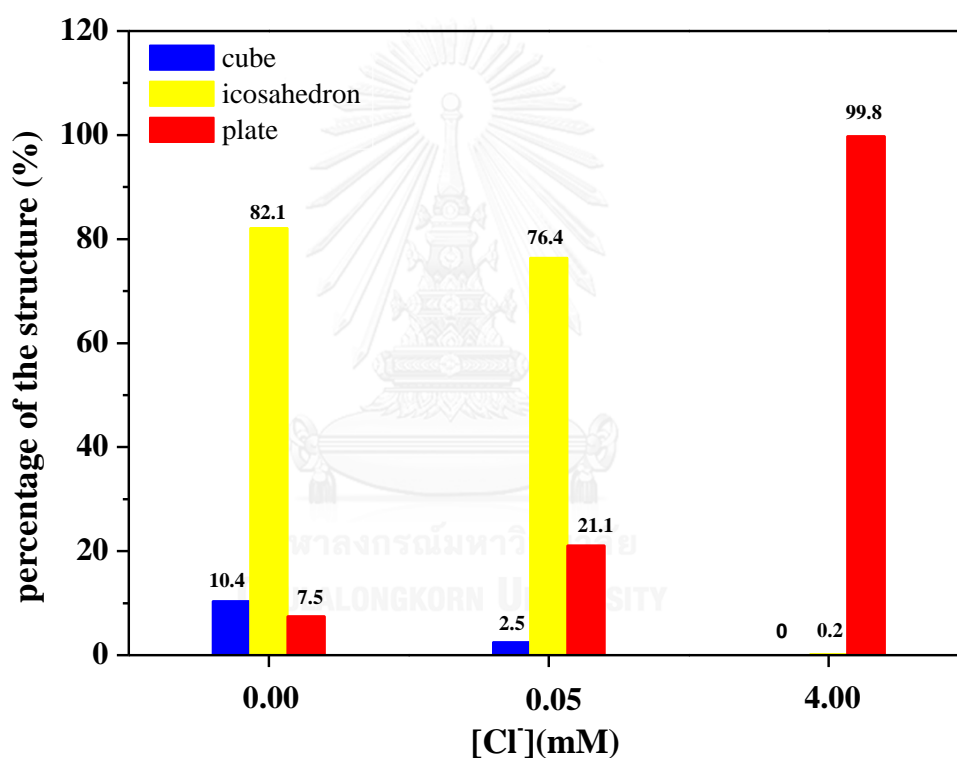
Figure 2.5 Percentage of cubic, icosahedral, and microplate silver crystals in synthetic conditions shown in Figure 2.4. The results indicated that Cl^- played an important role as a structural controlling agent as it selectively destroys structure with Ag{100} facet (*i.e.*, cube, icosahedron) while preserves those with Ag{111} (*i.e.*, plate). At Cl^- concentrations greater than 4 mM, the survived population was plate-structures while cubes and icosahedra were disappeared [47].
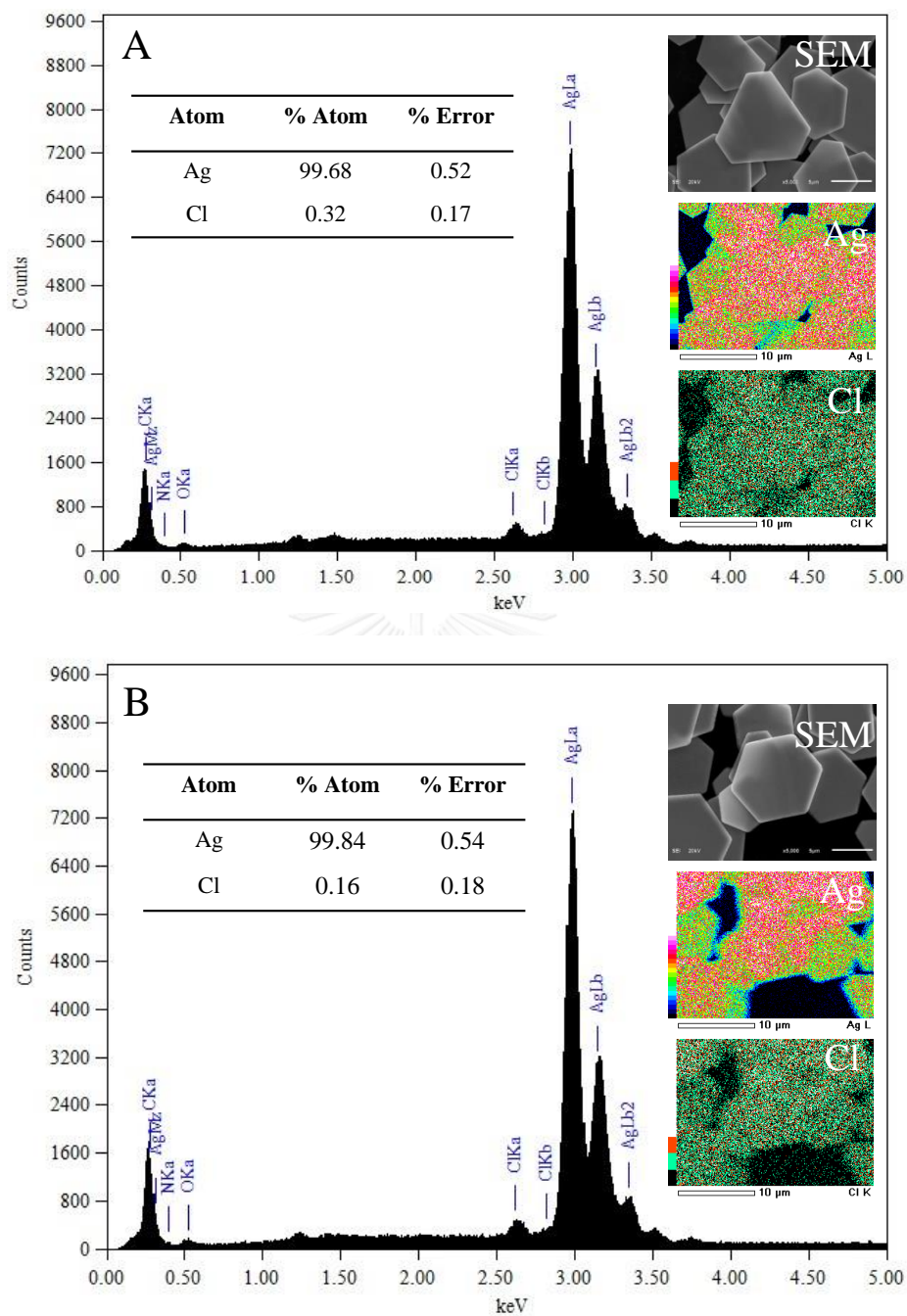
Figure 2.6 EDS spectra of AgMPls (A) before and (B) after washing with 0.1 M NH₄OH solution. The disappearance of chlorine after washing confirmed the presence of AgCl layer on the surface of as-synthesized AgMPls [47].
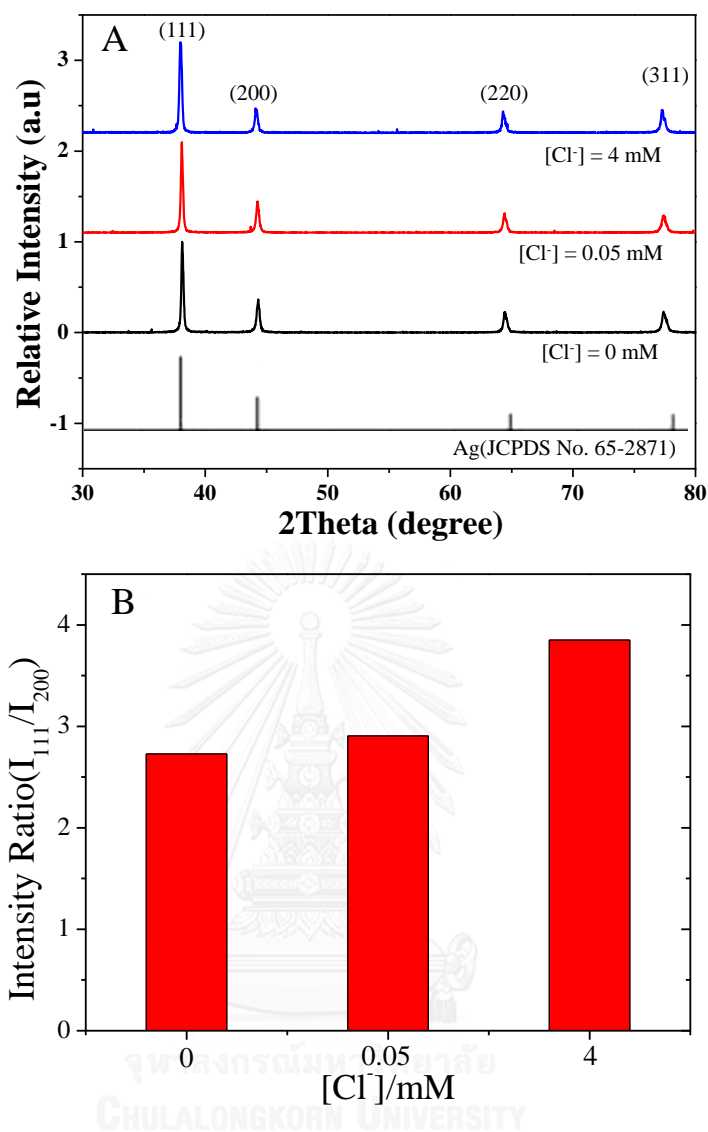
Figure 2.7 (A) XRD patterns of AgMPs synthesized with different Cl⁻ concentrations shown in Figure 2.3. (B) The plot of intensity ratios of (111) and (200) peaks indicates an increment of plate structure with [Cl⁻]. All patterns correspond to fcc crystal of silver metal (JCPDS No.65-2871) [47].

To gain an insight understanding on the selective formation of AgMPls under the etching environment, a systematic investigation was performed. Figure 2.8 shows the effect of NH_4OH, Ag^+, H_2O_2, and PVP on the morphology of silver

microstructures. In an acidic medium (pH<5) without NH_4OH (Figure 2.8A1), H_2O_2 cannot reduce Ag^+ or AgCl to metallic sliver at any concentration [58]. The reducing efficiency of H_2O_2 could be enhanced by increasing pH either by NH_4OH or NaOH [58, 59, 68] (Figure 2.9). When a minute amount of NH_4OH was added (Figure 2.8A2), AgNPls was formed. However, residual AgCl particles remained due to an incomplete reduction at a near neutral pH. The formation of AgNPls suggested that a seed selection process was initiated with an introduction of NH_4OH. Quasi-sphere AgMPs obtained when the reduction was conducted under NaOH (Figure 2.9). At NH_4OH concentration of 0.09–0.18 M, AgMPls (3–40 μm lateral size and 0.2–1.1μm thickness, Figures 2.8A3–2.8A5) were obtained. The reduction was very rapid as AgMPls formed and precipitated within 1 min after an addition of H_2O_2. At a relatively high NH_4OH concentration of 0.45 M, the reduction was incomplete with a formation of large AgMPls having a broad size distribution (10–120 μm lateral size). H_2O_2 was also rapidly exhausted due to the alkaline-induced decomposition and auto-decomposition on silver surface [53, 67].

Figure 2.8B1 confirmed that H_2O_2 is the sole reducing agent as AgCl crystals were obtained in the absence of H_2O_2. By adding a minute amount of H_2O_2 (0.05 M, Figure 2.8B2), AgNPls formed with a remaining solid AgCl. Under the employed condition, 0.11 M H_2O_2 was enough to completely convert $[Ag(NH_3)_2]^+$ complex to AgMPls (Figures 2.8B3–2.8B6). The plate size was increased from 4 μm to 23 μm while the plate thickness was increased from ~400 nm to 700 nm when H_2O_2 concentration was increased from 0.11 M (Figure 2.8B3) to 0.88 M (Figure 2.8B6). The sharp edges with smooth basal planes suggested that AgMPls tolerated the oxidative etching at high concentration of H_2O_2.
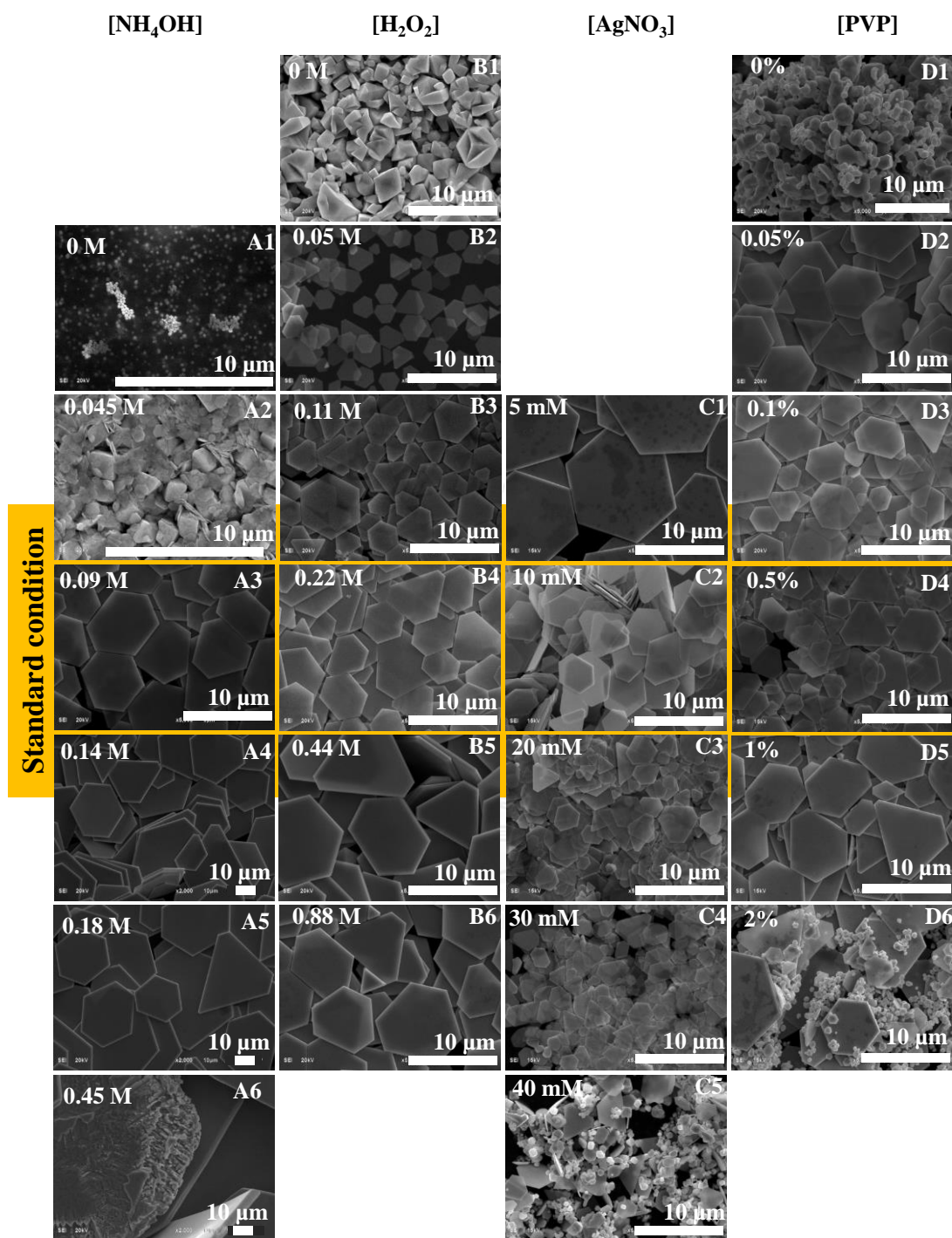
Figure 2.8 SEM micrographs show morphological change of AgMPs induced by the concentration of the reactants: (A) NH$_4$OH, (B) H$_2$O$_2$, (C) AgNO$_3$, and (D) PVP. The concentration is indicated in the figure. The scale bars indicate 10 μm [47].
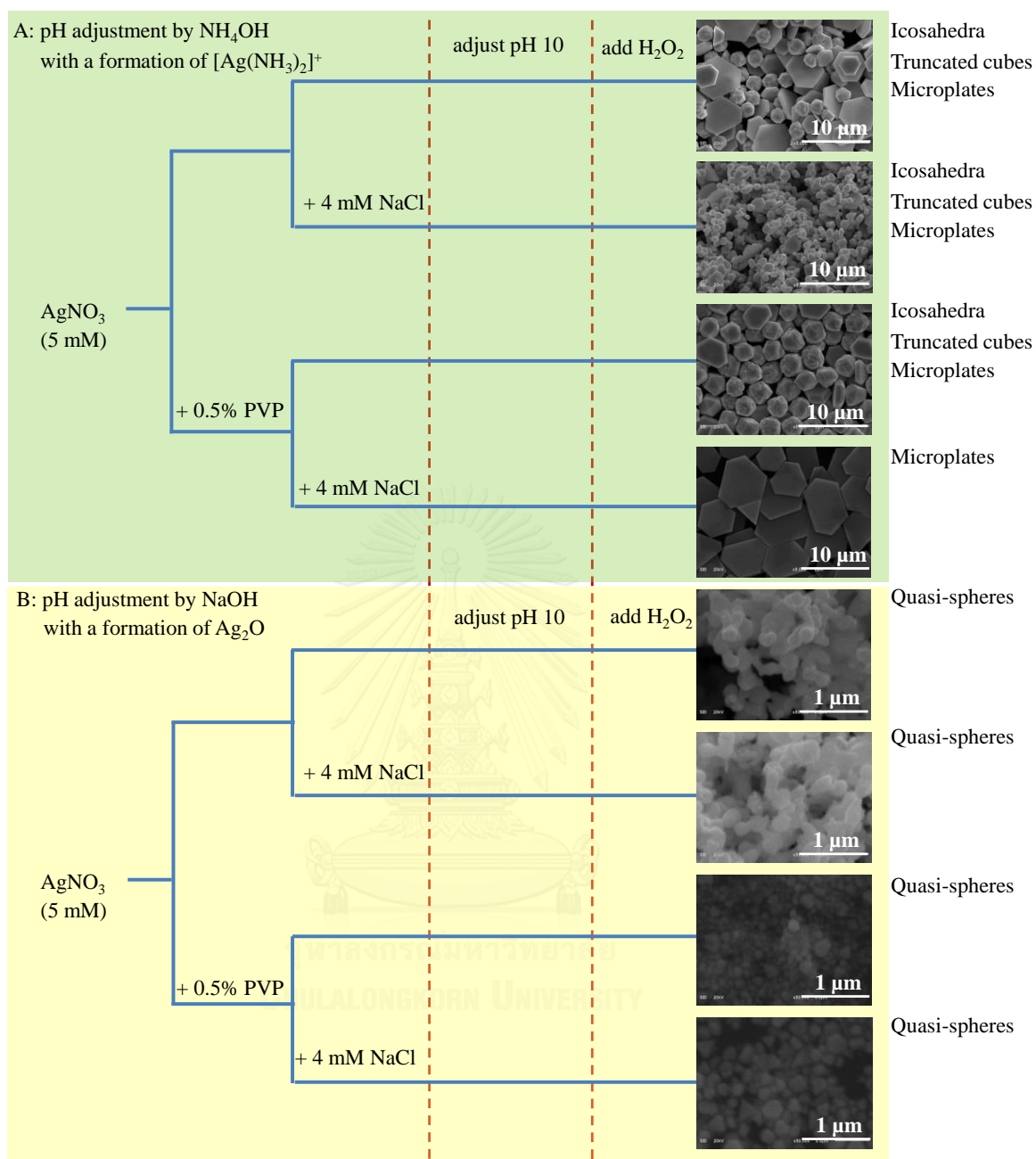
Figure 2.9 Influences of reaction media on the formation of silver micro/nanostructures under alkaline-H$_2$O$_2$ (pH 10) induced by (A) NH$_4$OH and (B) NaOH. The obtained silver micro/nanostructures suggested that the presence of Cl$^-$ and NH$_4$OH is crucial for the development of plate structure. PVP is an efficient stabilizer preventing the aggregation while assisting the formation of large silver microstructures [47].
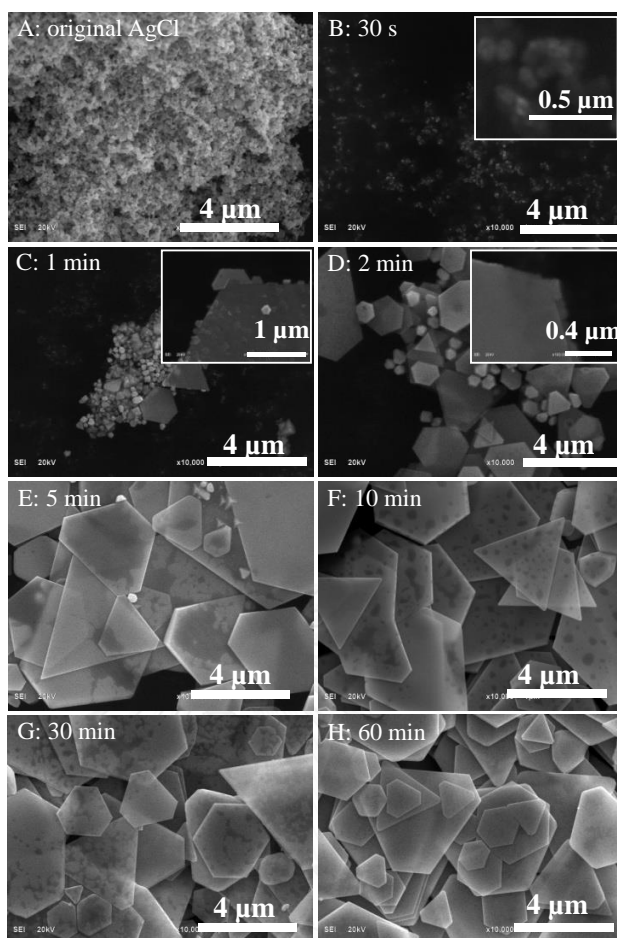
Figure 2.10 Time dependent SEM micrographs show evolution of AgMPls synthesized under the same condition as that of Figure 2.4F. The time was recorded after an injection of H_2O_2 reducing agent. Scale bars indicate 4 µm [47].

Figure 2.8C shows the influence of $AgNO_3$ concentration while the ratio of $[H_2O_2]:[Ag^+]$ was kept constant at 22. Large AgMPls were obtained at low concentration of $AgNO_3$ (5 mM, Figure 2.8C1). The AgMPls systematically transformed to AgNPls as the $AgNO_3$ concentration was increased. The lateral size was decreased from 15 µm to 3 µm while the thickness was decreased from 300 nm to 80 nm as the $AgNO_3$ concentration was increased from 5 mM to 30 mM (Figures 2.8C2–2.8C4). However, at an extremely high concentration of $AgNO_3$ (40 mM,

Figure 2.8C5), a mixture of AgMPls (lateral size of 4 μm and thickness of 200 nm) and microsphere (particle size of ~1–2 μm) was obtained. The structural change was due to: (1) a large number of seed generated under a high concentration of H_2O_2, (2) a rapid growth under an increased concentration of $AgNO_3$, and (3) an insufficient etching under a constant Cl^- concentration of 4 mM. Although O_2/Cl^- is known to efficiently etch multiply twinned seed [2, 35-37], silver microspheres in Figure 2.8B5 survived due to a low concentration of Cl^-. A significant aggregation was also observed at high concentration of $AgNO_3$ (40 mM, Figure 2.8C5) due to an insufficient stabilization of PVP (0.5% w/v).

From the previous investigations (Figures 2.8A–2.8C), PVP (0.5% w/v) functions as a good stabilizer preventing aggregation of AgMPls and AgNPls. PVP is known to preferentially adsorb on Ag{100} facet [24, 69, 70]. Without an addition of PVP (Figure 2.8D1), only aggregated AgMPs (1–5 μm) were obtained. Surprisingly, an insignificant structural change of AgMPls (lateral size of ~6 μm and thickness of 150 nm) was observed as the concentration of PVP was increased from 0.05 to 1 % w/v. This minor structural variation suggested that PVP functioned only as a stabilizer without any interference on nucleation and growth of AgMPls (Figures 2.8D2–2.8D5). The expansion of the basal plane was induced by the weaker adsorption of PVP on Ag{100} facets [24, 69, 70] with a passivation of NH_3 [4], Cl^- [40-44], and AgCl [44-46] on Ag{111} facets. These resulted in a greater deposition rate of silver atoms on Ag{100} facet than Ag{111} facet. However, a relatively high concentration of PVP of 2% w/v induced an incomplete reduction as AgCl microparticles (AgClMPs) were the main product with a formation of large AgMPls (lateral size of ~15 μm and thickness of ~300 nm, Figure 2.8D6). As the

concentration of H_2O_2 was kept constant at 220 mM, the formation of AgClMPs indicated an insufficient reduction power of H_2O_2 at high concentration of PVP as it forms stable complex between PVP [71-74].

Based on the observed phenomena, we believed that the water soluble $[Ag(NH_3)_2]^+$ complex is the sole species being reduced by alkaline peroxide. With the available NH_4OH, all Ag^+ were transformed into the complex [48, 64]. However, when the alkalinity was adjusted by NaOH, quasi-sphere AgMPs (Figure 2.9) were obtained instead of AgMPls. NH_4OH is one of the key factors for the development of plate shape structures as it imposes the following constraints: (1) NH_4OH decreases the rate of reduction by forming a stable $[Ag(NH_3)_2]^+$ complex with lower E^0 compared to that of Ag^+ [62] and (2) NH_4OH/H_2O_2 selectively etches single crystal particles [38, 39].

One of the interesting phenomena in this system is the survival and systematic growth of large AgMPls under a highly corrosive environment containing O_2/Cl^-, NH_4OH/H_2O_2, and H_2O_2. Figure 2.10 shows evolution of AgMPls as the water soluble $[Ag(NH_3)_2]^+$ complex was reduced by H_2O_2 solution. After a 30-s of H_2O_2 injection (Figure 2.10B), quasi-sphere silver particles (100–200 nm) were generated. At 1-min (Figure 2.10C), the quasi-sphere developed into silver crystals including truncated cubes, icosahedra, and plates. At 2-min (Figure 2.10D), those crystals grow into microstructures. Interestingly, the plate structures grow larger in terms of number and size (1–4 µm lateral size) compared to those of icosahedra and truncated cubes (0.6–0.8 µm). At 5-min, the majority of the silver structures are large AgMPls (1–10 µm lateral size) with rough surface (Figure 2.10E). A few numbers of small icosahedra and truncated cubes (~0.5 µm) were occasionally observed in SEM

micrographs. The change in population and morphology indicated a selective dissolution of icosahedra and truncated cubes as those structures completely disappeared after 10-min (Figure 2.10F). One interesting morphological change of the AgMPls is the increased smoothness of the basal planes after a prolong reaction time, as indicated by SEM micrographs in Figures 2.10E–2.10H. AgMPls with flat and smooth surfaces were obtained after 60-min.

Figure 2.8B6 suggested that the AgMPls were very stable under the extremely high concentration of H_2O_2 (0.88 M). The stability of AgMPls was due to the passivation of Ag{111} by Cl$^-$ [40-44] and AgCl [44-46]. H_2O_2 and NH_4OH/H_2O_2 selectively destroyed the truncated cubes (single crystal particles) [38, 39], while O_2/Cl^- selectively etched the multiply twinned particles [2, 35-37]. Our results indicated that the O_2/Cl^- also etched the truncated cubes (Figures 2.4A and 2.4E).

In Figure 2.11, we proposed a mechanism explaining the rapid growth of AgMPls under the employed etching environment. As shown in Figure 2.1, H_2O_2 could reduce water soluble $[Ag(NH_3)_2]^+$ complex into silver crystals. The growths of cubes from single crystal seeds, icosahedra and pentagonal rods from multiply twinned seeds, and hexagonal and triangular plates from seeds with stacking faults were thoroughly explained [1, 12, 25]. An addition of Cl$^-$ initiated an etching environment with selective survival of plate structures. The asymmetric twinned nanoplates bound by Ag{111} planes with alternated Ag{100} and Ag{111} lateral sides were formed [75, 76]. The surface passivation of Ag{111} by Cl$^-$ and AgCl limited the atomic deposition on the basal planes and decreased the rate of thickness growth. The adsorption of Cl$^-$ on the basal planes of AgMPls was confirmed by the EDS and XPS data. The XPS results show that AgCl was adsorbed on the basal planes

of as-prepared AgMPls as indicated by the binding energy of Cl 2p at 197.5 and 199.0 eV,[77-80] Figure 2.12B. To confirm the presence of AgCl, as-prepared AgMPls were washed by 0.1 M NH$_4$OH. The trace AgCl was completely removed after washing (Figures 2.6B and 2.12B). The bare surface of AgMPls was slowly oxidized to Ag$_2$O after a prolong storage under an ambient condition, as indicated by O 1s at 531.5 eV (Figure 2.12C) [80-82].

In addition, the adsorption of PVP-Ag$^+$ complex on Ag{100} facets promotes growth along the lateral side [50, 60, 70, 83-86] (Figure 2.13). An anisotropic growth due to a faster expansion of Ag{100} compared to that of Ag{111} induces a cyclic structural transformation of triangular, truncated triangular, and hexagonal structure [75, 76]. The growth continued until the [Ag(NH$_3$)$_2$]$^+$ complex was depleted.
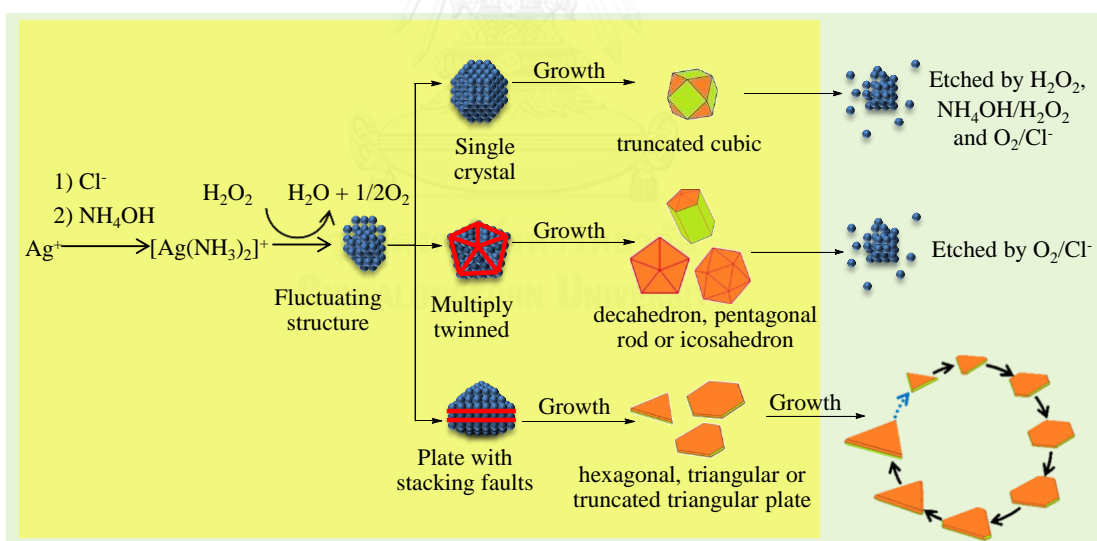
Figure 2.11 Proposed mechanism on the selective formation of AgMPls under an etching environment containing NH$_4$OH/H$_2$O$_2$, H$_2$O$_2$, O$_2$/Cl$^-$. The single crystal and multiply twinned crystal were selectively destroyed. The stability of the plate structure was due to the passivation of Ag{111} facets. The green facets indicate Ag{100} while the orange facets indicate Ag{111} [47].
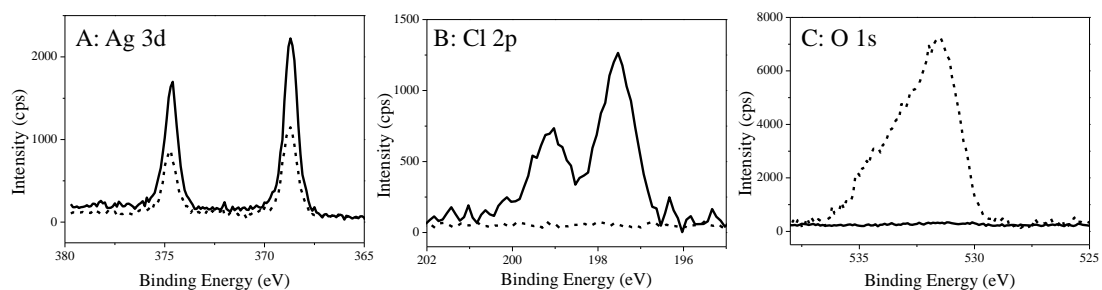
Figure 2.12 XPS spectra of as-prepared AgMPls (solid line) and 6-month storage AgMPls (dotted line). The as-prepared AgMPls were metallic silver with AgCl passivation as indicated by Ag 3d (A) and Cl 2p (B) spectra. The surface of cleaned AgMPls was oxidized into Ag_2O after a prolong storage as indicated by O 1s spectrum (C) [47].
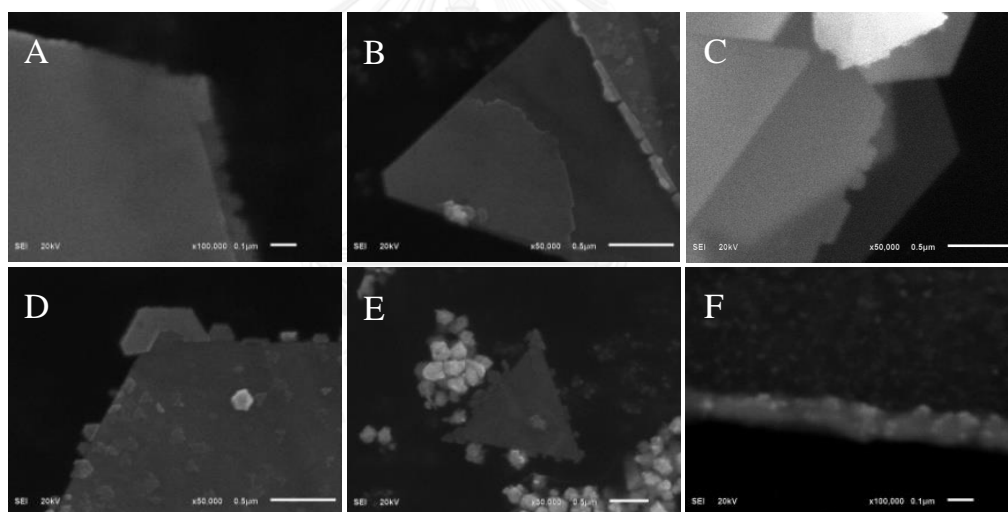
Figure 2.13 SEM micrographs show evidences of the lateral growth of AgMPls [47].

One of the potential applications of our developed technique is the direct fabrication of AgMPs and AgMPls from AgCl precipitates. The silver wastes were normally digested or leached into Ag^+ before precipitating as solid AgCl for easy separation. The AgCl precipitates were then converted to metallic silver by electrochemical deposition [87], galvanic replacement [88], chemical reduction [89]

and hydrometallurgical recovery [90, 91]. However, the processes are labor intensive, expensive, and generate more chemical wastes. Due to the 1:1 mole ratio of $Ag^+:Cl^-$ in the precipitated AgCl, the procedure employed in Figure 2.4H could only partially convert AgCl into metallic silver after a prolong reaction of 15 h (Figure 2.14A). The inefficient reduction was due to a very slow conversion of AgCl to $[Ag(NH_3)_2]^+$ complex at a relatively low $[NH_4OH]$ of 0.09 M while H_2O_2 cannot reduce solid AgCl to metallic silver. To improve the conversion, NH_4OH concentration was increased to 0.18 M (Figure 2.14B). Large AgMPls were precipitated when NH_4OH concentration was increased to 0.27 and 0.36 M (Figures 2.12C and 2.12D). In the absence of PVP, for comparison, the precipitates contained microplates, truncated cubes, and icosahedra (Figure 2.15).
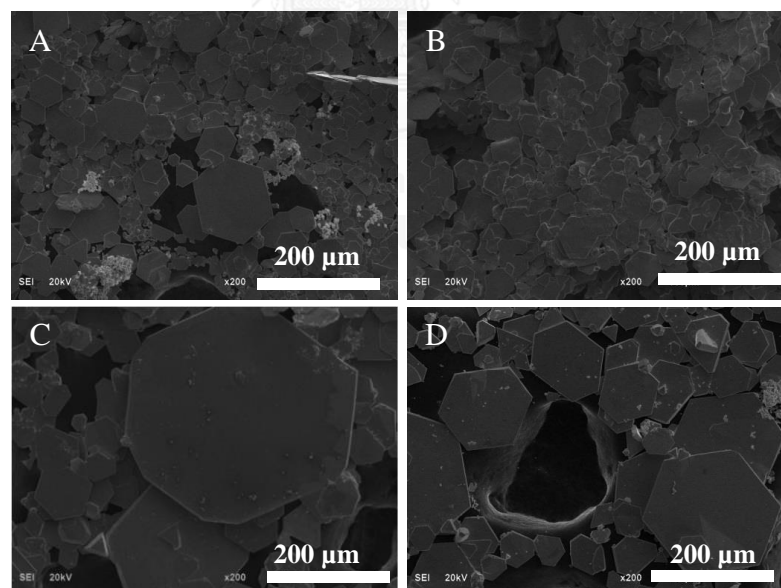
Figure 2.14 SEM micrographs show AgMPls directly fabricated from solid AgCl using our developed technique. The experimental condition is the same as that of Figure 2.4H with NH_4OH concentration of (A) 0.09, (B) 0.18, (C) 0.27, and (D) 0.36 M. The scale bars are 200 μm [47].
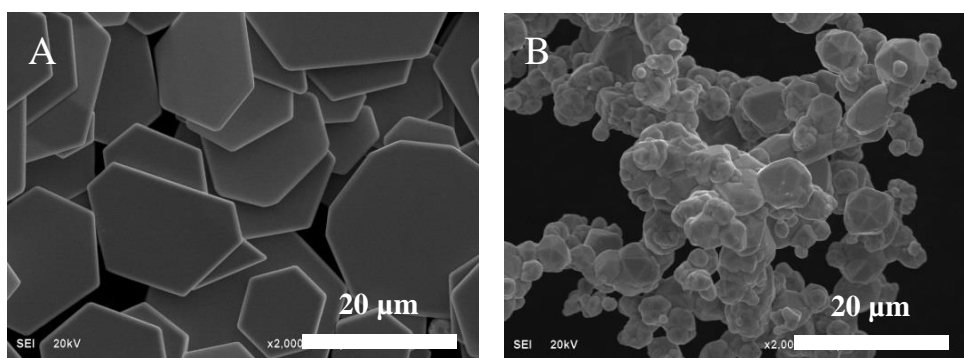
Figure 2.15 SEM micrographs show AgMPls and AgMPs recovered from wasted AgCl using the developed method: (A) with PVP of 0.5% w/v and (B) without PVP. The recovery conditions were [AgCl] = 10 mM, [H_2O_2] = 220 mM, and [NH_4OH] = 0.18 M. Scale bare indicate 20 μm [47].

Our technique offers a rapid, economic, and environmentally friendly protocol for silver recovery under an ambient condition. It does not create additional chemical waste as H_2O_2 was employed as the sole reducing agent. The main advantages of our developed technique include: (1) high recovery ratio of greater than 95%, (2) easily separated AgMPls precipitates (3) highly pure recovered AgMPls (99.99%, Figure 2.16), (4) tap water or water with Cl⁻ contamination can be employed instead of DI water, and (5) environmentally friendly process (by-products included O_2, H_2O, and NH_4Cl).
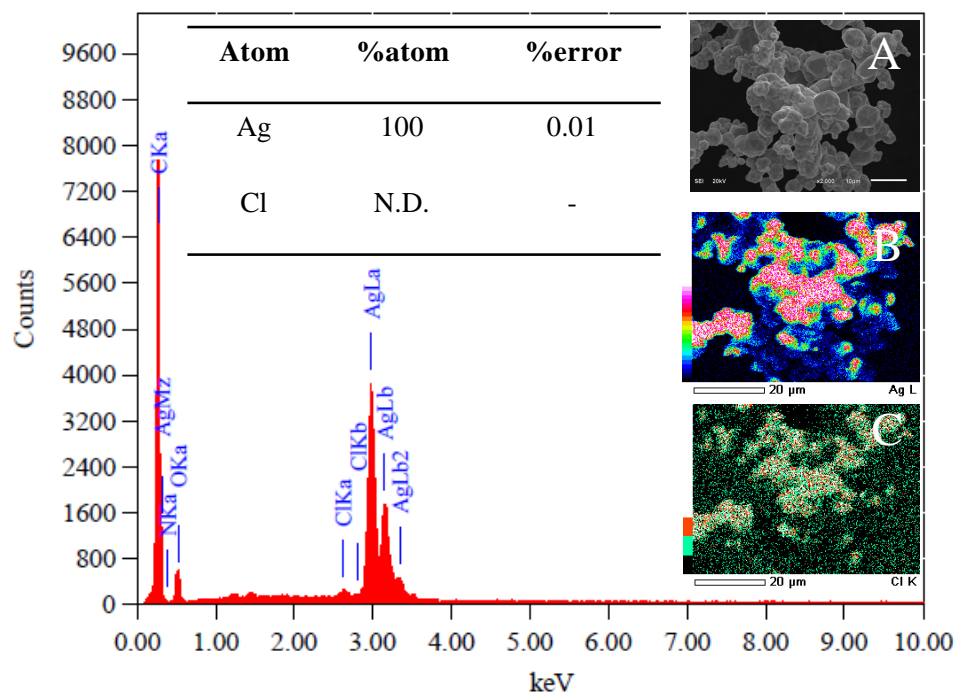
Figure 2.16 EDS spectrum of AgMPs recovered from waste AgCl using our developed protocol (A) SEM micrograph (B) silver map and (C) chloride map. By rinsing the AgMPs several times with 0.1 M NH₄OH solution, the residual AgCl on the surface can be completely removed, as suggested by EDS measurement [47].

2.4 CONCLUSIONS

We have developed a simple yet rapid technique for a large scale synthesis of AgMPls from $[Ag(NH_3)_2]^+$ using H_2O_2 as the reducing agent under an etching environment containing O_2/Cl^-, NH_4OH/H_2O_2, and H_2O_2. A trace Cl^- induced an etching environment that only plate structures could withstand as it passivated the Ag{111} facets of the plates. The time dependent SEM investigations confirmed that Cl^- promoted the survival of plate structures while selectively destroyed truncated cubes, icosahedra, and pentagonal rods containing Ag{100} envelops. In the system without Cl^-, etchants capable of structural selectivity does not exist. As a result, H_2O_2

reduction of $[Ag(NH_3)_2]^+$ complex produce silver microparticles including truncated cubic, icosahedral, pentagonal rod, and plate microstructures with icosahedra as the major product. A potential application of the developed protocol for a fabrication of highly pure AgMPls directly from AgCl precipitates has been demonstrated.

CHAPTER III

3D AgCl MICROSTRUCTURES SELECTIVELY FABRICATED *VIA* A Cl⁻-INDUCED PRECIPITATION FROM $[Ag(NH_3)_2]^+$

3.1 INTRODUCTION

Morphology-controlled synthesis of inorganic materials has attracted significant research attention as their physical, chemical, optical, magnetic and catalytic properties can be tuned by tailoring their size, shape, and composition [1]. Highly-branched inorganic micro/nanostructures synthesized by induced anisotropic growth [12] and selective etching method [39, 92] have been studied. For example, octapod Pt nanocrystals fabricated *via* an environmentally controlled wet chemical synthesis exhibited particularly high activity in formic acid oxidation [11-13]. Morphology-controlled synthesis has focused on the fabrication of structures with high-index facets in order to enhance the photocatalytic activities. Pd and Pt crystals, having crystal growth along <111> and <100> directions, showed exceptionally high electrocatalytic activities due to high index facets including {720}, {730}, {520}, and {830} [93-95].

Silver chloride (AgCl) is well-known as a photosensitive material in photographic industry and imaging. A recent discovery of its excellent visible

light photocatalytic activity derived from the surface plasmon resonance (SPR) induced electron transfer triggered by the surface silver nanoparticles has drawn considerable further researches [58, 96-101]. Various AgCl micro/nanostructures including nanoparticles [102], nanospheres [103], nanocubes [96, 103-106] and caged cubes [107] were synthesized and explored for potential applications as advanced functional material. A morphology-controlled synthesis of concave cubic and 3D AgCl hierarchical superstructure *via* the facet selective growth protocol has been demonstrated [108, 109]. To allow a slow crystal growth, the oxidation-controlled release of Ag^+ in a solution with high Cl^- concentration was performed. The kinetic growth along the <111> and <100> directions of the cubic seeds enables a formation of concave cubes and AgCl hierarchical superstructures as the surface energies of the Cl^--bonded {100} facets are much greater than those of the Cl^--bonded {110} and {111} facets. Interestingly, the 3D AgCl hierarchical superstructures show a better photocatalytic activity compared to those of cubes and concave cubes. To explore and realize the potential applications offered by the novel structural controlled materials, efficient methods for the fabrication of precisely controlled complex micro/nanostructures are still required.

In this contribution, we present a strategic morphology-controlled synthesis that enables a selective fabrication of 3D AgCl microstructures from silver ammine ($[Ag(NH_3)_2]^+$) complex by an addition of Cl^-. The 3D AgCl microstructures including octapods (8pAgCl), 8pAgCl with fishbone pods, hexapods (6pAgCl), 6pAgCl with 4-blade arrowhead pods, concave octahedrons, and octahedrons could be selectively precipitated and separated.

The photocatalytic activity of the synthesized 3D AgCl microstructures were explored by a decomposition of methyl orange (MO) solution under a visible-light irradiation.

3.2 EXPERIMENTAL SECTION

3.2.1 Chemicals

Silver nitrate (AgNO$_3\geq$99.8%), sodium chloride (NaCl$\geq$99%), ammonium hydroxide solution (NH$_4$OH 25% w/w) and methyl orange (MO) were purchased from Merck$^\circledR$ and were used as received. Prior to use, all glassware and magnetic bars were thoroughly cleaned with detergent, rinsed with deionized (DI) water, rinsed with 6 M nitric acid, and thoroughly rinsed with DI water.

3.2.2 Synthesis of 3D AgCl microstructures

Various 3D AgCl microstructures were selectively synthesized *via* a Cl$^-$-induced precipitation from silver ammine ([Ag(NH$_3$)$_2$]$^+$) complex precursor. Briefly, a solution of [Ag(NH$_3$)$_2$]$^+$ was prepared by rapidly mixing AgNO$_3$ solution (0.1 M, 5 mL) with NH$_4$OH solution (5.308 M, 2.83 mL) under a vigorous stir. A dark brown colloid of silver (I) oxide (Ag$_2$O) was observed for a brief moment prior to the formation of a colorless solution of [Ag(NH$_3$)$_2$]$^+$ complex. To induce a formation of 3D AgCl microstructures, the complex solution was quickly poured into NaCl solution (1.08 M, 92.17 mL). The clear solution instantaneously turned milky white indicating a formation of solid AgCl. The colloid was then vigorously stirred for 5 min before allowing the solid AgCl to precipitate. The clear supernatant was decanted. The

precipitate was 5-time washed with DI water and once with ethanol before drying under a dark ambient condition. Under this condition, the concentrations of AgNO₃, NaCl, and NH₄OH in the reacting medium were 5 mM, 1 M, and 0.15 M, respectively. To investigate the influence of Ag^+, Cl^-, and NH₄OH on the morphology of AgCl microstructures, their concentrations were systematically manipulated within the range of 2.5–10 mM, 0.1–2 M, and 0–0.3 M, respectively.

3.2.3 Selective etching of AgCl microstructures

The dissolution of certain crystallographic facet of AgCl microstructures under a continuous rinsing of NH₄OH solution (0.1 M for cubes and truncated cubes and 0.5 M for octahedrons) was performed. Briefly, precipitated AgCl was immobilized on filter paper by a simple filtration. The remaining AgCl on the paper was continuously rinsed by the NH₄OH solution. The structural changes were investigated after 1- and 2-min rinsing.

3.2.4 Structural transformation of AgCl microstructures

A colloid of cubic AgCl was prepared by mixing a solution of $[Ag(NH_3)_2]^+$ (*i.e.*, prepared by mixing AgNO₃ (0.1 M, 5 mL) with NH₄OH (5.308 M, 1 mL)) with NaCl solution (6.5 mM, 100 mL). The AgCl cubes (average size of 1–2 µm) formed within 1 min. To induce a structural transformation, NH₄OH solution (5.308 M, 1 mL) was added into the colloid and the product was collected after 30 s, 1, 2, 5, 10, 30, and 120 min for further characterization.

3.2.5 Characterization

Morphology (size and shape) of the 3D AgCl microstructures was recorded by a scanning electron microscope (SEM, JEOL JSM-6510A) operating at 20 kV under a high vacuum mode with a secondary electron image (SEI) detector. The X-ray diffraction (XRD) patterns were collected by an X-ray diffractometer (Rigaku D/MAX-2200) operated at room temperature with a scanning rate of 0.02 deg/min, using Cu K_α irradiation (40 kV, 30 mA). The diffractograms were recorded within 20°–80° region.

3.2.6 Photocatalytic activity investigation

A selected 3D AgCl microstructure (0.1 g) was mixed with methyl orange (MO) solution (20 mg/L, 100 mL). The mixture was incubated for 60 min in the dark. The photocatalytic activity under a visible light irradiation (250 W Xe arc lamp) was carried out. An aliquot (5 mL) was taken out every 2 min for visible adsorption measurement (USB4000 fiber optic spectrometer coupled with a DH-2000 deuterium/halogen light source, Ocean Optics).

3.3 RESULTS AND DISCUSSION

The $[Ag(NH_3)_2]^+$ solution prepared from $AgNO_3$ and NH_4OH is a colorless solution with excess NH_4OH. A precipitation of solid AgCl from the complex can be achieved by an addition of NaCl solution, as shown in Equation 3.1 [110].

$$[Ag(NH_3)_2]^+(aq) + Cl^-(aq) + 2H_2O(l) \rightleftharpoons AgCl(s) + 2NH_4OH(aq) \quad (Eq.\ 3.1)$$
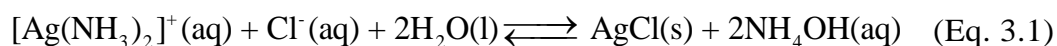
The concentrations of NH_4OH, NaCl as well as $AgNO_3$ strongly affect the morphology (size and shape) of the precipitated AgCl. By systematically adjusting their concentrations, 3D AgCl microstructures including 8pAgCl, 8pAgCl with fishbone pods, 6pAgCl, 6pAgCl with 4-blade arrowhead pods, concave octahedrons, octahedrons, a mixture of small concave cubes, small 6pAgCl, and small 8pAgCl, and microspheres, as shown in Figure 3.1, could be selectively precipitated.

According to the morphologies shown in Figure 3.1, 3D AgCl microstructures with unique exposed surfaces could be selectively precipitated from $[Ag(NH_3)_2]^+$ complex under a controlled environment. Microstructures with symmetric pod length indicate a uniform crystal growth while the uniform sizes indicate a complete separation between the nucleation and growth periods in this one-pot synthetic protocol. Although AgCl is sparingly soluble in water ($K_{sp} = 1.77 \times 10^{-10}$) [62], its solubility in NH_4OH solution increases as it forms water soluble $[Ag(NH_3)_2]^+Cl^-$ complex [64]. As a result, a relatively high Cl^- concentration was necessary to induce the precipitation (Figure 3.2). In an initial investigation, a clear solution of $[Ag(NH_3)_2]^+$ complex was prepared by mixing $AgNO_3$ solution (0.1 M, 2.5 mL) with NH_4OH solution (5.308 M, 2.83 mL). The $[Ag(NH_3)_2]^+$ complex solution was rapidly poured into NaCl solution (1.06 M, 94.67 mL) to induce a formation of solid AgCl. Under this condition the concentrations of Ag^+, Cl^-, and NH_4OH, respectively, were 2.5 mM, 1 M, and 0.15 M with the mole ratios $[Cl^-]/[Ag^+]$, R1 = 400 and $[NH_4OH]/[Ag^+]$, R2 = 60. The precipitated 3D AgCl microstructure was 8pAgCl with fishbone triangular pods, as shown in Figure 3.3Aa and Table 3.1. The precipitation of

8pAgCl was expected as the crystals were formed in an environment with high Cl^- concentration. The Cl^--rich environment promotes the growth in <111> directions of cubic seeds [13, 108]. As the concentration of Ag^+ increased to 3.5 and 5 mM, a mixture of 8pAgCl and 6x4pAgCl were obtained (Figures 3.3Ab and 3.3Ac). A mixture of small 8pAgCl, concave cubes, and 6pAgCl were obtained when Ag^+ concentration increased to 7.5 mM (Figure 3.3Ad). An instantaneous precipitation of AgCl microspheres occurred when Ag^+ concentration increased to 10 mM (Figure 3.3Ae).
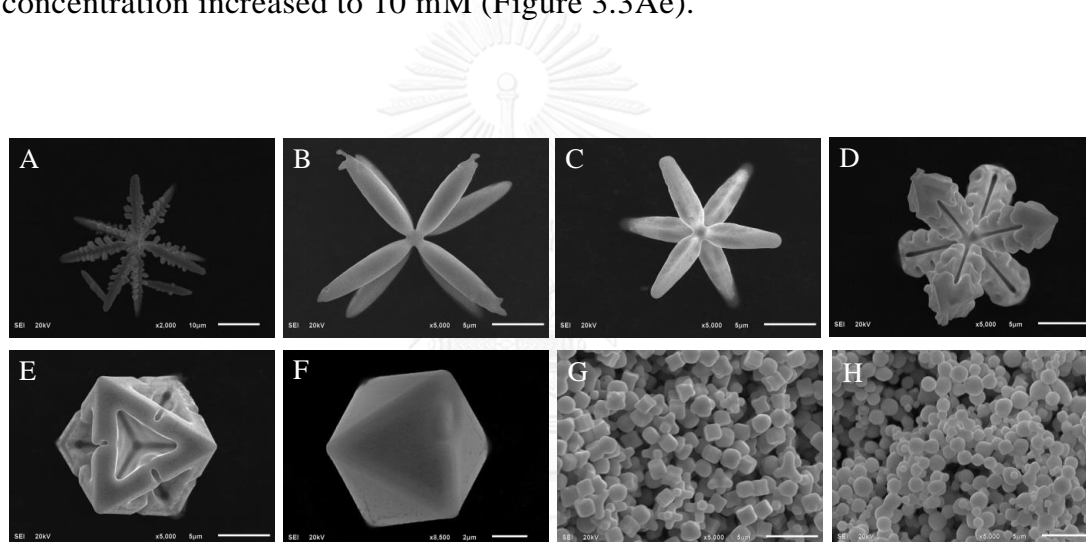
Figure 3.1 AgCl microstructures precipitated from $[Ag(NH_3)_2]^+$ complex by an addition of Cl^-: (A) 8pAgCl with fishbone pods, (B) 8pAgCl, (C) 6pAgCl, (D) 6pAgCl with 4-blade arrowhead pods, (E) concave octahedrons, (F) octahedrons (G) mixture of small concave cubes, small 6pAgCl, and small 8pAgCl, and (H) microspheres [48].
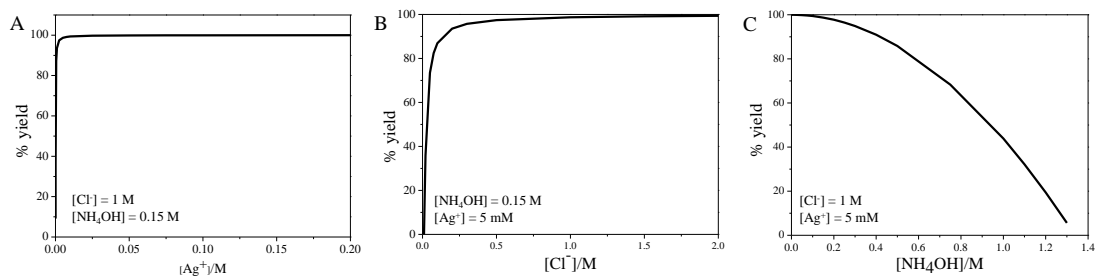
Figure 3.2 Theoretical yield of AgCl precipitates from a solution containing Ag$^+$, Cl$^-$, and NH$_4$OH. The yield is given in terms of concentration of each reactant. Under the employed conditions, nearly 100% of AgCl was precipitated. Note: the concentration of NH$_4$OH was always lower than 0.3 M [48].

The formation and growth of 8pAgCl with fishbone pods, 8pAgCl, and concave cubes from cubic seeds under the influence of Cl$^-$ were clearly explained by Huang's group [108, 109]. In our investigation, the formation of eight-pod family from cubic seeds in Cl$^-$-rich environment is expected. However, the co-precipitation of 6pAgCl and 6x4pAgCl in Figures 3.3Ab– 3.3Ad was unexpected since they could not grow from the cubic seeds. The formation of six-pod family could be associated with the presence of NH$_4$OH.
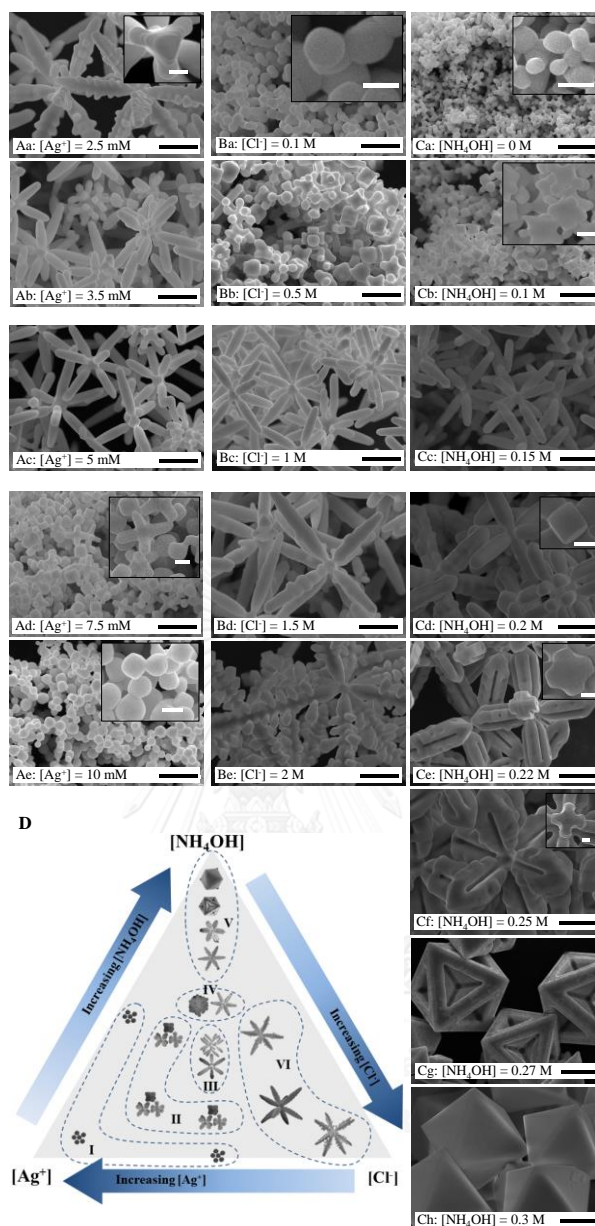
Figure 3.3 SEM micrographs of precipitated 3D AgCl microstructures under: (A) [Ag$^+$] = 2.5–10 mM, (B) [Cl$^-$] = 0.1–2 M, and (C) [NH$_4$OH] = 0–0.3 M. The concentrations were varied over those of the standard condition (Figures 3.3Ac, 3.3Bc, and 3.3Cc). (D) a map of 3D AgCl microstructures revealing the influence of reactant concentrations. The structures were divided into 6 groups circumscribed by the dashed lines. The scale bars are 5 μm (main figures) and 1 μm (insets) [48].

Table 3.1 Experimental condition for the selective fabrication of 3D AgCl microstructures. The concentration and mole ratio are given with respect to those in Figure 3.3 [48].

Figure	$[Ag^+]$ (M)	$[Cl^-]$ (M)	$[NH_4OH]$ (M)	R1	R2	Products	Group	Note
			Effect of $[Ag^+]$					
3.3Aa	2.5×10^{-3}	1	0.15	400	60	8pAgCl with fishbone triangular pods	VI	++
3.3Ab	3.5×10^{-3}	1	0.15	285	43	8pAgCl, 6x4pAgCl	III	++
3.3Ac	**5×10^{-3}**	**1**	**0.15**	**200**	**30**	**8pAgCl, 6x4pAgCl**	**III**	**++**
3.3Ad	7.5×10^{-3}	1	0.15	133	20	8pAgCl, 6pAgCl, concave cube	II	+++
3.3Ae	1×10^{-2}	1	0.15	100	15	sphere	I	+++
			Effect of $[Cl^-]$					
3.3Ba	5×10^{-3}	0.1	0.15	20	30	sphere	I	++
3.3Bb	5×10^{-3}	0.5	0.15	100	30	8pAgCl, 6pAgCl, concave cube	II	++
3.3Bc	**5×10^{-3}**	**1**	**0.15**	**200**	**30**	**8pAgCl, 6x4pAgCl**	**III**	**++**
3.3Bd	5×10^{-3}	1.5	0.15	300	30	8pAgCl with fishbone triangular pods	VI	+++
3.3Be	5×10^{-3}	2	0.15	400	30	8pAgCl with fishbone triangular pods	VI	+++
			Effect of $[NH_4OH]$					
3.3Ca	5×10^{-3}	1	0	200	0	sphere	I	+++
3.3Cb	5×10^{-3}	1	0.1	200	20	8pAgCl, 6pAgCl, concave cube	II	+++
3.3Cc	**5×10^{-3}**	**1**	**0.15**	**200**	**30**	**8pAgCl, 6x4pAgCl**	**III**	**++**
3.3Cd	5×10^{-3}	1	0.2	200	40	6pAgCl, 8x3pAgCl	IV	++
3.3Ce	5×10^{-3}	1	0.22	200	44	6pAgCl with 4-blade arrowhead pods	V	++
3.3Cf	5×10^{-3}	1	0.25	200	50	6pAgCl with 4-blade arrowhead pods	V	++
3.3Cg	5×10^{-3}	1	0.27	200	54	caged octahedron	V	+
3.3Ch	5×10^{-3}	1	0.3	200	60	octahedron	V	+

Note: +++ precipitate instantaneously, ++ precipitate within 1 min,

+ precipitate within 4 min,

R1 = $[Cl^-]/[Ag^+]$

R2 = $[NH_4OH]/[Ag^+]$.

In Figure 3.3B, the influence of Cl⁻ concentration was verified over the range of 0.1–2 M corresponding to R1 = 20–400 (the concentrations of Ag^+ and NH_4OH were fixed at 5 mM and 0.15 M, respectively). At low Cl⁻ concentration of 0.1 M (Figure 3.3Ba) AgCl microspheres with an average diameter of 1 μm instantaneously precipitated. At Cl⁻ concentration of 0.5 M (Figure 3.3Bb), the product was a mixture of 6pAgCl with an average pod length of 2 μm, concave cubes with an average size of 2.5 μm, and 8pAgCl with an average pod length of 1 μm. However, when the Cl⁻ concentration increased to 1.5 M (Figure 3.3Bd), the large 8pAgCl with an average pod length of 10 μm was the sole product. At an extremely high Cl⁻ concentration of 2 M (Figure 3.3Be), 8pAgCl with 10-μm long fishbone triangular pods was obtained. This morphology is in good agreement with that in Figure 3.3Aa as they were precipitated at the same R1 (see Table 3.1).

The influence of NH_4OH concentration was conducted over 0–0.3 M while the concentration of Ag^+ and Cl⁻ were fixed at 5 mM and 1 M (R1 = 200 and R2 = 0–60), respectively. In the absence of NH_4OH (Figure 3.3Ca), AgCl microspheres with an average size of 500 nm instantaneously precipitated. At 0.1 M NH_4OH (Figure 3.3Cb), a mixture of small 8pAgCl, small concave cubes, and small 6pAgCl was obtained. At 0.2 M NH_4OH (Figure 3.3Cd), the precipitate consisted of 6pAgCl and 8x3pAgCl. At 0.22 and 0.25 M NH_4OH (Figures 3.3Ce and 3.3Cf), the product was 6pAgCl with 4-blade arrowhead pods. The 4-blade pods originated from crystal growth in the <100> directions along the pod length. The grove between adjacent blades on the same pod was the growth-suppressed {110} facets. As NH_4OH concentration increased to

0.27 M (Figure 3.3Cg), as the 6pAgCl developed into a concave octahedrons, the <100> orthogonal blades on the adjacent pods grew until their edges joint together. The jointed edges created triangular vacancies with a tri-pod grove of the growth-suppressed {111} facets. When the NH_4OH concentration was further increased to 0.3 M (Figure 3.3Ch), the edges of the concave octahedrons over grown along the <100> directions until the triangular vacancies were filled. The caged octahedron then transformed into an octahedron bounded by {111} facets.

To simplify the structural development under an influence of all three reacting components, 3D AgCl microstructures were projected on a triangular map (Figure 3.3D). The microstructures can be classified into six groups. Group I consisted of microspheres that rapidly precipitated at high Ag^+ concentration with relatively low Cl^- and NH_4OH concentration (Table 3.1). Group II consisted of small concave cubes, 8pAgCl, and 6pAgCl formed at moderate Cl^- and NH_4OH concentrations. As the NH_4OH concentration was increased, group III microstructure consisting of 8pAgCl and 6x4pAgCl was obtained. When NH_4OH concentration further increased, group IV microstructure containing 6pAgCl and 8x3pAgCl was obtained. At extremely high NH_4OH concentration, group V microstructure (6pAgCl, 6pAgCl with 4-blade arrowhead, concave octahedrons and octahedrons) was precipitated. At extremely high Cl^- concentration, the 8pAgCl with triangular pod and 8pAgCl with fishbone triangular pods were obtained (group VI microstructure).

The variation of 3D AgCl microstructures shown in Figure 3.3 suggested that Cl^- and NH_4OH played an important role on the structural development.

The preferential growth along <111> directions was promoted in Cl$^-$-rich environment [108, 109]. However, the preferential growth along <100> directions in an NH_4OH-rich environment that produced six-pod family has never been reported. To gain an insight understanding on the role of NH_4OH, dissolution of cubic, truncated cubic and octahedral AgCl by NH_4OH were investigated. The cubes turned into quasi-spheres within a 2-min rinsing by 0.1 M NH_4OH, as shown in Figure 3.4A indicating a faster dissolution of {111} corners than {110} edges and {100} facets, respectively. The same phenomena were also observed during the dissolution of truncated cube as the predominant dissolution occurred at the truncated {111} facets (Figure 3.4B). The selective dissolution of {111} facets was clearly evident in the octahedrons (Figure 3.4C). Surprisingly, after a 2-min rinsing with 0.5 M NH_4OH, the six {100} tips of the octahedrons remained (Figure 3.4Cc). The observed structural change in Figure 3.4 suggested that NH_4OH preferentially etched the {111} facets. The etching was predominant at the {111} corners and the {110} edges of the cube as well as the {111} facets of octahedrons. The {100} square tips of the octahedron were not disturbed even under a treatment with higher concentration of NH_4OH (Figure 3.4C).

When cubic AgCl was incubated in the NH_4OH solution, the transformation of cubes into big truncated cubes indicates the growth in the <100> directions as shown in Figure 3.5. The structural change indicates a preferred structural transformation towards that with a greater fraction of {111} facets. An appearance of small microspheres (in yellow circle) indicates that the formation of bigger truncated cube involved Ostwald ripening. The structural

transformations in Figures 3.4 and 3.5 imply a selective preservation of octahedral seeds in the NH_4OH-rich environment where the cubic seeds are selectively destroyed. The structural transformation of fcc crystal (Ag and Pd) from cubes to truncated cubes and octahedrons has been reported [34, 111].
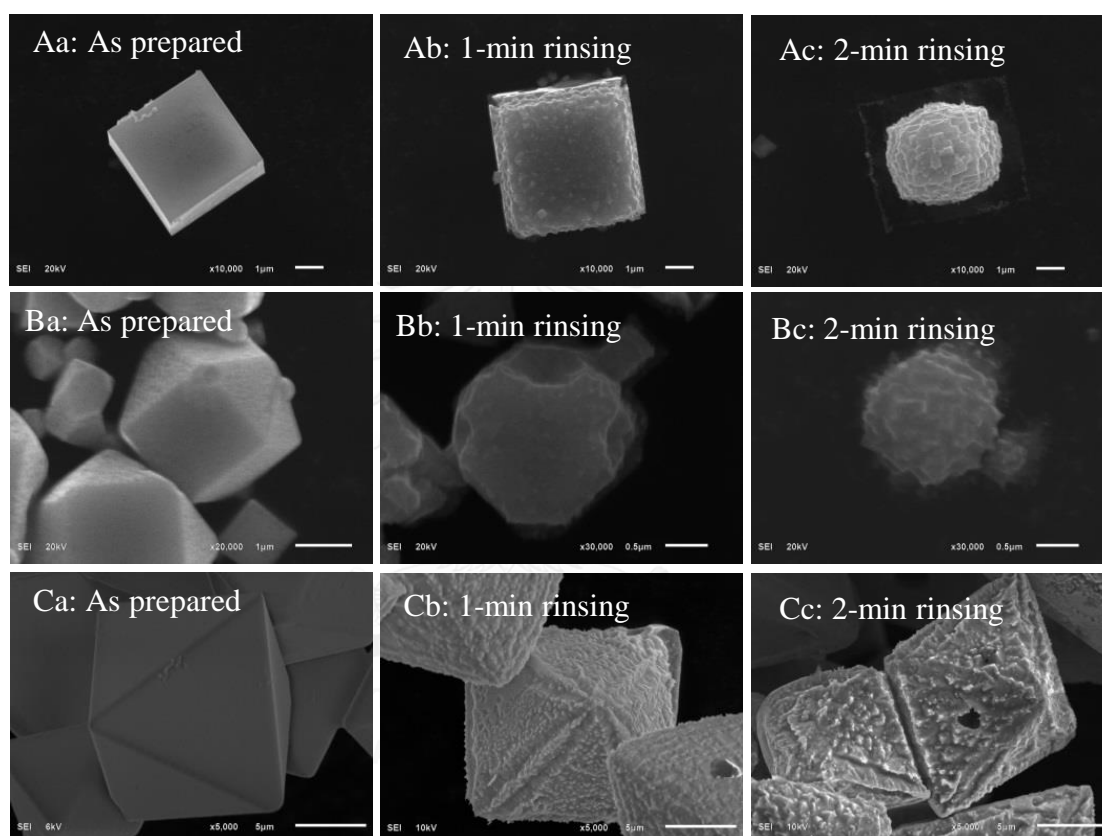
Figure 3.4 Dissolution of AgCl by NH_4OH (A) cube, (B) truncated cube, and (C) octahedrons. The etching was performed by continuously rinsing the immobilized AgCl microstructures with 0.1 M NH_4OH (A and B) and 0.5 M NH_4OH (C) [48].
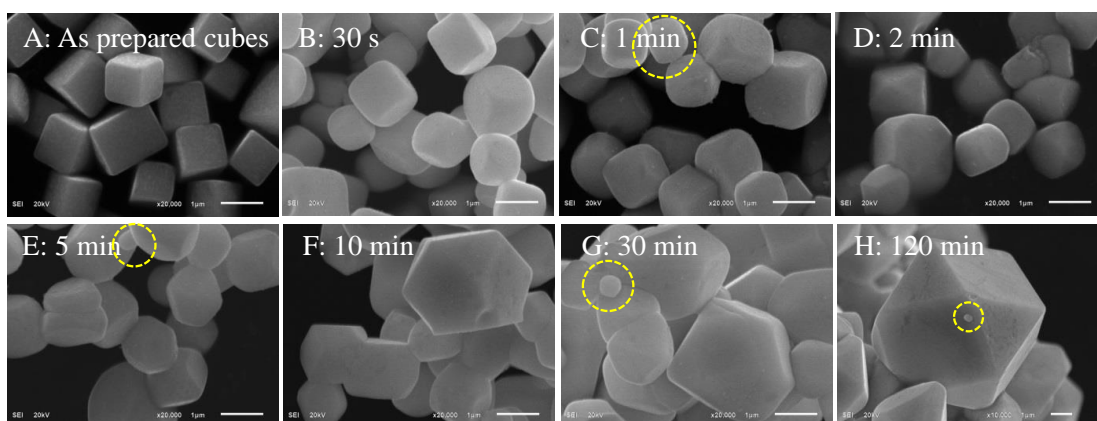
Figure 3.5 Structural transformation of cubic AgCl to bigger truncated cubes under the influence of NH$_4$OH: (A) as prepared cubes, and after an addition of NH$_4$OH for (B) 30 s, (C) 1 min, (D) 2 min, (E) 5 min, (F) 10 min, (G) 30 min, and (H) 120 min. The scale bars are 1 μm [48].

According to the classified structures in Figure 3.3D and Table 3.1, a structural evolution in the Cl$^-$-rich and NH$_4$OH-rich growth environment is summarized in Figure 3.6. Based on the minimum surface energy hypothesis [108, 112], we proposed that cubic seeds were firstly developed during the early stage of nucleation as it is the most thermodynamically favorable structure. The survival of the seed, the structural transformation, and further development were dictated by the growth environment. With the presence of NH$_4$OH, the cubic seeds were truncated and transformed into octahedral seeds. Under the moderate condition, both octahedral and cubic seeds survived and further growth into group II structure.
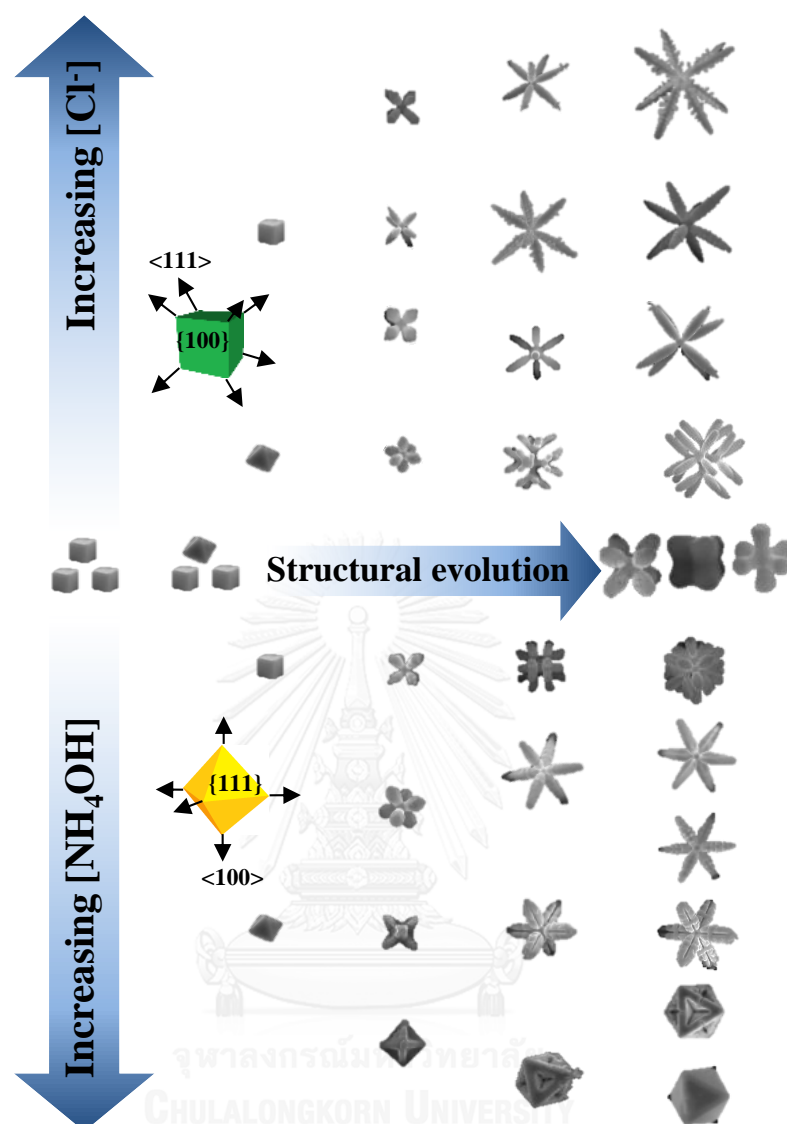
Figure 3.6 Schematic illustration shows seed selectivity and concomitant structural development of 3D AgCl microstructures under the influence of Cl$^-$ and NH$_4$OH [48].

The development of 6x4pAgCl (Group III structure) indicates the conversion of growth from <100> to <111> directions while that of 8x3pAgCl (Group IV structure) indicates the opposite phenomena. The conversion on the preferential growth direction indicates the influence of seed morphology and

the growth environment on the final microstructures. The initial growth is dictated by the seed morphology while the concomitant growth is governed by the environment. For 6x4pAgCl, initially, the tips of the octahedral seed grew along the <100> into a small 6pAgCl under a moderate concentration of NH_4OH. Each pod is bound by five {100} facets, eight {110} edges, and four {111} corners (Figure 3.7). However, the environment favored the Cl^--induced growth, the small 6pAgCl further grew along <111> directions from the twenty four corners of the six pods into a 6x4pAgCl. Similarly, in the case of 8x3pAgCl, the cubic seed grew along the <111> directions into 8pAgCl with square pods under a moderate Cl^- concentration. However, the tip of each pod was truncated as the seed was grown in an NH_4OH-rich environment (*i.e.*, similar to those in Figure 3.5). The crystals then further growth along the <100> directions from the twenty four tips of eight pods into an 8x3pAgCl (Figure 3.8).

The previous reports have proven that the octapod AgCl microstructures were grown from cubic seed under the preferential growth along <111> directions in Cl^--rich environment without a presence of NH_4OH [108, 109]. We hypothesize that the six-pod family (Group V microstructure shown in Figure 3.3D) was developed from octahedral seeds where NH_4OH plays a major role on the formation and survival of the seeds. A similar phenomenon was reported where the single crystalline nano-hexapod silver was grown from an octahedral seed [113]. To verify our hypothesis, the time dependent structural evolution of several microstructures was investigated and the results are shown in Figure 3.9.
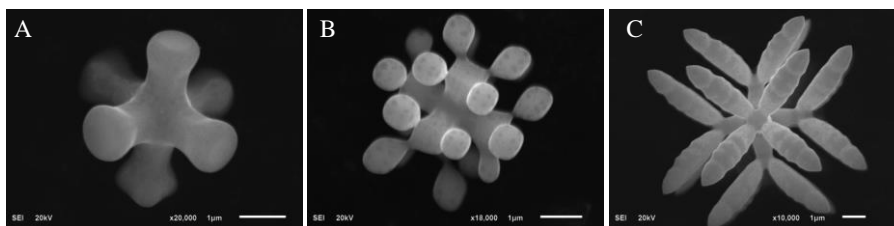
Figure 3.7 SEM micrographs show structural evolution of 6x4pAgCl from octahedral seeds in Cl⁻-rich environment. Initially, the short cubic pods in Figure 3.7A grew out from the six square tips of the octahedral seed. However, in Cl⁻-rich environment, the growth along <111> directions was predominantly promoted [108, 109]. As a result of the constraint imposed by the growth environment, four pods grew out of the {111} corners of each pods. The twenty four short pods in Figure 3.7B then further grew in the Cl⁻-rich environment. Finally, 6x4pAgCl was obtained when an octahedral seed was growth in a Cl⁻-rich environment (Figure 3.7C). The scale bars are 1 µm [48].
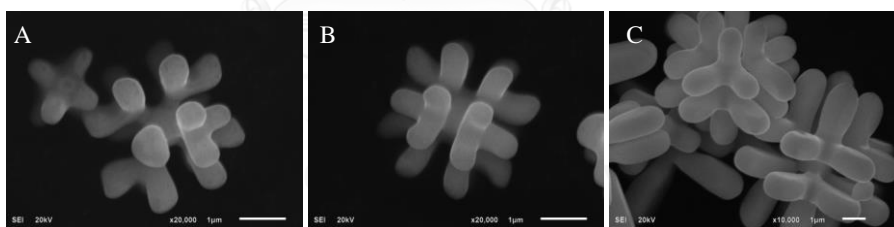
Figure 3.8 SEM micrographs show structural evolution of 8x3pAgCl from cubic seed in NH₄OH-rich environment. In contrast to those in Figure 3.7, the short pods in Figure 3.8A grew out from the eight triangular tips of the cubic seed. However, in an NH₄OH-rich environment, the growth along <100> directions was promoted. Three square pods grew out of the tip of the eight short pods (Figures 3.8A–3.8B). The twenty four square pods the further grow along <100> directions in the growth environment with high concentration of NH₄OH (Figure 3.8C). The scale bars are 1 µm [48].

The 8pAgCl grew out of cubic seeds while the 6pAgCl and octahedrons grew out of octahedral seeds (Figures 3.9, 3.10, and 3.11). The nucleation and growth of 3D AgCl microstructures are rapid as they are completed within 5 min. The square pods in 6pAgCl symmetrically grew out in the <100> directions of the tips of octahedral seeds. According to the crystallographic facets, the development of triangular groove corroborates that the six pods of 6pAgCl grew out of the tips of the octahedral seeds not from the face of the cubic seeds. Their square pods developed into 4-blade arrowhead pods. The rapid growth at high NH_4OH concentration connected the orthogonal blades on adjacent pods and the structure was transformed into concave octahedrons and octahedrons, respectively, as shown in Figures 3.9E–3.9F.

The XRD patterns of 3D AgCl microstructures in Figure 3.12 show characteristic diffraction peaks of (111), (200), (220), (311) and (222) planes indexed to the fcc structure of AgCl (JCPDS No. 85-1355). All diffractions except that of octahedrons showed a more intense (200) peak compared to (111) peak as the structures were dominated by the {100} facets. As the octahedrons are encased by {111} facets, the (111) peak is more pronounced with the intensity ratio of peak (111) to that of (200) greater than 1.
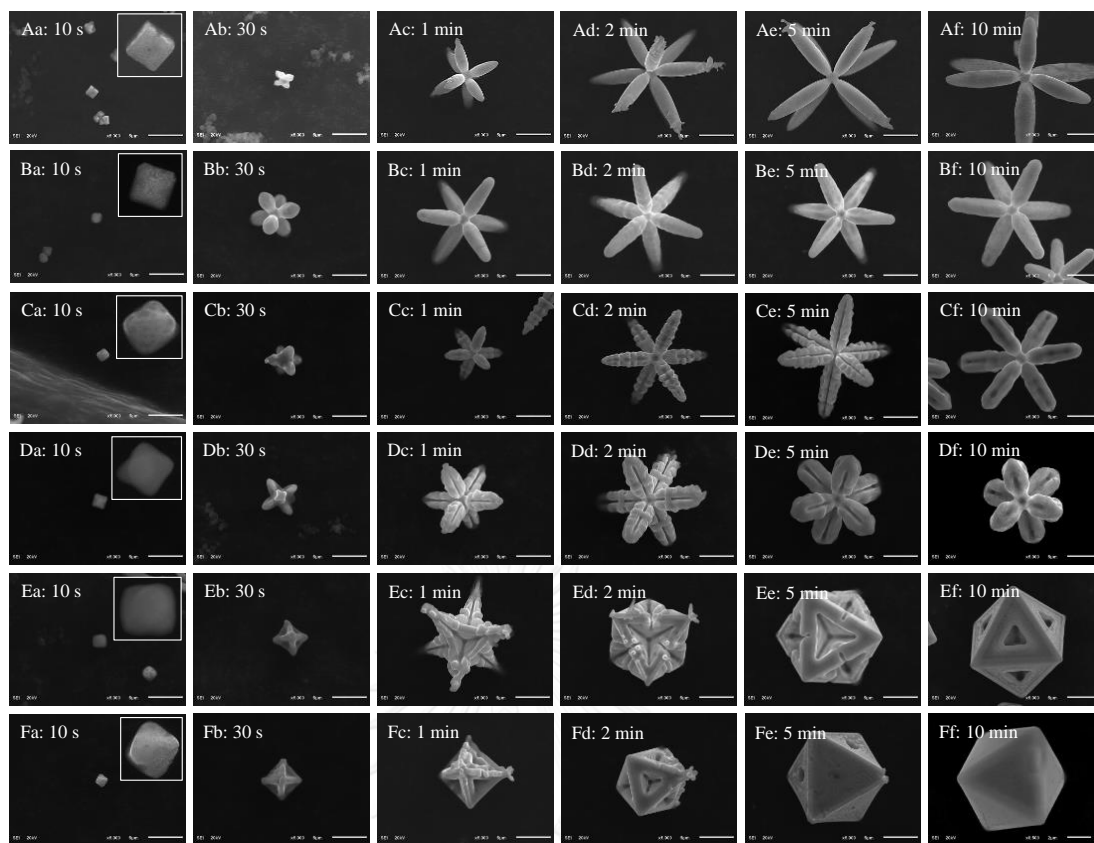
Figure 3.9 Time dependent structural evolution of (A) 8pAgCl, (B) 6pAgCl, (C and D) 6pAgCl with 4-blade arrowhead, (E) caged octahedron, and (F) octahedron. The structures fully developed within 5 min. The scale bars are 5 µm [48].
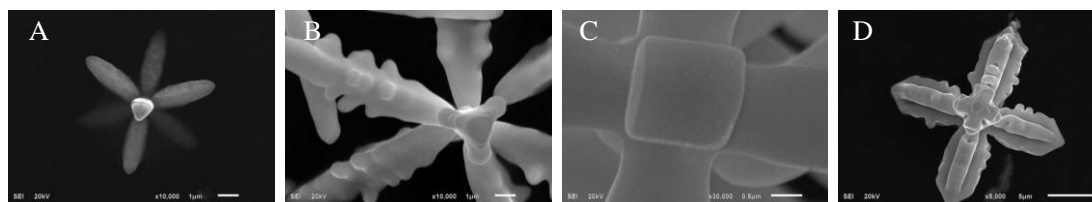
Figure 3.10 High magnification SEM micrographs of pods in selected 3D AgCl microstructures: (A) triangular pods of 8pAgCl, (B) triangular fishbone of 8pAgCl with fishbone pods, (C) square pods of 6pAgCl, and (D) square pods of 6pAgCl with 4-blade arrowhead pods [48].
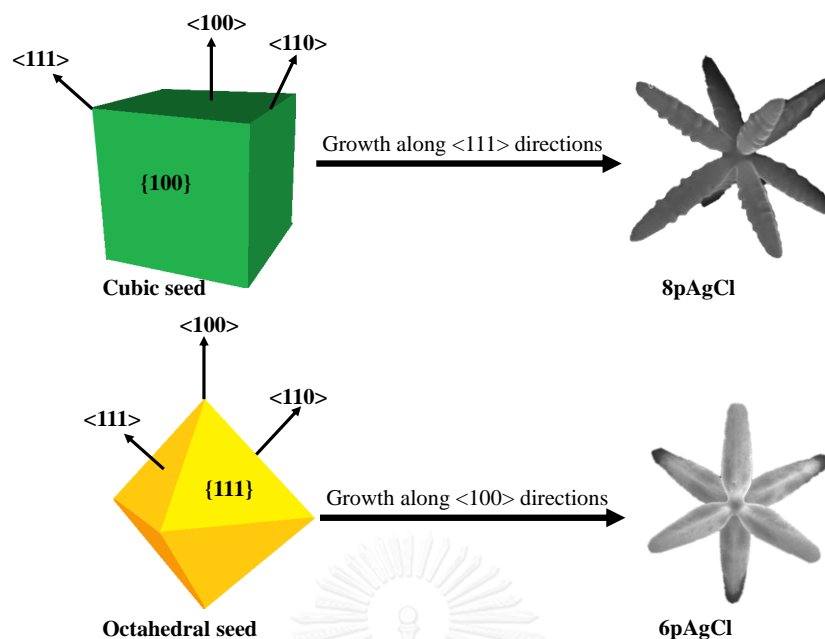
Figure 3.11 Schematic drawing shows facets and growth directions of 3D AgCl microstructures from cubic and octahedral seeds [34, 111]. The cubic seed consists of six {100} facets, eight {111} corners and twelve {110} edges. The octahedral seed consists of eight {111} facets, six {100} corners and twelve {110} edges. The 8pAgCl develops from cubic seed *via* a preferential growth along <111> directions in the Cl^--rich environment. On the other hand, the 6pAgCl develops from octahedral seed *via* a preferential growth along <100> directions in the NH_4OH-rich environment [48].

In Figures 3.9 and 3.10, the triangular pod in 8pAgCl is originated by the <111> growth out of the triangular tips of a cube in the Cl^--rich environment. The formation of fishbone triangular pod in 8pAgCl is the result of the competitive <111> growth along the pot length at a relatively high concentration of Cl^-. Similarly, the formation of square pod in 6pAgCl is the result of the <100> growth out of the square tip of an octahedron in NH_4OH-

rich environment. The square pods with 4-blade arrowhead in 6pAgCl were formed at a relatively high NH$_4$OH concentration. The thick square pods is due to a rapid growth in <100> directions along the pod length at an extremely high NH$_4$OH concentration.
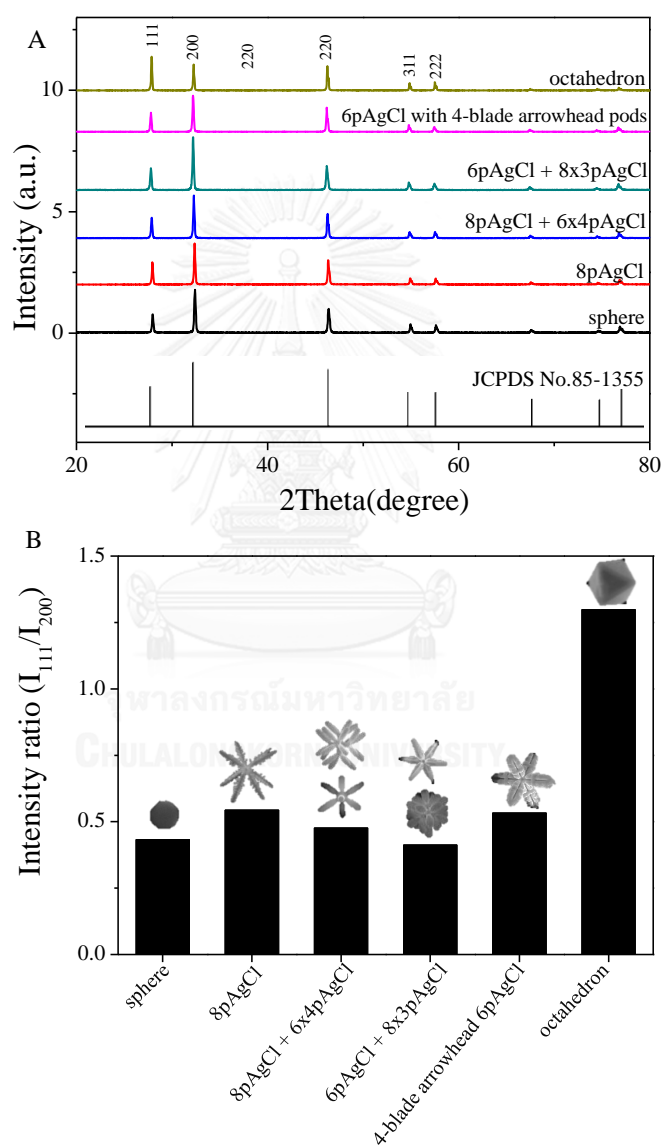
Figure 3.12 (A) XRD patterns of precipitated 3D AgCl microstructures. (B) The plot of intensity ratios of (111) and (200) peaks. The XRD patterns confirm that all precipitates are pure AgCl [48].
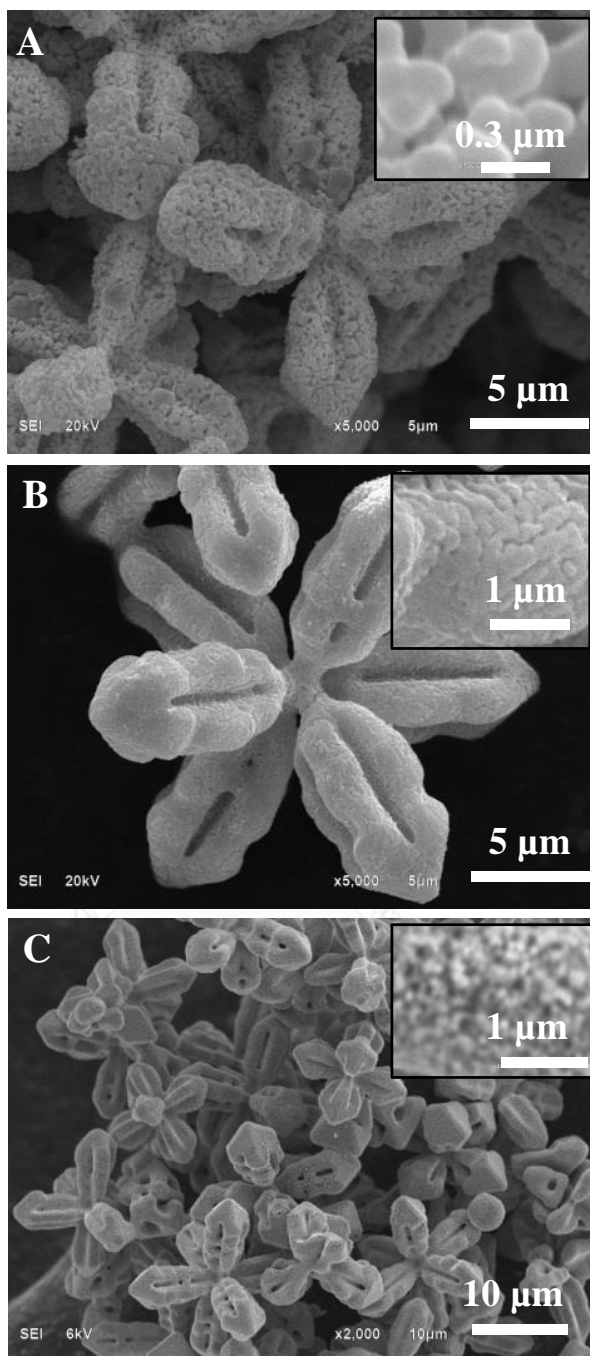
Figure 3.13 (A) Nanoporous silver microstructures derived from the 6pAgCl with 4-blade arrowhead pods using 0.5 M L-AA as the reducing agent. AgNP film on AgCl prepared by (B) a partial reduction with 0.2 M L-AA (flash reduction) and (C) an electron beam bombardment in SEM sample chamber [48].
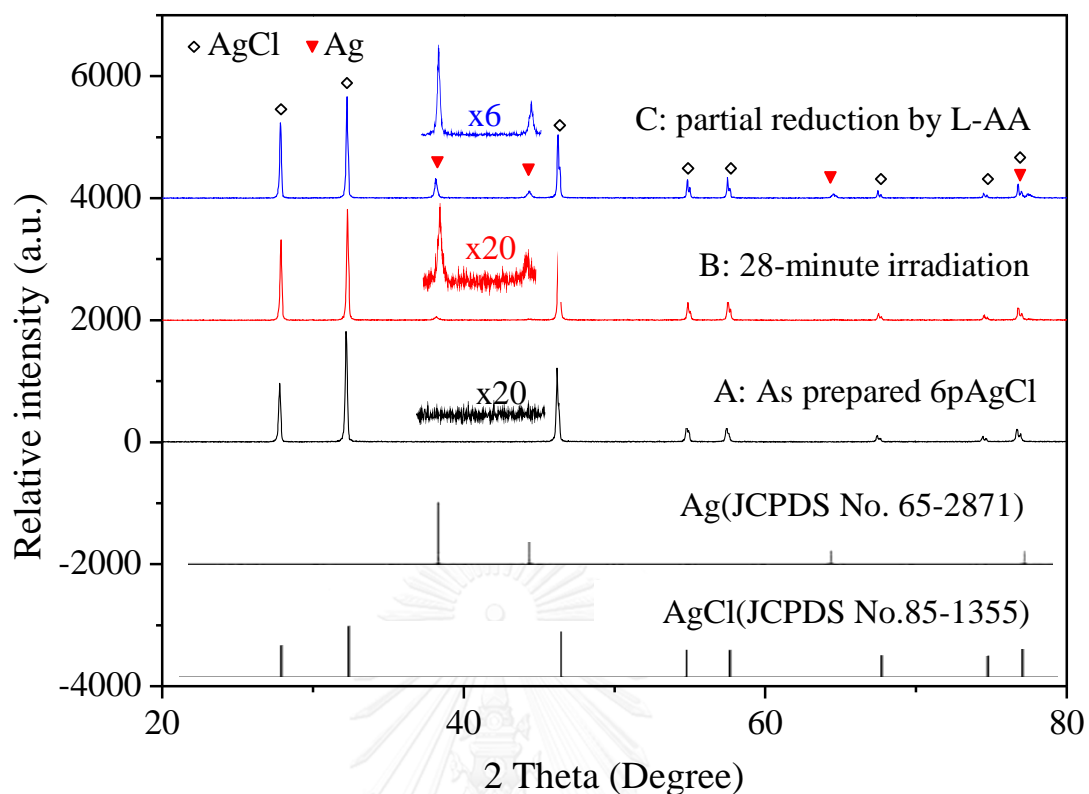
Figure 3.14 XRD patterns of (A) as synthesized 6pAgCl with 4-blade arrowhead pods, (B) after a 28-minute irradiation, and (C) after a partial reduction by L-ascorbic acid (L-AA). The standard XRD patterns of Ag and AgCl were added for comparison [48].

To explore their potential application, the morphologically-controlled 3D AgCl microstructures were converted to porous silver microstructure and silver nanoparticle-decorated AgCl microstructures. The porous silver microstructures were prepared by a chemical reduction of 6pAgCl with 4-blade arrowhead using 0.5 M L-ascorbic acid (L-AA). The size and shape of the grey nanoporous silver microstructures are the same as those of original AgCl (Figure 3.13A). However, when the AgCl microstructures were briefly treated with a diluted L-AA solution (0.2 M), only surface AgCl was reduced into

silver nanoparticle (AgNP) thin film covering the AgCl microstructures (Figures 3.13B and 3.14) which has a dark brown color. When the AgCl microcrystals were reduced *via* an electron beam bombardment, domains of large AgNPs developed (Figures 3.13C and 3.14). The photocatalytic activities of the synthesized 3D AgCl microstructures were also experimentally compared with that of dendritic silver microstructure synthesized by a previously report technique [101].
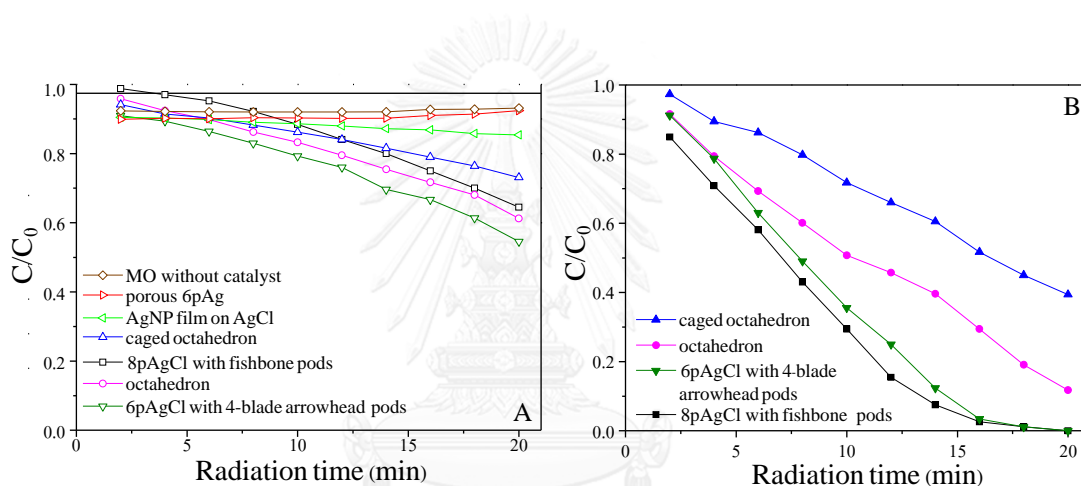
Figure 3.15 Catalytic decomposition profiles of MO under the visible light irradiation using (A) freshly prepared 3D AgCl microstructures and (B) Ag@AgCl microstructures as photocatalysts. The photocatalysts included dendritic Ag, nanoporous 6pAg microstructures, AgNP film on 6pAgCl, 8pAgCl with fishbone pods, 6pAgCl with 4-blade arrowhead pods, caged octahedral, and octahedral AgCl [48].

The transformation to nanoporous silver microstructures indicates that the 3D AgCl microstructures can be employed as a building block for the fabrication of complex micro/nanostructures unachievable *via* a conventional

means [114, 115]. The obtained porous silver microstructures could be further employed as a template for surface modifications as well as porous catalysts [116-120].

The decomposition of methyl orange (MO) under the visible-light-induced photocatalytic activity of 3D AgCl microstructures was investigated. As shown in Figure 3.15A, the porous 6pAgCl and AgNP film on AgCl did not exhibit photocatalytic activity. Freshly prepared 3D AgCl microstructures of 8pAgCl with fishbone, 6pAgCl with 4-blade arrowhead, concave octahedrons, and octahedrons expressed moderate photocatalytic activity as 20–40% drop of MO concentration was achieved after a 20-min irradiation. The pre-exposed AgCl microstructures were excellent photocatalysts as 8pAgCl and 6pAgCl induced a completed decomposition after a 20-min irradiation as shown in Figure 3.15B. The increased catalytic activity was due to the formation of isolated AgNPs as indicated by SEM micrographs and XRD patterns shown in Figures 3.14 and 3.16 [96, 108, 109]. The increasing of catalytic activities of Ag@AgCl microstructures was due to the ultrafast plasmon-induced electron transfer processes [97-99, 101, 103, 104, 107, 121-123]. The oscillating dipole on isolated AgNPs enable an oxidation of MO anchored to the surface of AgNPs as surface plasmon resonance (SPR) of AgNPs upon a visible-light irradiation triggers an electron transfer from AgNPs to AgCl. The photocatalytic effect exploits the ultrafast plasmon-induced electron transfer from AgNPs to AgCl. A large numbers of isolated AgNPs become crucial for an efficient photocatalytic activity. As the frequency of the oscillating dipole is unique to the nano-size silver particles, the bulk-like AgNP film and porous

silver microstructure do not show a photocatalytic activity since they do not exhibit SPR in the visible region.
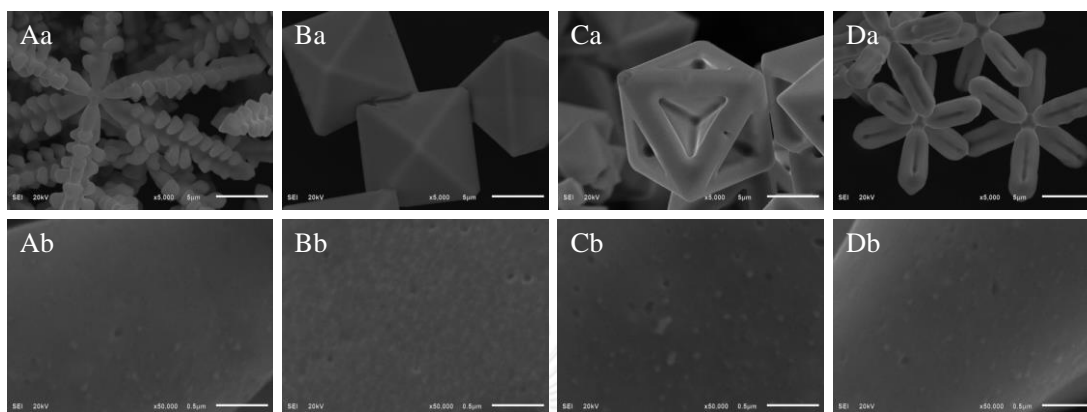
Figure 3.16 Low magnification and high magnification SEM micrographs of 3D AgCl microstructures after the 20-min irradiation by a xenon arc lamp: (A) 8pAgCl with triangular fishbone pods, (B) octahedron, (C) caged octahedron, and (D) 6pAgCl with 4-blade arrowhead pods. The high magnification SEM micrographs reveal isolated silver nanoparticles (AgNPs) on AgCl surface after the irradiation. The SEM results agree with the visual observation as the white precipitates turned black after the 20-minute irradiation [48].

A repeating usage of the Ag@AgCl photocatalyst was explored and a 40% drop of the catalytic activities was observed after 10 test cycles, as shown in Figures 3.17 and 3.18 (note: the exposure time was kept at 28 min). The decreased catalytic efficiency was due to the formation and increasing of large AgNPs on the surface of Ag@AgCl photocatalyst upon repeated exposures (Figure 3.19). The EDX results confirm the increment of silver content as

Ag/Cl ratio was increasing from 1.05 (virgin) to 1.12 (1st exposure) and 1.32 (10th exposure), respectively, as shown in Figure 3.20 and Table 3.2. A slightly greater than unity of the ratio in the virgin AgCl microstructures is due to the decomposition of AgCl under the exposure of electron beam [114]. The formation of AgNPs was also confirmed by XRD characterization (Figure 3.14) as the characteristic peaks of the fcc silver crystal developed after the 1st exposure.
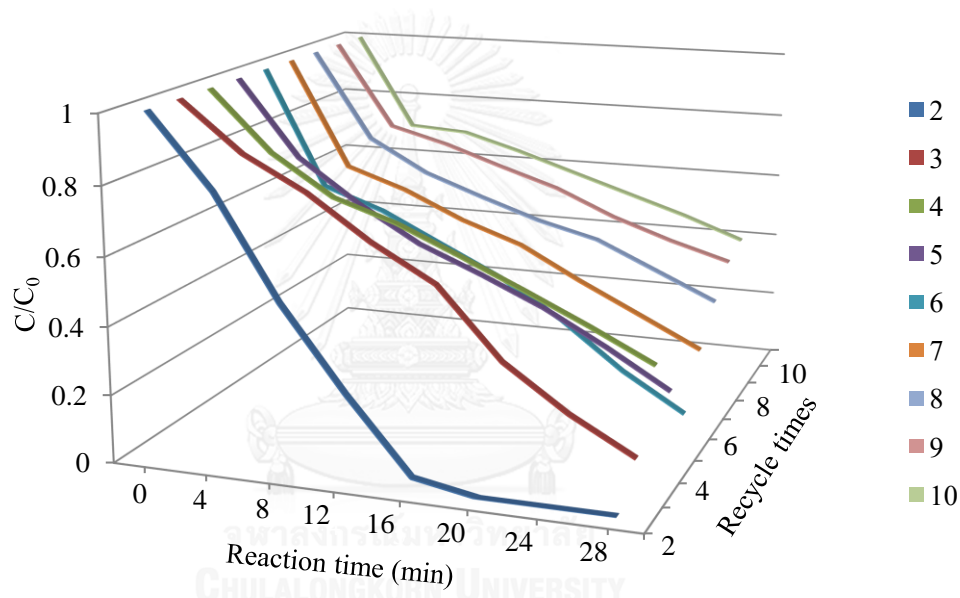
Figure 3.17 Degradation kinetics of methyl orange (MO) by 6pAgCl with 4-blade arrowhead pods under a visible-light irradiation. All 10-cyclic tests were conducted consecutively using the same catalyst. The catalyst was thoroughly cleaned with DI water before performing the next catalytic test. The experimental conditions (weight of catalyst, concentration and volume of analyte, and irradiation condition) are the same as those of Figure 3.15 [48].
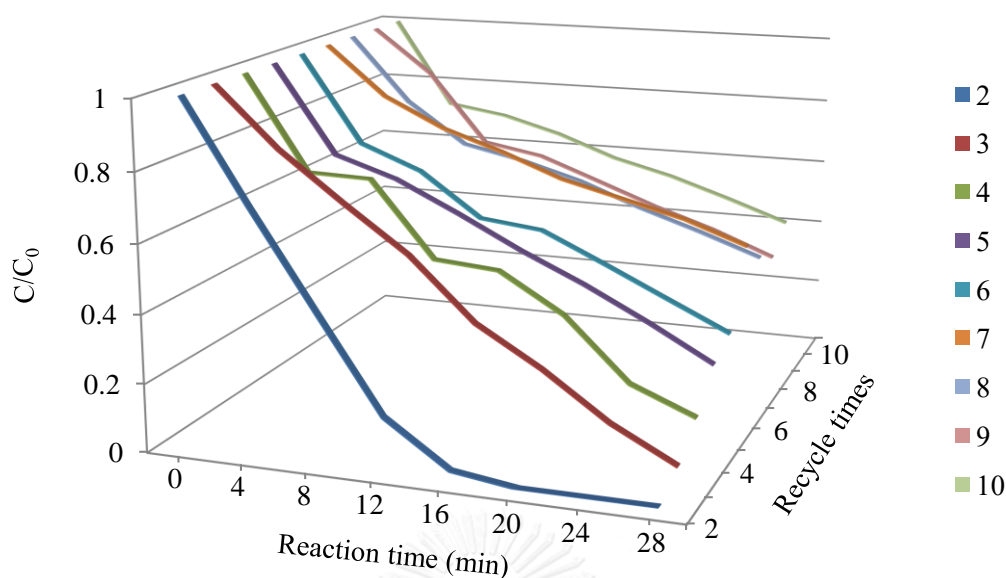
Figure 3.18 Degradation kinetics of methyl orange (MO) by 8pAgCl with triangular fishbone pods under a visible-light irradiation. All 10-cyclic tests were conducted consecutively using the same catalyst. The catalyst was thoroughly cleaned with DI water before performing the next catalytic test. The experimental conditions (weight of catalyst, concentration and volume of analyte, and irradiation condition) are the same as those of Figure 3.15 [48].

Surprisingly, the 6pAgCl with 4-blade arrowhead pods was very stable as an insignificant structural change was not observed after the 10th test cycle (Figure 3.19). Moreover, a structural break down due to agitation was not observed. However, in the case of 8pAgCl with fishbone pods, the structure broke down after a 10-cycle photocatalytic test. The pods broke down at the joint into rod-like structures as the fishbone feature transformed into AgNPs upon irradiation.

6pAgCl with 4-blade arrowhead pods
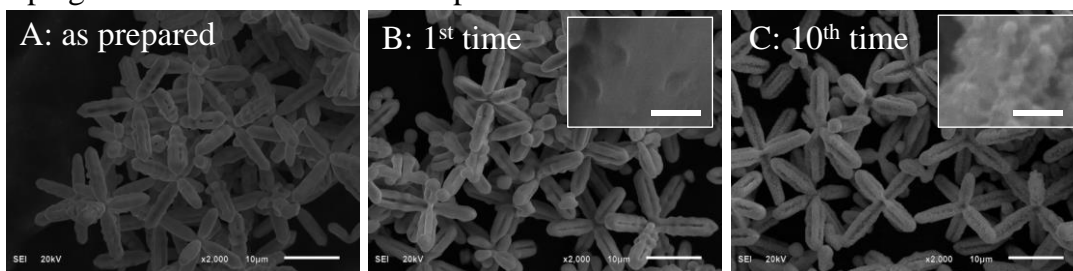
8pAgCl with triangular fishbone pods
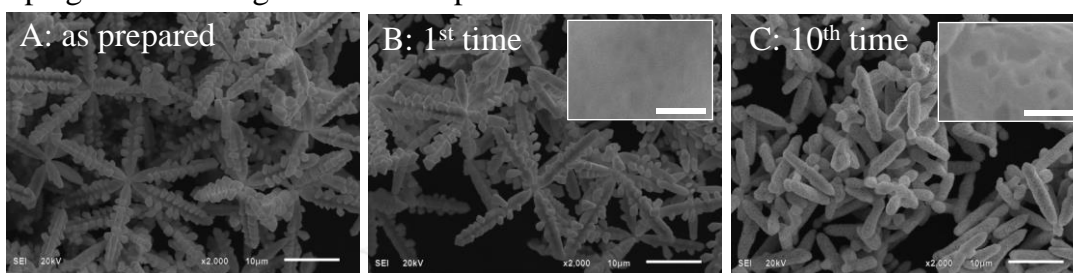
Figure 3.19 SEM micrographs show structural change of catalyst: (A) virgin, (B) after the 1st test cycle, and (C) after the 10th test cycle. The scale bars are 10 µm and 0.5 µm (insert) [48].

The 6pAgCl with 4-blade arrowhead pods and 8pAgCl with fishbone pods were also excellent photocatalyst for methylene blue (MB) degradation as they can decompose more than 95% of the original concentration within a 28-min irradiation (Figures 3.21 and 3.22).
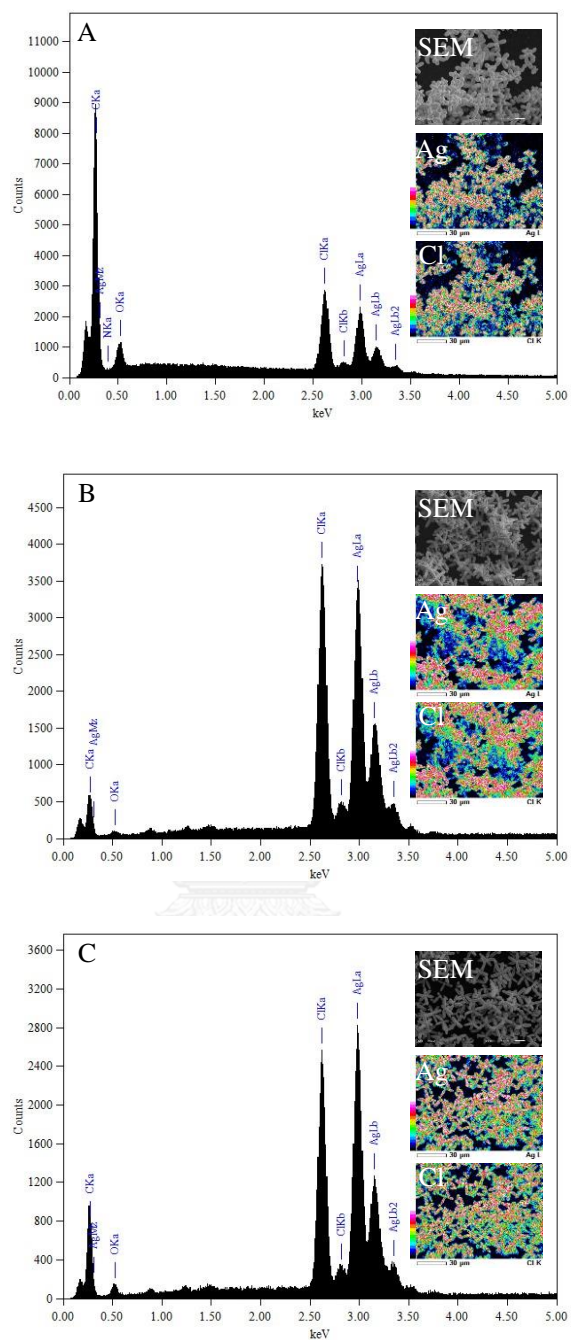
Figure 3.20 EDS spectra and EDS maps of 6pAgCl with 4-blade arrowhead pods (A) virgin (B) after the 1st and (C) after the 10th cycle photocatalytic decomposition of MO. The elemental contents of Ag and Cl were further employed for the calculation of Ag/Cl ratio (shown in Table 3.2) [48].
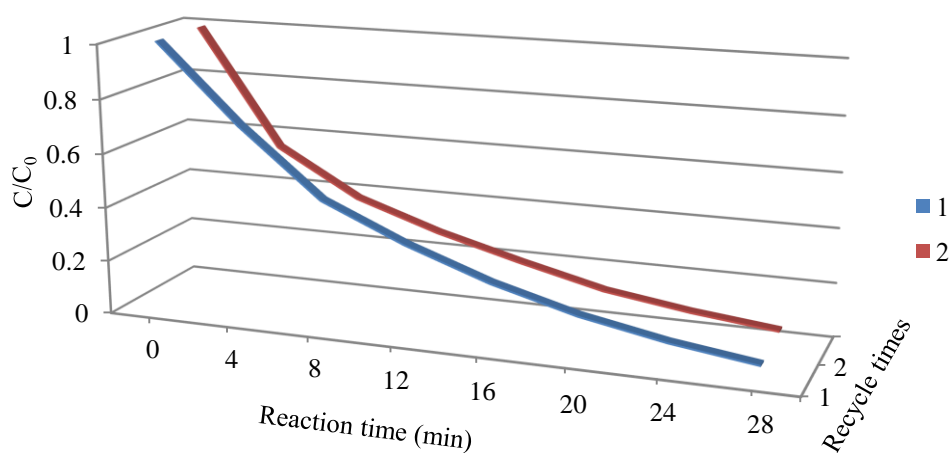
Figure 3.21 Degradation kinetics of 10 mg/L methylene blue (MB) by 6pAgCl with 4-blade arrowhead pods under a visible-light irradiation. All cyclic tests were conducted consecutively using the same catalyst. The catalyst was thoroughly cleaned with DI water before performing the next catalytic test. The experimental conditions (weight of catalyst, volume of analyte, and irradiation condition) are the same as those of Figure 3.15 [48].

Table 3.2 Elemental composition (Ag and Cl) of 6pAgCl with 4-blade arrowhead pods measured by EDS technique [48].

Sample	Composition (%atom)		Ag : Cl
	Ag	Cl	
Virgin AgCl microstructure	51.27	48.73	1.05 : 1
After the 1st exposure	52.93	47.07	1.12 : 1
After the 10th exposure	56.84	43.16	1.32 : 1
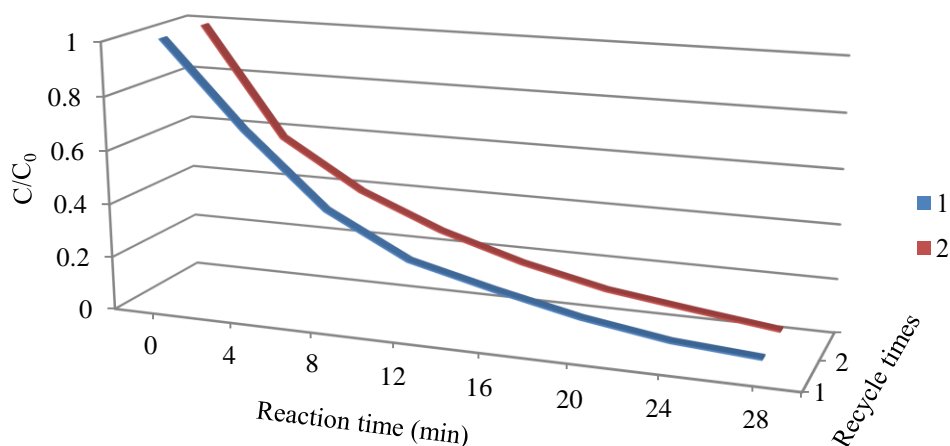
Figure 3.22 Degradation kinetics of 10 mg/L methylene blue (MB) by 8pAgCl with triangular fishbone pods under a visible-light irradiation. All cyclic tests were conducted consecutively using the same catalyst. The catalyst was thoroughly cleaned with DI water before performing the next catalytic test. The experimental conditions (weight of catalyst, volume of analyte, and irradiation condition) are the same as those of Figure 3.15 [48].

3.4 CONCLUSION

We have successfully developed a simple, rapid, and template-free technique for a selective fabrication of structurally controlled 3D AgCl microstructures *via* a precipitation from $[Ag(NH_3)_2]^+$ by an addition of Cl^- where seed morphology and growth environment dictate the final microstructure. The eight-pod family (8pAgCl and 8pAgCl with fishbone pods) grew from the cubic seeds in Cl^--rich environment. The six-pod family (6pAgCl, 6pAgCl with 4-blade arrowhead pods, caged octahedral, and octahedral AgCl), on the other hand, grew from an octahedral seeds in an NH_4OH-rich environment. The 8x3pAgCl microstructures are obtained as the

cubic seeds grow in an NH$_4$OH-rich environment while the 6x4pAgCl microstructures are obtained when the octahedral seeds are grown in a Cl$^-$-rich environment. The 3D AgCl microstructures can be employed as a building block for the fabrication of novel structures such as nanoporous silver microstructures with controllable pore size. The precipitated 3D AgCl microstructures became an efficient Ag@AgCl visible-light photocatalyst by a partial photo-reduction of the surface AgCl into isolated AgNPs.

CHAPTER IV

3D NANOPOROUS Ag MICROSTRUCTURES FABRICATED FROM AgCl MICROCRYSTAL TEMPLATES *VIA* CONCERTED OXIDATIVE ETCHING/RE-DEPOSITION AND GALVANIC REPLACEMENT

4.1 INTRODUCTION

Porous noble metals have attracted extensive attention due to the interesting physical, chemical, and mechanical properties. These unique properties have led them to be used in a wide range of applications including porous electrodes [124, 125], actuators [126], catalysts [127-129], biosensors [130] and transport media [131]. In order to optimize the properties of porous noble metals for specific applications, it is crucial to control their pore size and grain size. In recent years, silver nanostructures such as nanowires [4, 5], nanoparticles [132-134], nanocubes [34] and nanoplates [6-8, 58, 135, 136] have been synthesized and extensively studied because of their particular antimicrobial, catalytic, and optical properties. However, nanoporous silver has attracted only scant attention due to its relatively large characteristic ligament size [137].

Various methods have been developed to fabricate 1D and 2D porous silver. Dealloying method is the most popular one since it can control pore and grain particle sizes. For example, to fabricate nanoporous silver powder, single-phase binary alloys

such as Ag-Al [137, 138], Ag-Fe [139], Ag-Ni [139] and Zn-Ag [140] were treated using diluted acid solutions *e.g.,* H_2SO_4, H_3PO_4, and HCl to selectively dissolve other metals. Then, Ag metal was remained with porous structures. Nevertheless, the grain size of nanoporous silver is still large (approximately 100–500 nm). As well as the dealloying method, using soft sacrificial template such as poly(ethyleneimine) hydrogel also provided the large grain particles [141]. The spray dry pyrolysis of silver salt such as Ag_2CO_3 [142] and $AgNO_3$ [143] at high temperature (300 °C and 700 °C, respectively) was also applied to synthesize porous silver. Moreover, electrochemical deposition technique [144-147] was widely used for fabrication of this material. However, the complex 3D structure of nanoporous silver is rarely fabricated. From our previous study, the 3D nanoporous silver microstructures (np-AgMSs) was employed as a surface-enhanced Raman scattering (SERS) substrate and it provided highly enhanced Raman signal with exceptional stability [148].

Here, we introduce a simple, rapid, and stabilizer-free synthetic protocol of 3D np-AgMSs *via* galvanic replacement approach using AgCl microcrystal as templates. The formation mechanism of np-AgMSs under a Cl^--rich environment is revealed. This work not only proposes a method to fabricate np-AgMSs, but also provides an in-depth understanding on the crystal growth mechanisms and how to manipulate them efficiently. Moreover, we also demonstrate the potential application of np-AgMSs as a catalyst for the reduction of *p*-nitrophenol with high efficiency.

4.2 EXPERIMENTAL SECTION

4.2.1 Chemicals

Silver nitrate ($AgNO_3$, purity $\geq 99.8\%$), sodium chloride (NaCl, purity $\geq 99\%$), ammonium hydroxide solution (NH_4OH, 25%w/w), sodium borohydride

($NaBH_4$, purity $\geq 98\%$), sodium nitrate ($NaNO_3$, purity $\geq 99\%$), and sodium sulfate (Na_2SO_4, purity $\geq 99\%$) were purchased from Merck[®]. L-ascorbic acid ($C_6H_8O_6$, purity $\geq 99\%$) was purchased from Sigma-Aldrich Co., Ltd. All chemicals were used as received without further purification. Zinc, lead, tin, copper, and aluminum foil with 0.2 mm thickness are the commercial available grade. Prior to use, all glassware and magnetic bars were thoroughly cleaned with detergent, rinsed with DI water, rinsed with 6 M nitric acid, and thoroughly rinsed again with DI water.

4.2.2 Synthesis of hexapod AgCl (6pAgCl) microcrystals as a template

The 6pAgCl microcrystals were synthesized using our previous protocol [48]. Briefly, $AgNO_3$ solution (0.1 M, 5.0 mL) was mixed with NH_4OH solution (5.3 M, 4.7 mL) to form silver ammine complex ($[Ag(NH_3)_2]^+$). To induce the formation of 6pAgCl microcrystals, the complex solution was quickly poured into a NaCl solution (1.1 M, 90.3 mL). The 6pAgCl microcrystals were instantaneously precipitated. Then, the mixture was further stirred for 5 minutes to ensure that the formation of 6pAgCl microcrystals was completed. The precipitate was washed with DI water for 5 times and once with ethanol before drying under dark ambient conditions before performing the galvanic replacement with sacrificial metals.

4.2.3 Galvanic replacement of 6pAgCl microcrystals with sacrificial metals

The 6pAgCl microcrystals were used as a template while various sacrificial metals (Sn, Pb, Cu, Al and Zn), whose standard reduction potentials are lower than Ag^+, were used as an electron supplier for galvanic replacement reaction. The sacrificial metals with 0.2 cm thickness were cut to 2×2 cm^2, and then rinsed with 0.1 M HNO_3, water, and ethanol before using. The 6pAgCl was placed on a

sacrificial metal plate in a 50 mL of 0.5 M NaCl solution. The galvanic replacement instantaneously occurred while the color of solid 6pAgCl microcrystals turned from white into dark grey indicating the formation of metallic silver. When the reaction was completed (no white solid observed), the obtained solid was filtered, washed with DI water for 3 times, with 0.1 M NH_4OH for 1 time (in order to remove residual AgCl), and with DI water for 3 times. The samples were dried in vacuum chamber for 1 hour before further investigation.

4.2.4 Characterization

Morphology (size and shape) of the porous silver was recorded by a scanning electron microscope (SEM, JEOL JSM-6510A) operating at 20 kV under a high vacuum mode with a secondary electron image (SEI) detector. A built-in energy-dispersive X-ray spectroscopy (EDS) was employed for monitoring elemental compositions of np-AgMSs. The X-ray diffraction (XRD) patterns were collected by an X-ray diffractometer (Rigaku D/MAX-2200) operated at room temperature with a scanning rate of 0.02 deg/min, using Cu K_α irradiation (40 kV, 30 mA) recorded in the 2θ range of 20–80 degrees.

4.2.5 Catalytic activity investigation

Various types of np-AgMSs (*i.e.,* nanoporous hexapods, nanoporous octapods, nanoporous octahedra, and microplates) were employed as a catalyst for the reduction of *p*-nitrophenol. The reaction progress was investigated using UV-visible spectroscopy (USB4000 fiber optic spectrometer coupled with a DH-2000 deuterium/halogen light source, Ocean Optics). A 1-mL of 0.2 mM *p*-nitrophenol was mixed with 1 mg of np-AgMSs. After that, 1 mL of 0.1 M $NaBH_4$ was rapidly injected into the mixtures. Then, time-dependent UV-visible spectra of the mixtures

were recorded every 1 minute for 15 minutes. A decrease in absorbance at 400 nm in UV-visible spectrum was analyzed as a degree of reduction.

4.3 RESULTS AND DISCUSSION

Figure 4.1 shows the SEM micrographs of 6pAgCl microcrystals before and after the galvanic replacement using Zn as a sacrificial metal in 0.5 M NaCl. The galvanic replacement reaction is shown in Equation 4.1. The developing of nanoporous hexapod silver microstructures (np-6pAgMSs) was easily monitored by following a change in a sample color from white to dark grey. From Figures 4.1A1 and 4.1B1, the same morphology of microstructures can be noticed. It means that np-6pAgMSs can retain the hexapod morphology of 6pAgCl microcrystals after the galvanic replacement. It further implies that the galvanic replacement does not affect the morphology of microcrystals during a process. The rougher surface with a grain structure can also be observed after the galvanic replacement, as shown in Figures 4.1A2 and 4.1B2. They suggest that 6pAgCl microcrystals are completely converted to np-6pAgMSs [115].

$$2AgCl(s) + Zn(s) \longrightarrow 2Ag(s) + ZnCl_2(aq) \qquad ; E_{cell}^0 = 0.984 \text{ V} \qquad \text{(Eq. 4.1)}$$
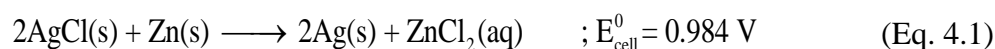
Table 4.1 shows the fastest completion time of galvanic replacement reaction. The completion time increases in the order of $t_{Al} < t_{Sn} < t_{Cu} < t_{Pb}$, respectively. However, this trend cannot be explained by according to the standard reduction potentials of the metals ($E_{Cu}^0 > E_{Pb}^0 > E_{Sn}^0 > E_{Zn}^0 > E_{Al}^0$). Under a Cl$^-$-rich environment, the galvanic reactions using Cu and Pb as a sacrificial metal are not complete, even the reactions are prolonged for 5 hours. It is because of the formation of water-insoluble salts of PbCl$_2$ and CuCl on the metal surface. The salts passivate the surface and prohibit an
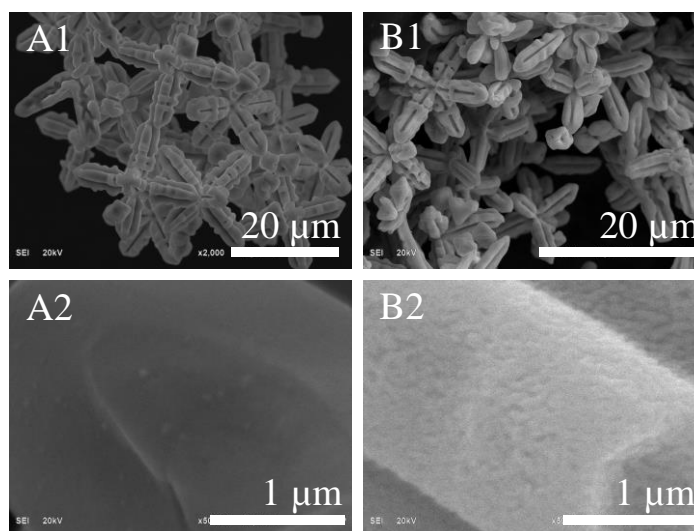
Figure 4.1 SEM micrographs of (A1) 6pAgCl microcrystals, (A2) 6pAgCl surface at high magnification, (B1) np-6pAgMSs and (B2) np-6pAgMSs surface with the porous structure at high magnification.

Table 4.1 Summary of np-6pAgMSs galvanized using different sacrificial metals.

Properties	Sacrificial metals				
	Sn	Cu	Pb	Al	Zn
Completion time (min)	150	N/A*	N/A*	120	10
Structural retaining (%)	partial	partial	partial	100	100
Average grain size (nm)	244.09 ± 68.56	321.45 ± 99.40	165.74 ±47.97	321.91 ±129.0	86.89 ±16.69
%Ag atom	99.83	99.79	100	100	100

*N/A: not completed in 5 hours

efficient electron transfer necessary for the galvanic replacement. When Al was employed as a sacrificial metal, the formation of highly stable and inert Al_2O_3 on the Al surface retarded the reaction. Only Zn and Al give a completed galvanic replacement with the perfect morphology retaining of 6pAgCl microcrystal template. It is because they did not form the water-insoluble salts and the reaction was fast enough to avoid the recrystallization and dissolution of AgCl.

The purity of np-6pAgMSs was investigated using XRD and EDS techniques. From Figure 4.2A, the original 6pAgCl microcrystals show the XRD pattern corresponding to a standard AgCl pattern (JCPDS No.85-1355) without any impurity peak. After the galvanic replacement using a sacrificial Zn metal, the XRD pattern of obtained np-6pAgMSs is in good agreement with a standard Ag pattern (JCPDS No. 65-2871) as well. The elemental maps which represent the distribution of atom in the sample show that 6pAgCl microcrystals have the Ag/Cl atomic ratio of 1:1 (Figure 4.3). After the galvanic replacement using Zn as a sacrificial metal, a high purity (>99.99%) of Ag was obtained, as shown in Figures 4.2B–4.2F. The EDS analyses of np-6pAgMSs developed by using other sacrificial metals show the high purities of >99.7 % (see Figure 4.4). The average grain size of the np-6pAgMSs is 86.89 ± 16.69, 165.74 ± 47.97, 244.09 ± 68.56, 321.45 ± 99.40 and 321.91 ± 129.0 nm when Zn, Pb, Sn, Cu and Al are employed as a sacrificial metal, respectively. A change in an average grain size is due to a difference in the galvanization rate of different metals (see completion time in Table 4.1). With a faster galvanization rate, the generation of Ag seeds is promoted and there is a shorter time for recrystallization. Therefore, small crystals were finally formed [115].
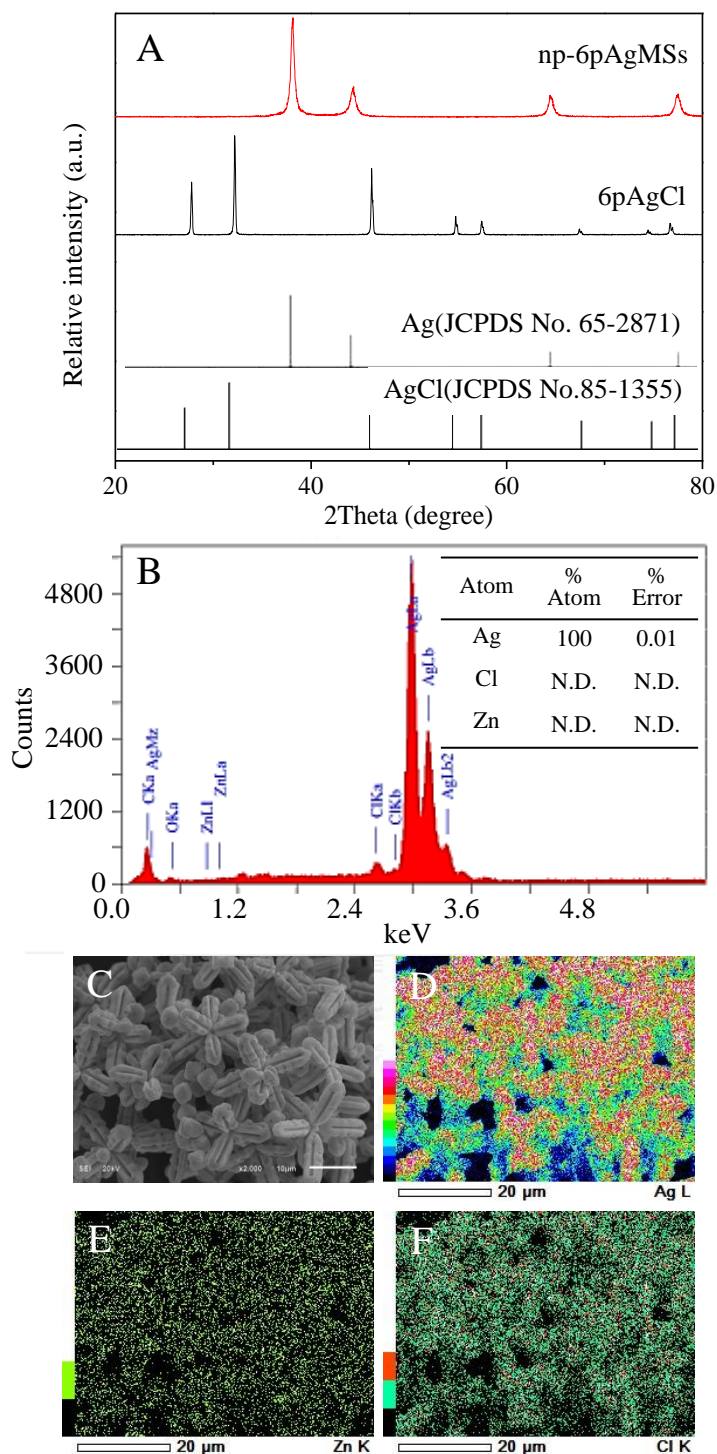
Figure 4.2 (A) XRD patterns of 6pAgCl microcrystals and np-6pAgMSs. (B) EDS spectrum of np-6pAgMSs galvanized using a sacrificial Zn metal in 0.5 M NaCl. (C) SEM micrograph and corresponding elemental maps representing the distribution of (D) Ag, (E) Zn and (F) Cl.

In this work, Zn is chosen as a sacrificial metal for further studies since it provides the shortest galvanization time, smallest average grain size, and the good template for retaining morphology.
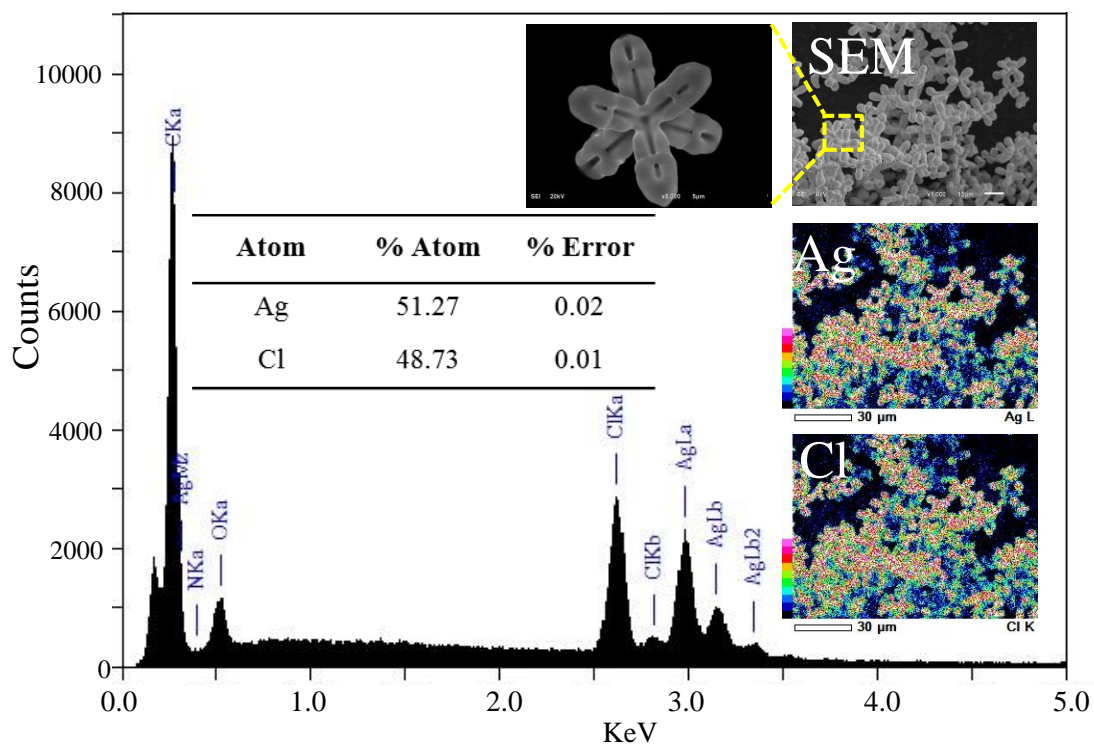
Figure 4.3 EDS spectrum and elemental maps of 6pAgCl microcrystals synthesized by the Cl$^-$-induced precipitation of $[Ag(NH_3)_2]^+$.
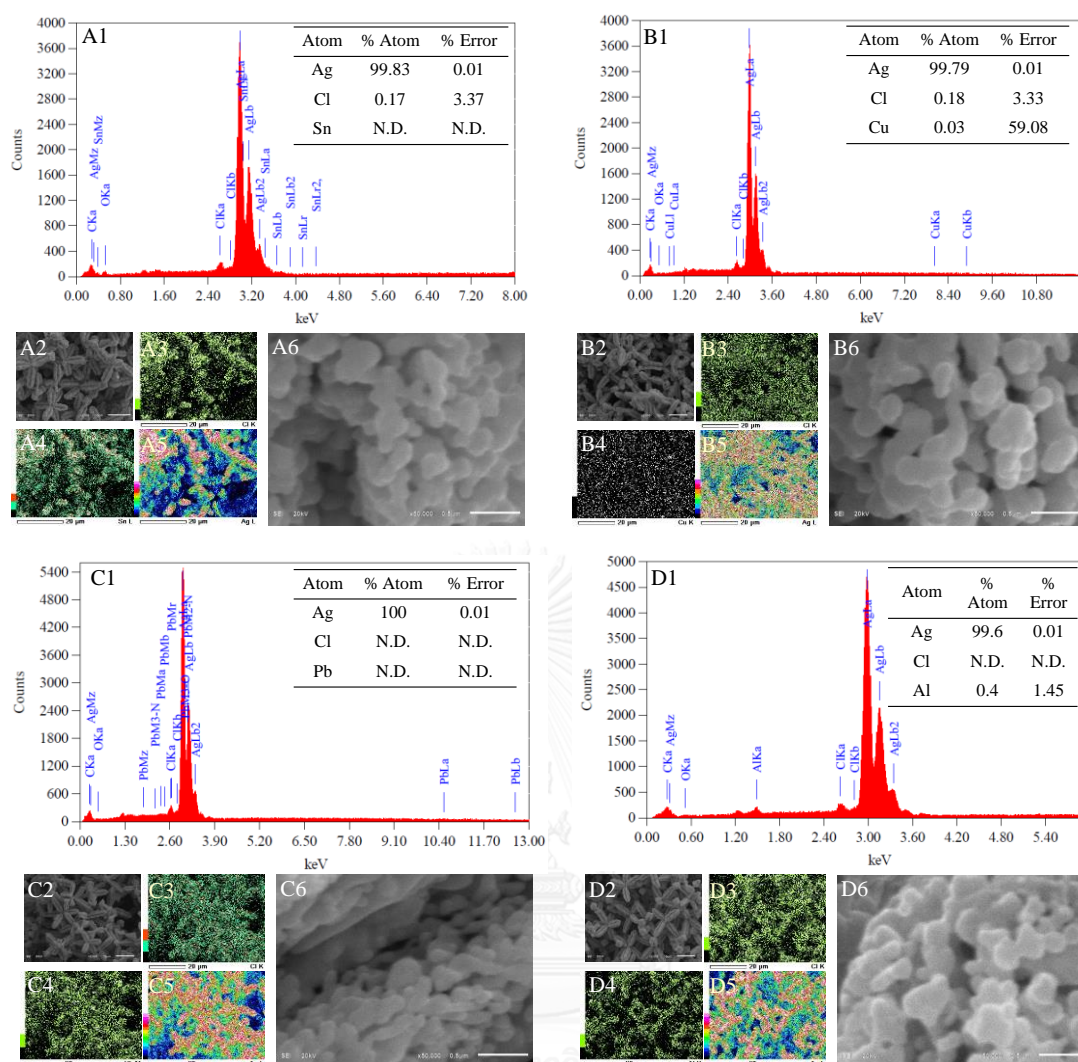
Figure 4.4 EDS spectra and elemental maps of np-6pAgMSs galvanized by (A) Sn, (B) Cu, (C) Pb and (D) Al in a solution of 0.5 M NaCl.

To investigate the effect of electrolyte concentration on the morphology of np-6pAgMSs, the concentration of NaCl was varied (0–2 M and saturated NaCl solution). The results show that all np-6pAgMSs can retain the template morphology in every NaCl concentration. However, the completion time decreases with an increase in NaCl concentration (35, 32, 20, 8, 6, 5 and 3 minutes for 0, 0.01, 0.1, 0.5, 1, 2 M and saturated NaCl solution, respectively). An increase in the galvanization

rate is due to faster oxidative etching of Zn by Cl⁻ [149-153], which generates electrons with a faster rate in higher Cl⁻ concentrations, as shown in Equation 4.2 [62]. In addition, the average grain size of np-6pAgMSs can be fine-tuned from 136.49 to 47.06 nm by increasing NaCl concentration, as shown in Figure 4.5. A decrease in an average grain size with an increase in Cl⁻ concentration can be explained by an increase in galvanization rate, as described above.

$$Zn(s) + 2Cl^-(aq) \longrightarrow ZnCl_2(aq) + 2e^-$$ (Eq. 4.2)
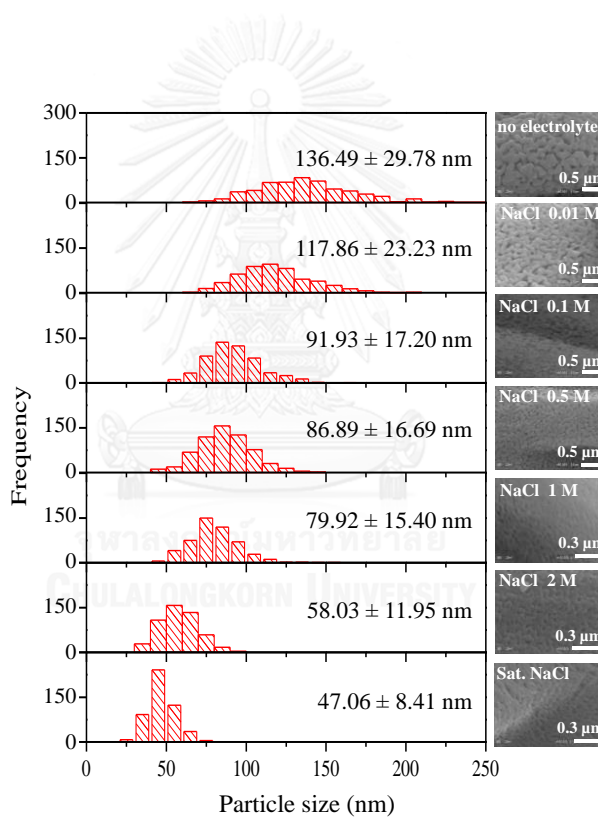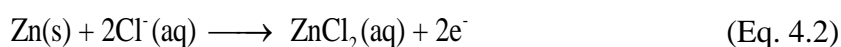
Figure 4.5 Average grain sizes of np-6pAgMSs galvanized using different concentrations of NaCl electrolyte (0−2 M and saturated solution).

We also observed a change in grain size along the distance from the surface of sacrificial metal. In NaCl solution, a systematic change of grain sizes is obvious. The grain size increases with an increase in a distance from the Zn surface, as shown in Figure 4.6A. On the other hand, in $NaNO_3$ solution, there is no significant change in grain size thorough np-6pAgMSs, as shown in Figure 4.6B. These results suggest that the re-deposition process of np-AgMSs should occur, which generates smaller grain particles. There are reports confirming that Cl^- [154, 155] and Cl^-/O_2 [2, 35-37, 47] can act as an etchant and O_2 (from air or dissolved O_2) is essential for the dissolution of Ag in the presence of Cl^- [2, 36]. Under a Cl^--rich environment, silver is etched and Ag^+ is liberated. During the galvanization process, Zn is continuously providing electrons. Simultaneously, the released Ag^+ accepts electrons and redeposits with a high deposition rate which Cl^- accelerates the etchant liberation of Zn. As a result, Ag has not enough time to recrystallize [115] and the small grain size is generated. The re-deposition process under an influence of Cl^- should be kinetically controlled due to the generation of smaller particle with higher surface area. However, the re-deposition process stops when AgCl is completely consumed. After the galvanization process is completed for 5 and 10 minutes, a further change was not observed (Figure 4.7). However, the growth of large Ag crystals can be observed after 3 days (Figures 4.7A4–4.7C4). It means that the re-deposition process still occurs but the rate is changed. This result suggests that the kinetically controlled growth mechanism becomes thermodynamically controlled process, after AgCl is completely depleted.

There are two possible mechanisms to create the np-AgMSs. The first mechanism is the electron transfer of sacrificial metal to reduce Ag^+ without any
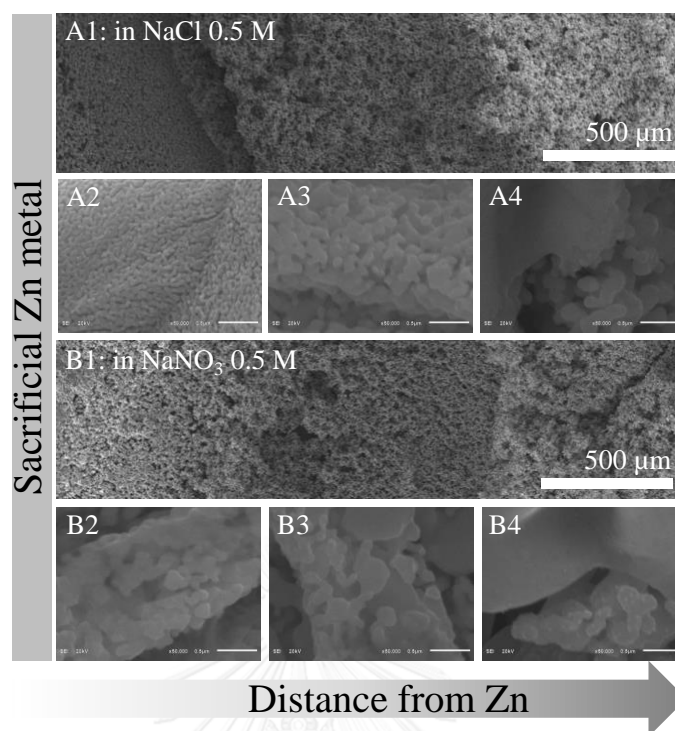
Figure 4.6 Grain particles of np-6pAgMSs at different positions away from the surface of sacrificial Zn metal using an electrolyte of (A) 0.5 M NaCl and (B) 0.5 M NaNO$_3$. The positions at 0, 1, and 2 mm away from the Zn surface are labeled by the number of 2, 3, and 4, respectively.

dislocation of Ag$^+$. In this process, Cl$^-$ is released from the AgCl microcrystal template, and then np-AgMSs is created. The second mechanism is the dissolution of silver ion species from AgCl microcrystal template. In this case, silver ion species move to receive electrons from sacrificial metal at the AgCl/metal interface and form the np-AgMSs. To verify the formation mechanism of np-AgMSs, the time-dependent SEM micrographs were captured from a AgCl microcrystal template galvanized by using Al as a sacrificial metal in water and a solution of 0.1 M NaCl, as shown in Figures 4.8A and 4.8B. The AgCl microtabular was fabricated *via* the evaporation of [Ag(NH$_3$)$_2$]$^+$Cl$^-$ under an ambient condition. The AgCl microtabulars were separated,
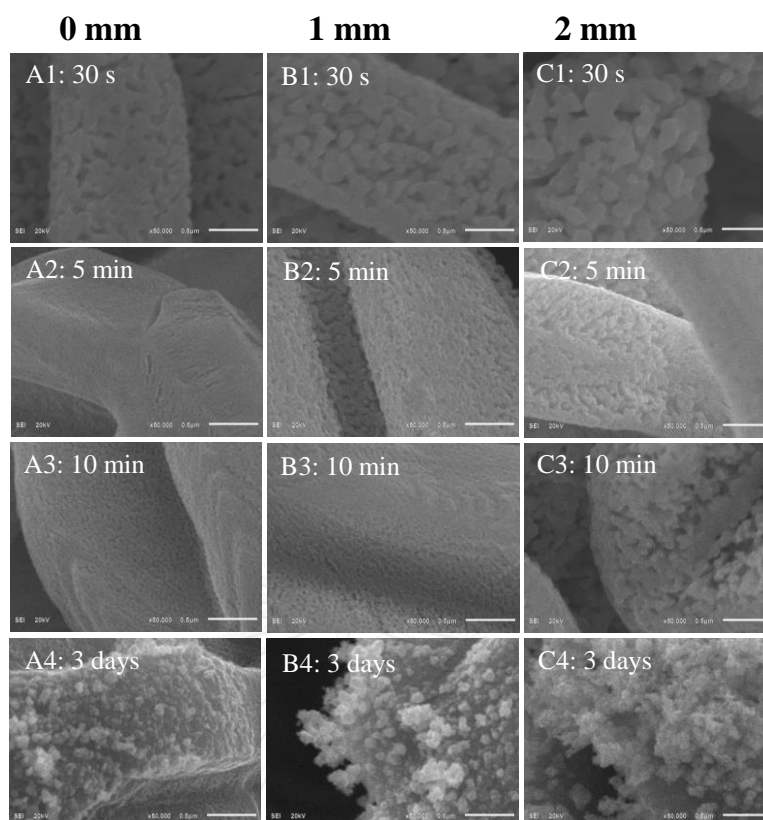
Figure 4.7 Morphological evolution of np-6pAgMSs at (A) 0, (B) 1, and (C) 2 mm away from the Zn surface. SEM micrographs were recorded at 30 seconds, 5 minutes, 10 minutes and 3 days after the starting of galvanization.

washed several time with DI water and dropped on carbon tape. Then, the AgCl microtabulars on carbon tape were attached on aluminum foil. Aluminum foil was employed as a sacrificial metal due to it provides a slower galvanization rate compared to Zn. It offers a clear observation on the morphological evolution. However, the galvanic replacement reaction was performed in a boiling solution to accelerate the reaction. DI water or 0.1 M NaCl was employed as media. The morphology of np-AgMSs was investigated at 1, 3 and 10 hours after the dipping of sample into a boiling solution. In water (see Figure 4.8A), AgCl was not completely
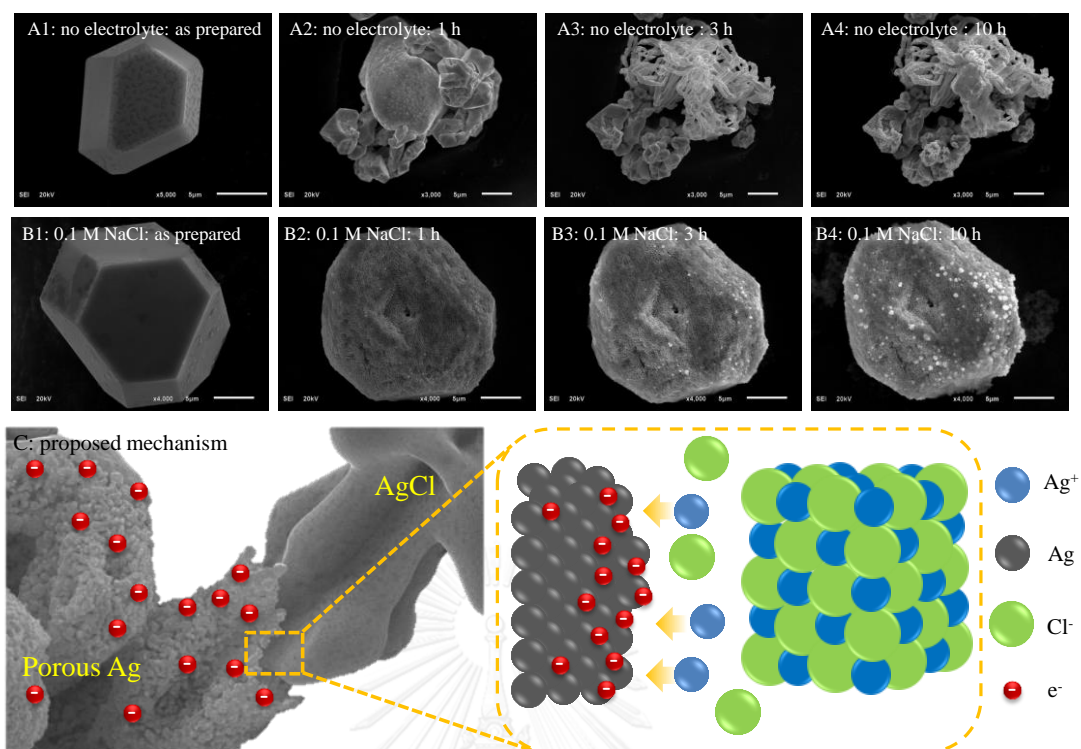
Figure 4.8 Conversion of AgCl into np-AgMSs (A) without and (B) with NaCl electrolyte using Al as a sacrificial metal. SEM micrographs were recorded at 1, 3 and 10 hours after the galvanization. (C) The proposed galvanization mechanism.

converted to porous silver within 1 hour. The AgCl microcrystal template was slowly galvanized and turned into silver microcrystals around the primary AgCl microcrystal template. The galvanization started from AgCl closed to the sacrificial Al metal then spread out to other parts of AgCl microcrystal template. With a high magnification of time-dependent SEM micrographs, the gaps between galvanized and non-galvanized AgCl can be observed (see Figure 4.9). This is a very strong evidence to conclude that the first mechanism should not be possible. It is because the gaps of several nanometers are too large for electron jumping from galvanized to non-galvanized AgCl. The second mechanism which a silver ion species moves and receives electrons

transferred from sacrificial metal at the AgCl/metal interface should be the correct mechanism. The microcrystals became bigger in size as a function of galvanization time. After 3 hours, all AgCl was completely transformed into metallic Ag and then Ag microcrystals were changed to small fibers (a re-deposition process to form smaller structures, as described above). After 10 hours, the morphology of Ag microstructures was not significantly changed, compared to that at 3 hours. In contrast, AgCl template was completely converted to np-AgMSs within 1 hour in a solution of 0.1 M NaCl. When the reaction was prolonged, the recrystallization process took place and larger Ag microcrystals developed, as shown in Figure 4.8B4. From these results, Cl$^-$ is an important factor to drive the recrystallization process. At very low concentration of Cl$^-$ (the galvanization in water), further recrystallization cannot undergo after the completion of galvanization process.
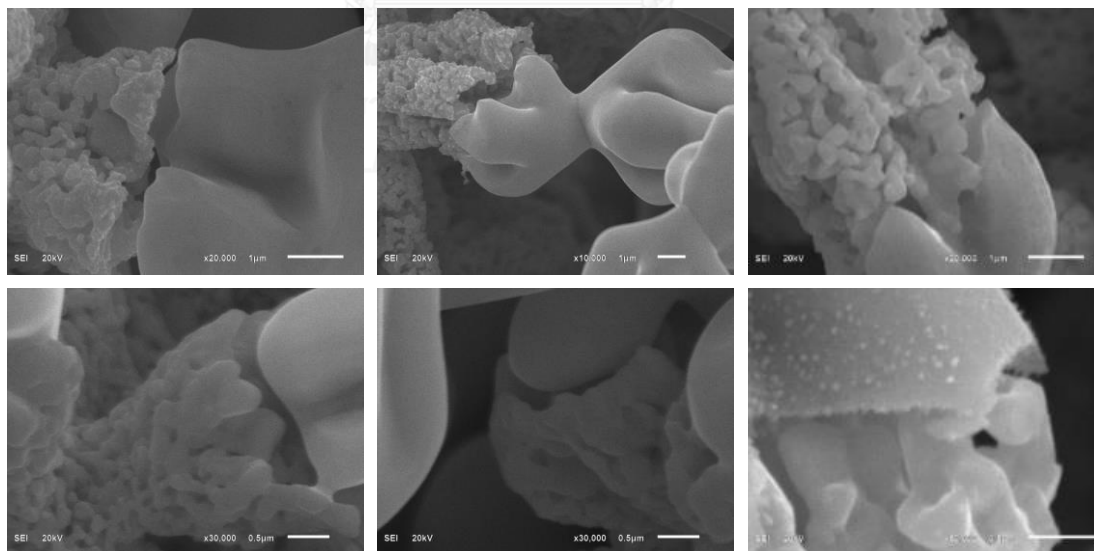
Figure 4.9 SEM micrographs show the gaps between galvanized and non-galvanized AgCl.

In this system, Cl⁻ involves in either a AgCl microcrystal template or an electrolyte. Therefore, the possible silver species which can get electrons transferred from sacrificial metals are Ag^+ or $AgCl_2^-$. To confirm the involving reduced silver species and the influence of Cl⁻ on the re-deposition process, the Ag_2SO_4 microstructures were employed as a template for galvanic replacement. The Ag_2SO_4 microstructures were synthesized by an addition of $AgNO_3$ solution (1 M, 5 mL) into Na_2SO_4 solution (0.25 M, 50 mL) and washed with DI water several times before using as a template. The processes were performed using Zn as a sacrificial metal in a solution of 0.5 M $NaNO_3$. In this system, there is no Cl⁻ involving in the reaction, the galvanic replacement still occurs. It confirms that the dissolved silver species from Ag_2SO_4 template which moves and gets electron at the AgCl/metal interface is Ag^+, not $AgCl_2^-$. The obtained np-AgMSs show the retaining of the original template shape with porous morphology. However, the grain size of np-AgMSs in this system is quite similar thorough whole np-AgMSs, as shown in Figure 4.10A. This is different from the reaction in a solution of 0.5 M NaCl, which the grain size at the position closed to sacrificial Zn metal is significantly different from that at 2 mm away from the Zn surface (see Figure 4.10B). Accordingly, Cl⁻ is the crucial parameter to promote the re-deposition process which decreases the grain size of np-AgMSs during the galvanic replacement reaction.

The overall growth mechanism of np-AgMSs is proposed in Figure 4.11. In an aqueous solution, AgCl microcrystal templates can release small amount of Ag^+ due to its low solubility. The dissolved Ag^+ can travel around the AgCl surface. In the presence of sacrificial metal, electrons provided by a sacrificial metal induce the movement of Ag^+. The dissolved Ag^+ move to get an electron and form a Ag seed on
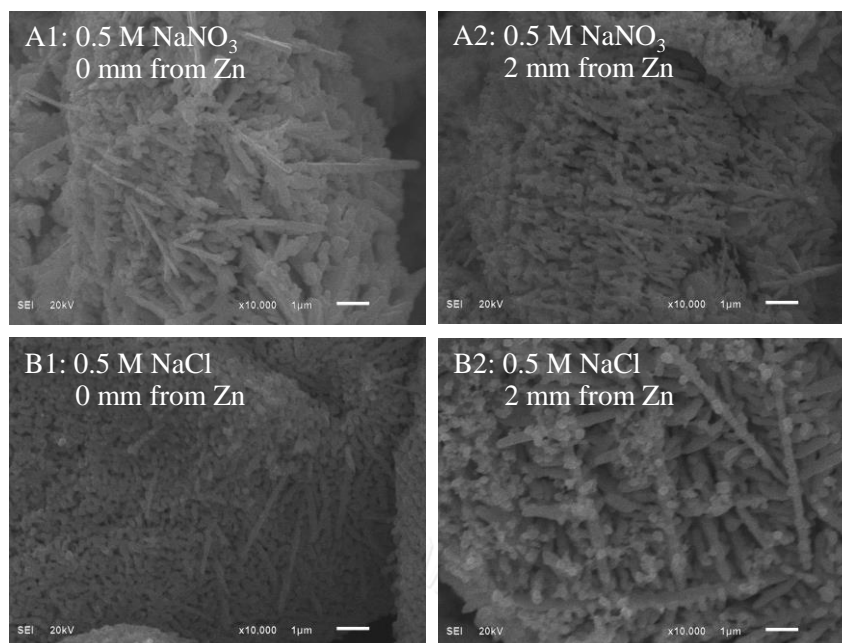
Figure 4.10 SEM micrographs of np-AgMSs galvanized from the Ag_2SO_4 microstructures using Zn as a sacrificial metal in a solution of (A) 0.5 M NaCl and (B) 0.5 M $NaNO_3$ at 0 and 2 mm away from the Zn surface.
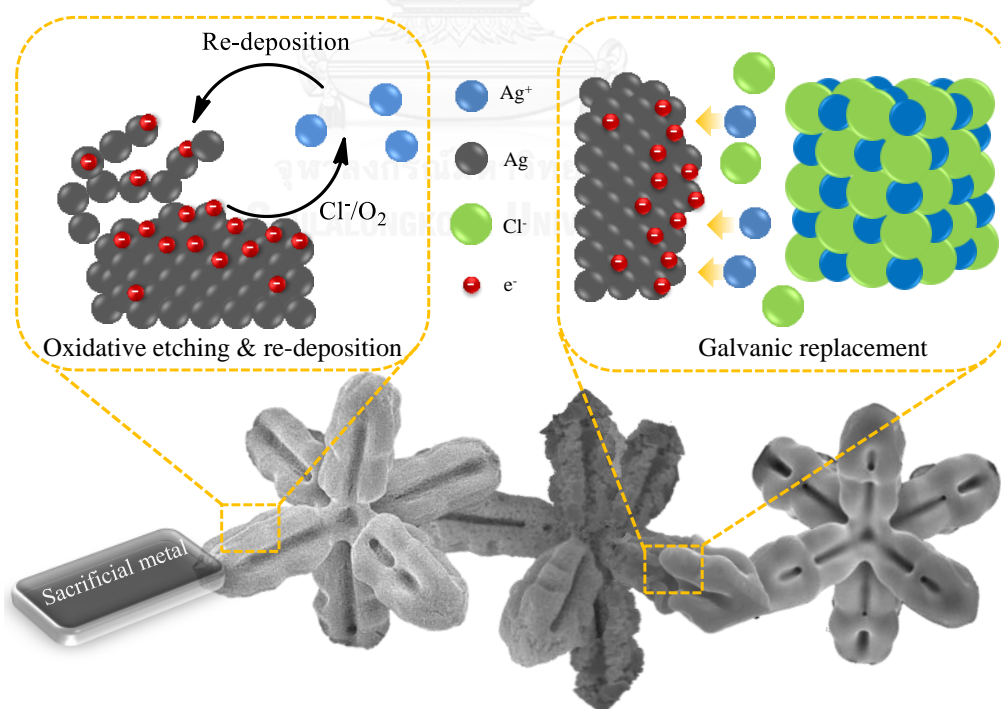
Figure 4.11 Proposed mechanism on the formation of np-AgMSs under the concerting of galvanic replacement and oxidative etching/re-deposition reaction.

a metal surface. Then, adjacent AgCl also continues this process and converts to Ag metal. The reaction starts at the surface of sacrificial metal, which is the closest electron source for reduction of Ag^+ then spreads out to whole AgCl microcrystal template and finally forms Ag microstructures. The grain size of Ag microstructures can be tuned by the concentration of Cl^-. The Ag microstructures are oxidatively etched by Cl^- or Cl^-/O_2 to form Ag^+, and then Ag^+ is reduced and re-deposited. This cycle continuously repeats during the galvanization process. The re-deposition process creates the smaller grain size of np-AgMSs, which is the kinetically controlled growth mechanism. The process takes place during the galvanic replacement proceeded. The galvanic replacement process and the formation of np-AgMSs spontaneously undergo until AgCl or sacrificial metal is depleted, as shown in Figure 4.12. After AgCl microcrystal template is completely converted to np-AgMSs, the kinetically controlled growth mechanism is terminated when the thermodynamically controlled growth mechanism is introduced.

We also employed this procedure with other morphologies of AgCl microcrystal templates synthesized *via* the protocol of our previous work [48]. In Figure 4.13, octapod AgCl and octahedral AgCl microcrystals were used as templates for galvanic replacement by Zn in 0.5 M NaCl. The grain sizes of nanoporous octapod silver microstructures (np-8pAgMSs) and nanoporous octahedral silver microstructures (np-OhAgMSs) are similar to that of np-6pAgMSs under the same galvanization condition. These results suggest that the grain size of np-AgMSs is independent from the morphology of AgCl microcrystal templates and the growth mechanism process should be the same.
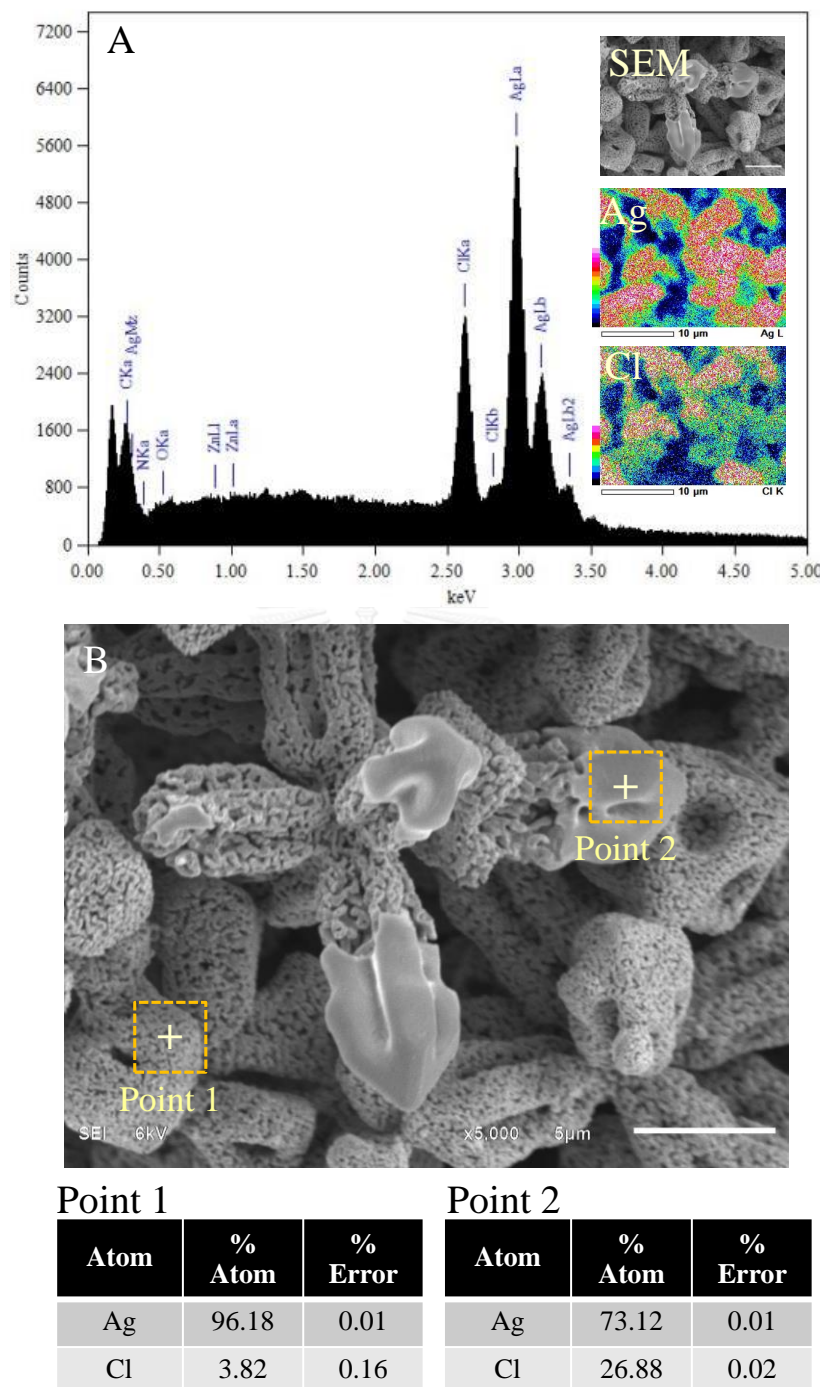
Figure 4.12 EDS spectrum and elemental maps of np-6pAgMSs during the galvanization with Zn in a solution of 0.5 M NaCl. The tables show the elemental compositions analyzed in the complete (point 1) and incomplete (point 2) galvanized area.
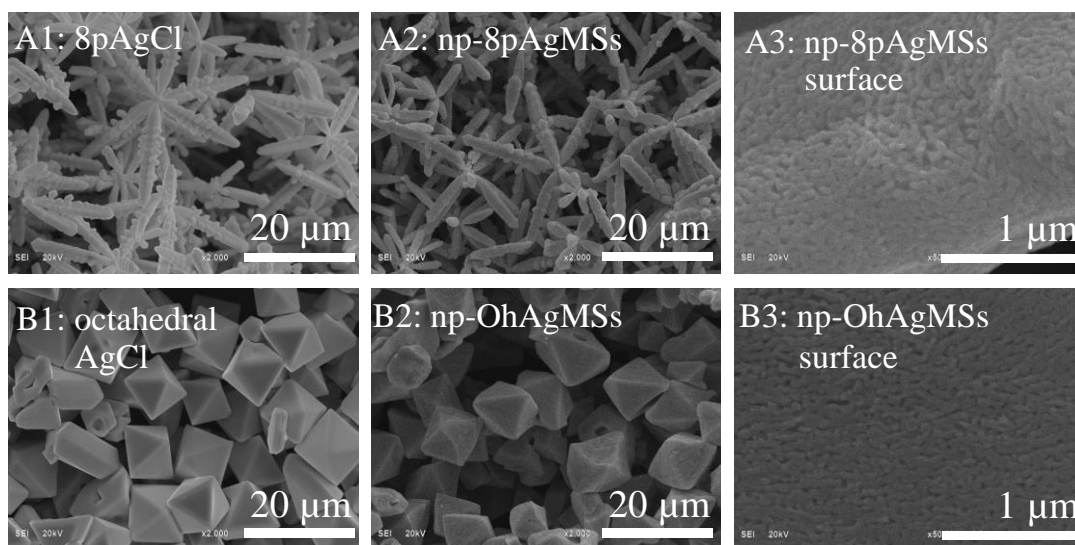
Figure 4.13 SEM micrographs of (A1) octapod AgCl microcrystals, (A2) np-8pAgMSs, (A3) the surface of np-8pAgMSs, (B1) octahedral AgCl microcrystals (B2) np-OhAgMSs and (B3) the surface of np-OhAgMSs fabricated by the galvanic replacement with Zn under 0.5 M NaCl.

Moreover, np-AgMSs can be synthesized *via* the chemical reduction approaches. Figures 4.14A and 4.14B show the morphology and EDS spectra of np-AgMSs reduced by $NaBH_4$ and L-ascorbic acid. The high purity (>99.99%) of Ag in np-AgMSs was obtained. The results show that thin film of silver was formed on the surface of np-AgMSs when 0.2 M $NaBH_4$ was employed as a reducing agent. Also, the np-AgMSs with grain size of 233.77 nm was created when 0.2 M L-ascorbic acid was applied as a reducing agent.

It is well-known that the precious metal such as gold, platinum, palladium and silver show a good catalytic activity for nitrobenzene reduction [156-159]. The catalytic reduction of nitrobenzene by $NaBH_4$ on metal surface was revealed in the term of Langmuir-Hinshelwood model. This model described that the metallic

nanoparticles reacted with the BH_4^- to form the metal hydride. Simultaneously, nitrobenzene adsorbs onto the metal surface. The adsorption/desorption of both reagents on the surface is fast and can be modeled in terms of a Langmuir isotherm. The rate-determining step is the reduction of the adsorbed nitrobenzene to aminobenzene, which desorbs afterward [160].

The experiments confirming the reduction mechanism were conducted. A solution of *p*-nitrophenol before an addition of catalyst and $NaBH_4$ has strong absorption band at 317 nm (see Figure 4.15). The adsorption at 317 nm was decreased with a developing band at 400 nm due to the formation of the *p*-nitrophenolate ion[158, 161] when only catalyst or $NaBH_4$ was introduced. However, the deprotonation of *p*-nitrophenol was not completed when catalyst was introduced with an absence of $NaBH_4$. After catalyst and $NaBH_4$ were introduced together, the *p*-nitrophenolate ion was reduced to *p*-aminophenol, which has the adsorption at 300 nm. The decreasing in the absorption of the *p*-nitrophenolate ion at 400 nm was not due to the adsorption on catalyst surface. In an absence of $NaBH_4$, the intensity at 400 nm was slightly decreased after 6 minutes without any developing of the peak at 300 nm whereas this peak was developed after an addition of $NaBH_4$ (see Figure 4.15). Figure 4.16 presents the intensity ratio at 400 nm between p-nitrophenol in a presence of np-8pAgMSs and p-nitrophenol in a presence of NaBH4. The intensity ratio is nearly constant during mixing process. It implies that the adsorption of *p*-nitrophenolate ion on the Ag surface is not a major factor in a decrease in the intensity at 400 nm.
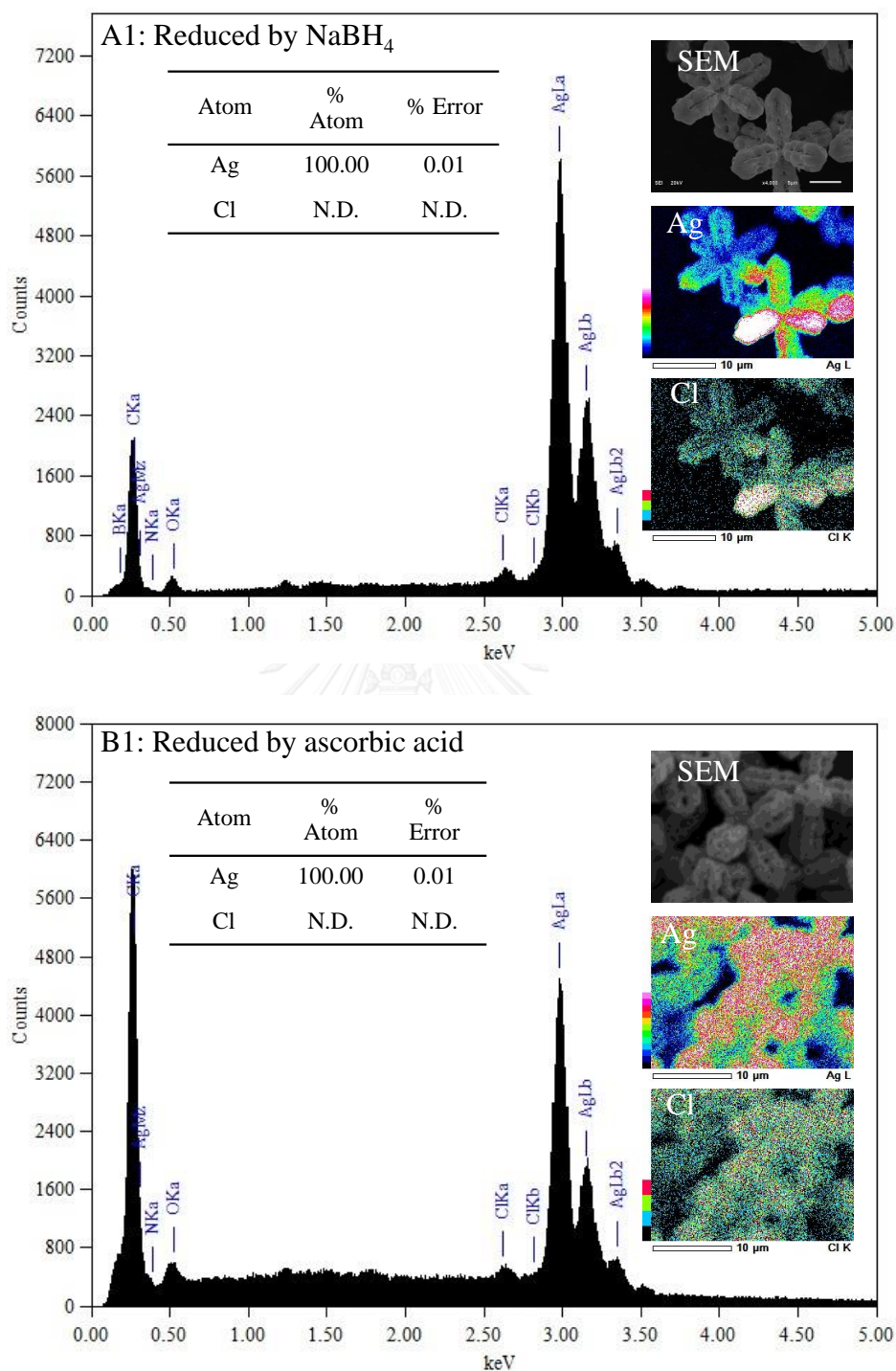
Figure 4.14 EDS spectra and elemental maps of np-6pAgMSs fabricated by the reduction of 6pAgCl microstructures using (A) 0.2 M NaBH$_4$ and (B) 0.2 M L-ascorbic acid.
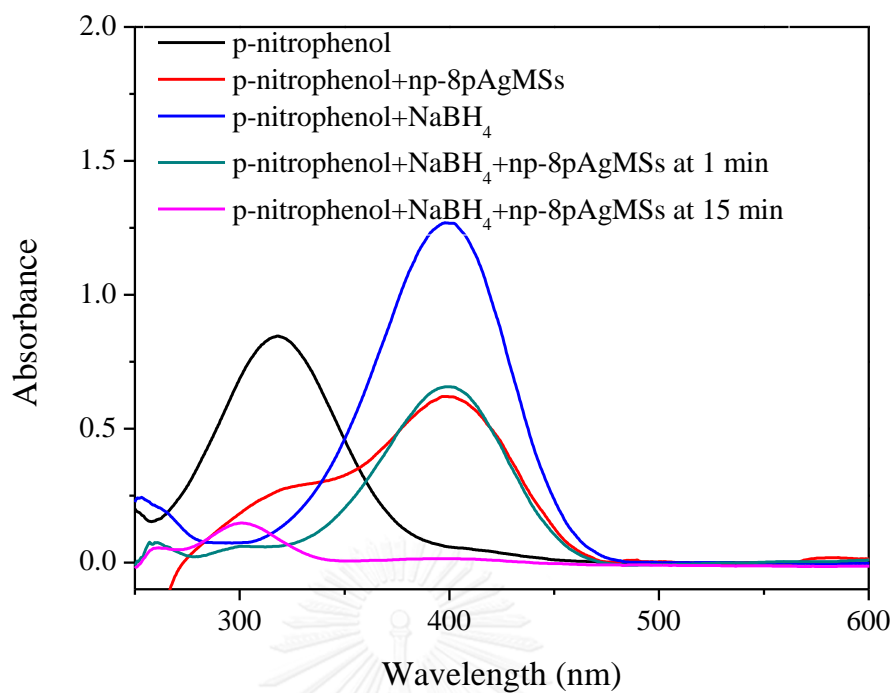
Figure 4.15 Absorption spectra of the catalytic reduction of *p*-nitrophenol by NaBH$_4$

using np-8pAgMSs (synthesized using 0.5 M NaCl as a galvanization media)
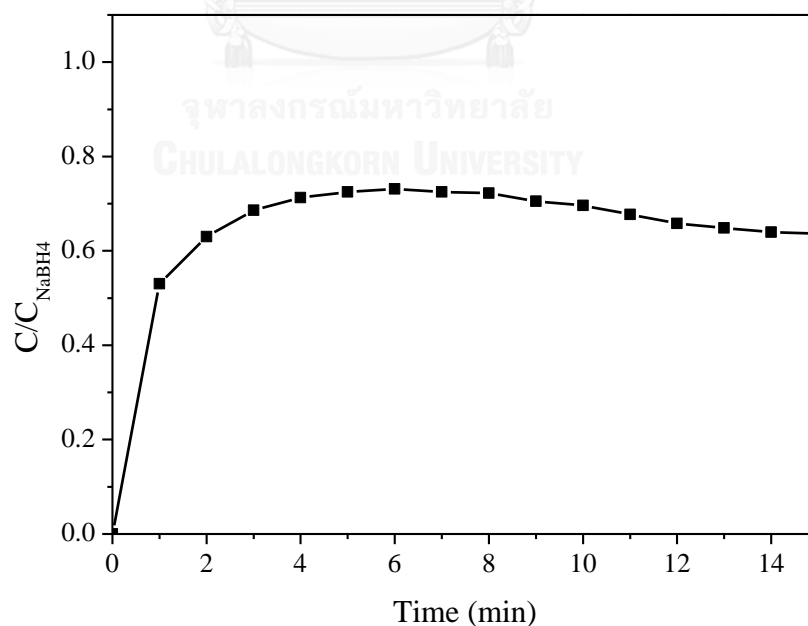
Figure 4.16 Intensity ratio at 400 nm between *p*-nitrophenol in a presence of np-

8pAgMSs and *p*-nitrophenol in a presence of NaBH$_4$.

Various morphologies of silver *i.e.*, np-6pAgMSs, np-8pAgMSs, np-OhAgMSs and silver microplates (average diameter and thickness of 20 and 1 μm, respectively) synthesized using the protocol of our previous work [47] were employed as a catalyst for the reduction of *p*-nitrophenol by NaBH$_4$. Figure 4.17A shows the catalytic activity of different Ag morphologies. The catalytic activities of Ag microstructures were monitored by following a decrease in absorbance at 400 nm in UV-visible spectra, which directly comes from the reduction of *p*-nitrophenol to *p*-aminophenol. Without catalyst, the reduction was not significantly observed within 15 minutes. Silver microplates and np-OhAgMSs show trivial catalytic activities which the concentration of *p*-nitrophenol was dropped to 60% and 50%, respectively. By using np-6pAgMSs as a catalyst, the *p*-nitrophenol was completely reduced within 15 minutes while it was achieved within 3 minutes using np-8pAgMSs. The effect of template morphology on the catalytic property is unexpected. This exceptional catalytic activity of np-8pAgMSs could be explained that np-8pAgMSs might contain more numbers of high index facets than others [93-95].

We also investigated the effect of grain size on the catalytic activity of np-8pAgMSs. The np-8pAgMSs were galvanized by Zn in DI water, 0.5 M and saturated NaCl, which have average grain sizes of 106.49, 80.15, and 55.69 nm, respectively. From Figure 4.17B, the catalytic activity increases with a decrease in grain size. The reductions using np-8pAgMSs galvanized in saturated NaCl, 0.5 M NaCl and DI waster were completely achieved in 2, 3 and 4 minutes, respectively. An increase in catalytic activity is due to an increase in surface area of catalysts. These results are in good agreement with using different grain sizes of np-6pAgMSs catalyst, as shown in Figure 4.18.
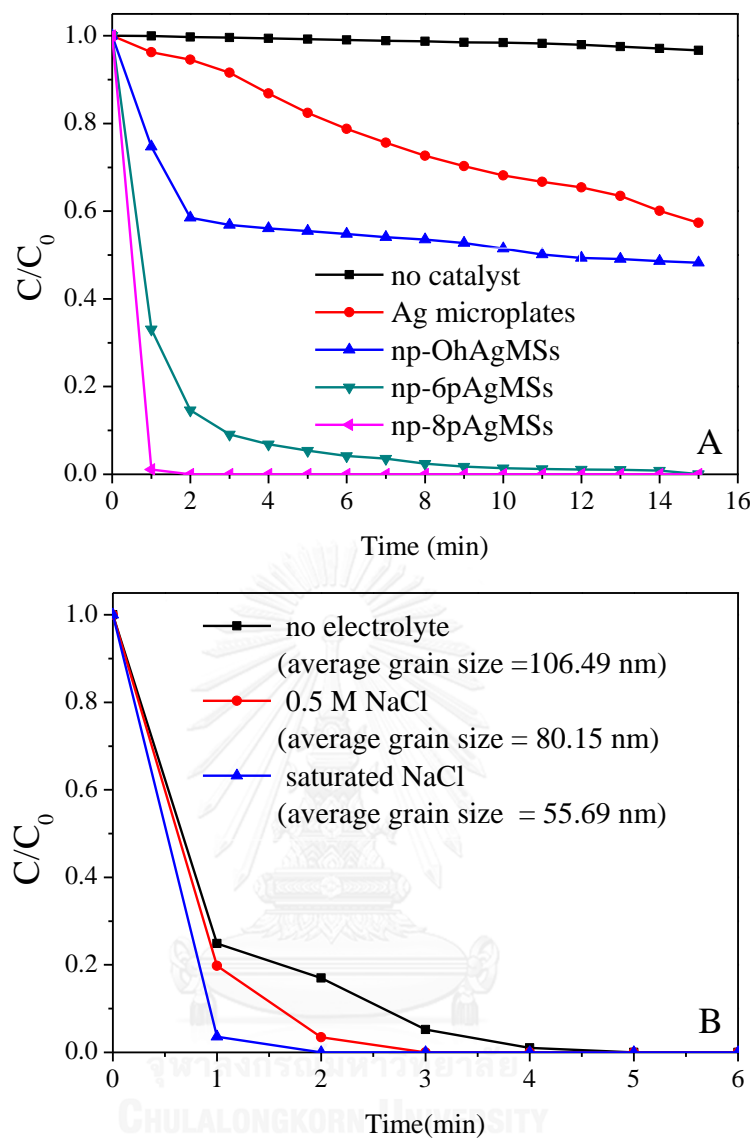
Figure 4.17 (A) The catalytic reduction of *p*-nitrophenol by NaBH$_4$ using silver microstructures with different morphologies as catalysts. (B) The effect of grain size in np-8pAgMSs on the catalytic reduction efficiency.
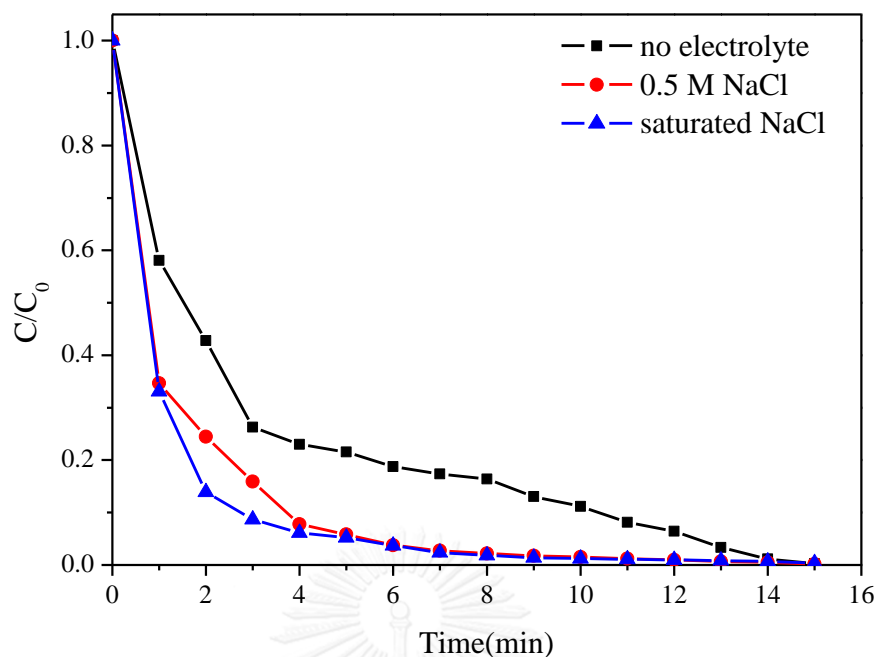
Figure 4.18 Effect of grain size in np-6pAgMSs on the catalytic reduction efficiency.

The np-8pAgMSs galvanized with a sacrificial Zn metal in a saturated NaCl solution was repeatedly employed as a catalyst for 10 cycles under the same experimental conditions (weight of catalyst, concentration and volume of analyte) as those in Figure 4.17. The catalyst was thoroughly cleaned with DI water before performing the next catalytic test. From Figure 4.19, the longer reduction time is observed when the catalyst is recycled. However, the reduction is completed within 6 minutes in all tests. The morphology of np-8pAgMSs is partially retained after 10th-cycle. The structural breakdown is due to the weak connecting joint of pods at the center of octapod structure, as shown in Figure 4.20.
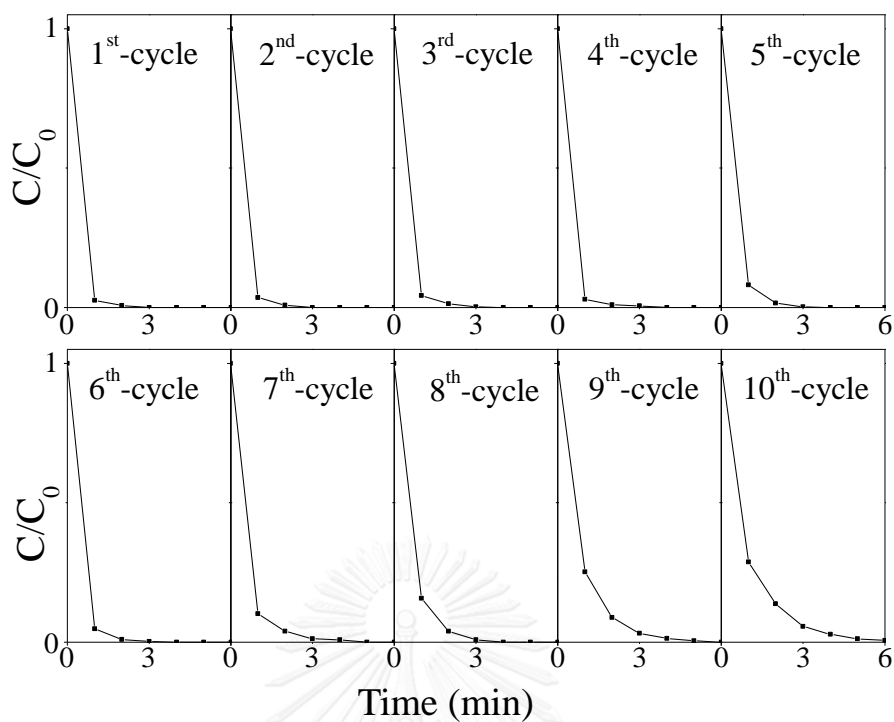
Figure 4.19 Recycling test for the catalytic reduction of *p*-nitrophenol by NaBH$_4$ using np-8pAgMSs as a catalyst.
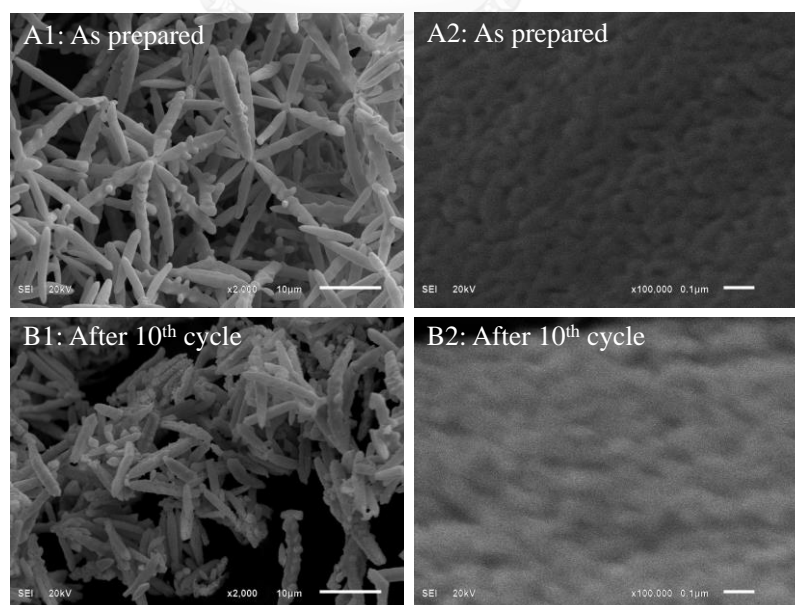
Figure 4.20 SEM micrographs of (A) as-prepared np-8pAgMSs and (B) np-8pAgMSs after 10th –cycle of the catalytic reduction.

Our technique offers a rapid, stabilizer free and grain size controllable protocol for fabrication of np-AgMSs under ambient conditions. The advantages of our developed technique are: (1) highly pure Ag (>99.99%) in np-AgMSs, (2) very clean surface of np-AgMSs due to the stabilizer or capping agent free protocol which open the opportunity for further surface modification, (3) easy, highly efficient, and rapid protocol and (4) easy separation of np-AgMSs precipitates.

4.4 CONCLUSIONS

We have successfully developed a simple, rapid and stabilizer-free technique for a fabrication of np-AgMSs *via* galvanic replacement of AgCl microcrystals using sacrificial Zn metal. Cl^- is the key parameter for tuning the average grain size of np-AgMSs as it facilitates the electron liberation of Zn. The Ag^+ dissolved from AgCl microcrystal template moves and receives electrons at the AgCl/metal interface to form Ag microstructures. The concerting reactions between the oxidative etching of np-AgMSs (by Cl^- and Cl^-/O_2) and the re-deposition of Ag atoms continuously takes place *via* kinetically controlled mechanism until AgCl microcrystal template is depleted. These processes convert large grains into small grains. The np-AgMSs efficiently catalyze the $NaBH_4$ reduction of *p*-nitrophenol into p-aminophenol. The catalytic reduction by np-8pAgMSs completes within 2 minutes. The reduction efficiency increases as the grain size becomes smaller. In addition, after a 10-repeating, np-8pAgMSs show insignificant decrease in catalytic activity.

CHAPTER V

ECO-FRIENDLY PROCESS FOR RECOVERY OF SILVER WASTE BY H_2O_2-INDUCED FORMATION OF SILVER MICROCRYSTAL FROM AgCl PRECIPITATES

5.1 INTRODUCTION

Due to their unique physical and chemical properties, silver metal and silver salt are widely used as catalysts, antibacterial substances, sensors, photographic materials, batteries and as part of electronic devices in various industries as well as in agriculture and medicine production. Recent reports have shown that silver is in great demand which is steadily increasing approximately 2–2.5% per annum [162, 163]. Since the extensive applications of silver, industrial wastes containing silver were also dramatically increased. The releasing of silver as silver nanoparticles (AgNPs) or silver ion (Ag^+) from silver-contained waste can cause a lot of damage to the environment and human health. The toxicity of AgNPs in zebrafish was reported to have the potential to cause health and ecotoxicity in a concentration-dependent manner [164]. The toxicity of Ag^+ has been reported that it can induce ion regulatory impairment and increased mortality in rainbow trout eggs [165]. Because of the limited natural availability and diminishing of silver mineral, the cost of silver production risen rapidly. Therefore, silver recovery process and regenerating silver from the industrial wastes have attracted much attention not only with respect to the

environmental sustainability and reduction of production costs but also the energy saving aspects.

Several processes developed for recycling the silver-contained wastes involve disassembling the metal from the non-metal part followed by a leaching process using hydrometallurgical (chemical) or biometallurgical technique. The final recovery step is the reduction of leachate by pyrometallurgical [91], galvanic replacement [88], chemical reduction [89], or electrochemical deposition [87]. Nevertheless, these recovery methods are costly, time consuming and require extensive labors. The addition of chemical reagents for precipitation and reduction in the processes generates large quantities of secondary wastes. Hence, an additional process for treating the secondary waste is required. The final product will be contaminated and the further purification will be necessary to obtain a high purity of metallic silver. The direct usages of the recovered product have never been mentioned or explored as the morphology (size and shape) and purity of recovered silver cannot be controlled. The modification and treatment of the recovered products substantially increase the recovery cost. As a result, silver recovery from wastes rarely achieves an economic scale. To overcome these problems, the development of new low-cost, eco-friendly and shape-controlled silver recovery systems from wastes is strongly recommended.

Hydrogen peroxide (H_2O_2) is well-known as a strong oxidizing agent, although it can be an efficient reducing agent under an alkaline condition [10, 47, 58-61]. The reducing capabilities of H_2O_2 were demonstrated [10, 58, 60, 61]. From our previous studies, we have observed that H_2O_2 can act not only as reducing agent but also a shape transformation reagent for silver nanospheres (AgNSs) to silver nanoplates (AgNPls) [58, 135, 166]. The concerted oxidation-reduction of H_2O_2 promotes the

growth of AgNPls. The prominent advantages of using H_2O_2 are: (i) it does not generate toxic products (it decomposes to oxygen and water), (ii) the process can be performed under ambient condition, (iii) the process is inexpensive, non-labor intensive, and fast, (iv) it has high recovery efficiency and generates highly pure silver crystals. Using of H_2O_2 as a reducing agent in the silver recovery process is considered as an attractive treatment process as it is eco-friendly process and low cost of operation. Moreover, H_2O_2 was also reported to be used for improving the leaching efficiency of silver from ore or metal alloy. The leaching rate was increased with an increasing of H_2O_2 concentration although the effect is eroded by the decomposition of H_2O_2 catalyzed by metal oxide [167]. Bas *et.al*. used H_2O_2 as an oxidizing agent to recover silver from the X-ray film processing effluents [168]. The concentration of H_2O_2 is the most significant parameter for recovery process which can be improved by an increasing of pH. Moreover, an addition of ethylene glycol can enhance the recovery efficiency due to its H_2O_2-stabilization effect. Mahdizadeh *et.al*. recovered silver from radiographic film processing effluents in similar protocol. The optimum conditions of the recovery process were determined by using response surface method [169].

The objective of this work is to develop an eco-friendly process and to evaluate its efficiency for recovering silver microcrystal from AgCl using H_2O_2 as a reducing agent under ambient condition. By turning precipitated AgCl (Equation 5.1) into silver ammine complex ($[Ag(NH_3)_2]^+$) (Equation 5.2), we could precipitate silver microcrystal and reduce it into silver microcrystal using H_2O_2 as a reducing agent (Equation 5.3) [62].

$$Ag^+(aq) + Cl^-(aq) \longrightarrow AgCl(s) \quad\quad\quad \text{(Eq. 5.1)}$$

$$AgCl(s) + 2NH_4OH(aq) \rightleftharpoons [Ag(NH_3)_2]^+(aq) + Cl^-(aq) + 2H_2O(l) \quad\quad \text{(Eq. 5.2)}$$

$$[Ag(NH_3)_2]^+(aq) + H_2O_2(l) \longrightarrow \quad\quad\quad \text{(Eq. 5.3)}$$
$$2Ag(s) + 4NH_3(aq) + 2H_2O(l) + 1/2 O_2(g)$$
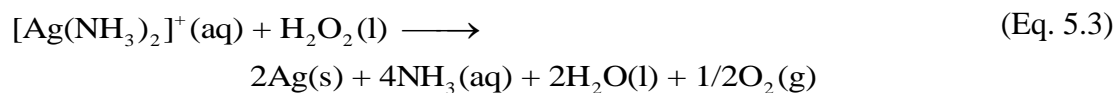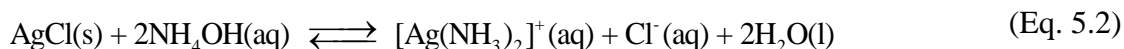
The morphology (size and shape), purity and recovery efficiency could be tuned by pH, concentration of Ag^+ and mole ratio of $H_2O_2:Ag^+$. To evaluate the recovery efficiency, the experiments were systematically performed using CCD approach, and the optimal conditions were determined by 3D-response surface plot. The developed process should be beneficial to environment as we employed the environmentally friendly process. The process is also highly economical as tab water with high Cl^- content can be used in the entire process without losing of recovery efficiency. The direct usages of the recovered silver microcrystals to be used for fabricating wearable silver jewelries were also demonstrated.

5.2 EXPERIMENTAL SECTION

5.2.1 Reagents and materials

Silver nitrate (AgNO$_3$, ≥99% purity), sodium chloride (NaCl, ≥99% purity), sodium hydroxide (NaOH, ≥99% purity), nitric acid (HNO$_3$, 65% w/v), ammonium hydroxide solution (NH$_4$OH, 25% w/w), sodium borohydride (NaBH$_4$, ≥98.0% purity) and hydrogen peroxide solution (H$_2$O$_2$, 30% w/w) were purchased from Merck$^{®}$. Poly(vinyl pyrrolidone) (PVP, M$_w$ ≈ 360,000) was purchased from Aldrich. All chemicals are analytical grade and used as received. Deionized (DI) water was used as solvent. Prior to use, all glassware and magnetic bars were

thoroughly cleaned with detergent, rinsed with DI water, rinsed with 6 M HNO$_3$, and thoroughly rinsed with DI water several times.

5.2.2 Preparation of saturated solution of AgCl

AgCl was prepared by adding 1.0 M NaCl into 500 mL of 1.0 M AgNO$_3$ until AgCl was completely precipitated. The precipitated AgCl was separated from the solution and washed for 5 times with DI water to get rid of the excess ions. Then, the sample was dried in oven at 60° C for 48 hours before storing in brown glass bottle to prevent the photo-reduction reaction. To get the saturated solution of AgCl, the excess amount of AgCl was added in to 100 mL of NH$_4$OH (5.3 M) until solid AgCl was remained. The solution was stirred under room temperature for 24 hours in the dark box to ensure the dissolution of AgCl was reached to the equilibrium and kept in the brown glass bottle for further investigation.

5.2.3 Reducing capability of H$_2$O$_2$

To demonstrate the reducing capability of H$_2$O$_2$ under alkaline conditions as shown in Equation 5.3 for silver recovery process, a 90-mL of saturated solution of AgCl in NH$_4$OH was adjusted the pH of 12.5 using 5 M NaOH and the total volume was adjusted to 172 mL by adding of DI water. The solution was stirred for 5 minutes before the addition of H$_2$O$_2$ (30% w/w, 18 mL). The reaction was prolonging for 2 hours until it was completed (no O$_2$ bubble). The product was collected and cleaned 3 times with 0.1 M NH$_4$OH and several times with DI water before drying in oven at 60° C for 24 hours for further characterizations.

5.2.4 Recovery percentage

The saturated solution of AgCl in 5.3 M NH$_4$OH 90 mL was reduced by 0.5 M NaBH$_4$ until the clear solution was obtained and the excess amount of

NaBH$_4$ was achieved. A 100-mL AgNO$_3$ solution was added in an aliquot supernatant. The precipitating of metallic silver was occurred if an excess amount of NaBH$_4$ was reached. The precipitated metallic silver was separated using the Whatman filter paper No.1. The filter paper was dried in oven at 60° C for 24 hours to get rid of the humidity and weighed before using. The precipitated metallic silver was washed 3 times with 0.1 M NH$_4$OH and 5 times with DI water and dried in oven at 60° C for 24 hours and weighed for a calculation of recovery percentage (%Recovery). The obtained weight here was defined as a perfect silver recovery. To determine the %recovery, the weight of each sample was divided by the weight of metallic silver obtained by the reduction of NaBH$_4$, as shown in Equation 5.4.

$$\%\text{Recovery} = \frac{\text{W2}}{\text{W1}} \times 100 \qquad\qquad (\text{Eq. 5.4})$$

where w_1 denotes the weights of metallic silver obtained by the reduction of NaBH$_4$ (perfect recovery) and w_2 is the weights of recovered metallic silver obtained by other conditions. After the reduction of [Ag(NH$_3$)$_2$]$^+$ using NaBH$_4$, a metallic silver of 5.9117 g. (corresponding to 0.604 M) is obtained as shown in Table 5.1. Therefore, it is assumed that NaBH$_4$ can perfectly reduce all Ag$^+$ species to achieve 100% recovery because of the strong reducing capability of NaBH$_4$.

5.2.5 Central Composite Design (CCD)

In order to obtain the good conditions for high %recovery, the setup experiments based on CCD were developed using three main factors which are solution pH (X$_1$), concentration of Ag$^+$ (X$_2$) and mole ratio of H$_2$O$_2$:Ag$^+$ (X$_3$). Fifteen different conditions were systematically setup follows CCD approach with at least three replicates. A total of 48 experiments (Table 5.2) were performed in order to get information related to experimental reproducibility and a good estimate of pure error.

The conditions of the recovery process using H_2O_2 were manipulated by adjusting the solution pH with either 5 M of NaOH or 5 M of HNO_3. The final volume before adding H_2O_2 was adjusted by DI water. The $[Ag(NH_3)_2]^+$ was spontaneously reduced into silver microcrystals by the rapid injection of 30% w/w H_2O_2 solution as shown in Equation 5.3. The brown precipitates were generated within 2 minutes. The reaction was prolonging for 4 hours to ensure that the completed reaction was reached. The obtained precipitates were washed and dried as the same procedure as mention above. The weight of metallic silver obtained from each condition is defined as w_2 in Equation 5.4 to calculate the recovery percentage.

5.2.6 Characterization of recovered silver

Morphology (size and shape) of the recovered products was recorded by a Scanning Electron Microscope (SEM, JEOL JSM-6510A) operating at 20 kV under a high vacuum mode with a secondary electron image (SEI) detector. A built-in Energy-dispersive X-ray spectroscopy (EDS) was employed for monitoring elemental compositions of the recovered silver. The X-ray diffraction (XRD) patterns were collected by an X-ray diffractometer (Philips PW3710) operated at room temperature with a scanning rate of 0.02 deg/min, using Cu K_α irradiation (40 kV, 30 mA). The diffractograms were recorded in the 30°–80° region with a 0.2° resolution.

5.3 RESULTS AND DISCUSSION

5.3.1 Reducing capability of H_2O_2

A 90-mL saturated solution of AgCl in 5.3 M NH_4OH (pH = 12.5) was used to express the reducing capability of H_2O_2 in order to reduce silver species into metallic silver. After the addition of H_2O_2, the white colloidal AgCl particles are

immediately generated and well-dispersed in the solution. After a few minutes of H_2O_2 injection, the colloids changed to brown with the evolution of O_2 bubbles and the exothermic reaction was occurred (solution temperature is increased to ~50° C). The shiny metallic silver was instantaneously formed within 10 minutes due to the positive value of standard potential cell (E_{cell}^0) [62] as shown in Equation 5.3. The reaction was completed after 2 hours (no O_2 bubbles). The overall scheme of the performed reaction is shown in Figure 5.1. The morphology of the obtained shiny metallic precipitant was characterized by SEM as shown in Figure 5.2. The variety of morphological structures consisting of microplates, icosahedra, truncated cubes and quasi-spheres were observed and all structures were in micrometer scale. These suggest that H_2O_2 is the efficient reducing agent for the reduction of $[Ag(NH_3)_2]^+$. The purity of the recovered silver microcrystals was examined by using EDS as shown in Figures 5.2B and 5.2C. From EDS map, only silver element without any contaminated chloride was determined. This suggests that a high purity (up to 99.99%) of metallic silver was obtained from the recovery process by using H_2O_2 as a reducing agent. It shows that the recovery protocol offers an easy, rapid, and non-toxic technique to recover silver microcrystals with a very high purity.

| Saturated solution of AgCl in 5.3 M NH4OH | Adjust pH and volume | Add H_2O_2 | 10 seconds | 2 minutes | 2 hours |
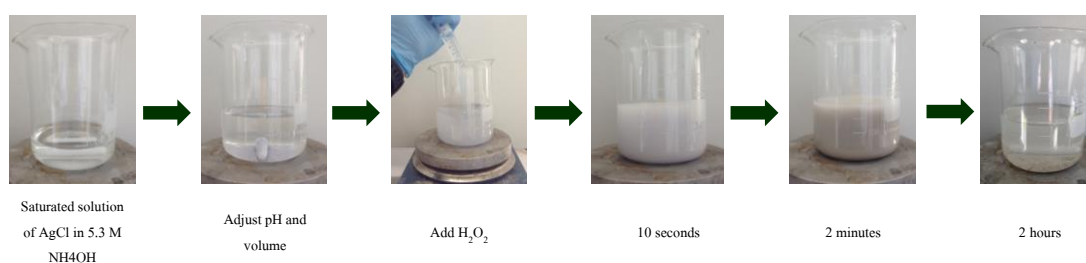
Figure 5.1 Silver recovery process using H_2O_2 as a sole reducing agent (under the condition of pH = 12.5, $[Ag^+]$ = 0.27 and mole ratio of $H_2O_2:Ag^+$ = 3.24). The reaction was prolonging for 2 hours.

Table 5.1 Weight of metallic silver obtained from the reduction of 90 mL saturated solution of AgCl in 5.3 M NH$_4$OH using DI water and tab water as a solvent and NaBH$_4$ as a reducing agent.

Sample number	Weight of Ag (g)	
	Using DI water	**Using tab water**
1	5.8326	6.0341
2	6.0206	6.0612
3	5.8401	5.9888
4	5.8336	5.9835
5	6.0617	6.0155
Average	5.9177	6.0166
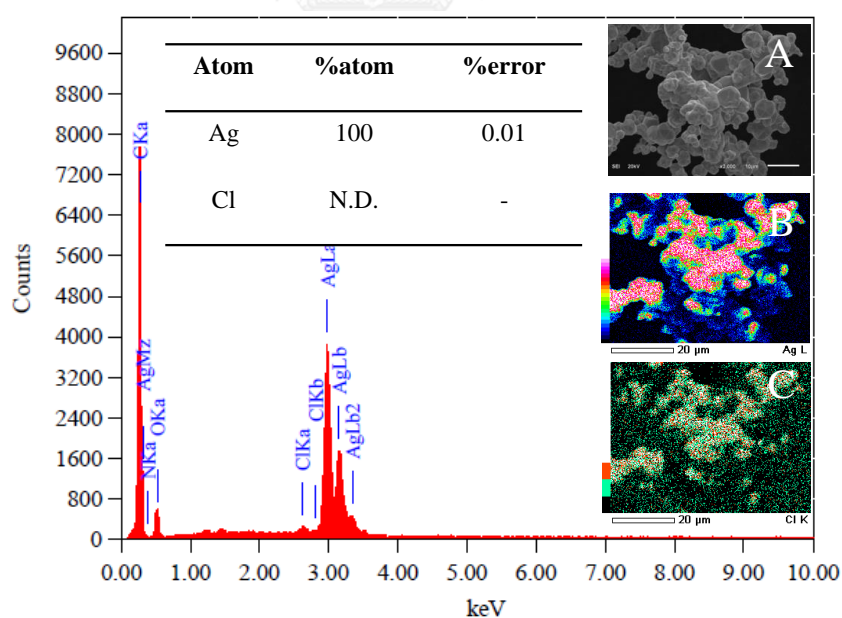
Figure 5.2 EDS spectra and EDS maps of the recovered silver microcrystals using H$_2$O$_2$ as a reducing agent. Inset figures demonstrate (A) SEM micrograph, (B) Ag composition map, and (C) Cl composition map. (N.D. represents not detected)

Table 5.2 Experimental matrix designed by using the central composite design approach. Each recovery condition was varied by parameter X_1: solution pH, X_2: $[Ag^+]$, and X_3: mole ratio of H_2O_2:Ag^+. The numbers in the table represent the actual values of each parameter. The numbers in bracket ( ) represent the coded value linearly corresponding to actual value. The average %recovery with standard deviation was determined using the gravitation analysis.

Experimental run	pH (X_1)	$[Ag^+]$ (X_2)	$[H_2O_2]/[Ag^+]$ (X_3)	% Recovery	
				DI water	Tab water
1	12.0 (1)	0.48 (1)	4.00 (1)	81.58 ± 0.94	79.99 ± 0.30
2	12.0 (1)	0.48 (1)	1.50 (-1)	76.18 ± 1.83	80.48 ± 0.07
3	12.0 (1)	0.20 (-1)	4.00 (1)	92.31 ± 1.43	91.67 ± 0.87
4	12.0 (1)	0.20 (-1)	1.50 (-1)	80.21 ± 1.93	80.38 ± 3.11
5	9.0 (-1)	0.48 (1)	4.00 (1)	0.00 ± 0.00	0.00 ± 0.00
6	9.0 (-1)	0.48 (1)	1.50 (-1)	0.00 ± 0.00	0.00 ± 0.00
7	9.0 (-1)	0.20 (-1)	4.00 (1)	0.44 ± 0.14	0.58 ± 0.03
8	9.0 (-1)	0.20 (-1)	1.50 (-1)	0.31 ± 0.15	0.51 ± 0.05
9	13.1 (1.732)	0.34 (0)	2.75 (0)	86.35 ± 2.16	86.84 ± 0.27
10	7.9 (-1.732)	0.34 (0)	2.75 (0)	0.00 ± 0.00	0.00 ± 0.00
11	10.5 (0)	0.58 (1.732)	2.75 (0)	60.30 ± 0.28	61.51 ± 0.29
12	10.5 (0)	0.10 (-1.732)	2.75 (0)	86.82 ± 1.07	76.90 ± 0.95
13	10.5 (0)	0.34 (0)	4.92 (1.732)	72.18 ± 1.06	74.10 ± 0.57
14	10.5 (0)	0.34 (0)	0.59(-1.732)	6.63 ± 0.51	10.80 ± 0.31
15	10.5 (0)	0.34 (0)	2.75 (0)	76.58 ± 0.81	70.99 ± 1.32

5.3.2 Morphology of the recovered silver

Due to the good advantages of using H_2O_2 as a reducing agent for silver recovery process [10, 47, 60, 61], the key parameters for the successful recovery of silver using H_2O_2 are the solution pH, the concentration of Ag^+, and the mole ratio of $H_2O_2:Ag^+$. From the reduction mechanism, it can be noted that the concentration of H_2O_2 should be greater than 0.5 times of silver species (following Equation 5.3) to ensure that the reduction process is completed. A solution pH plays an important role in the precipitation process as it affects the distribution and mobility of solute species, especially $[Ag(NH_3)_2]^+$, which able to be precipitated into AgCl at low pH [64]. The experimental conditions were systematically performed using CCD approach. The corresponding %recovery of each condition was determined using gravitation analysis. Morphology and composition of the chemical species can be observed in more details by using SEM and analyzed by using EDS, respectively. Figure 5.3 shows SEM micrographs of the recovered silver from each condition. By systematically adjusting the recovery conditions, a mixture of silver microstructures consisted of microplates, icosahedra, truncated cubes and quasi-spheres were obtained. However, it can be seen that the majority of the recovered structures is originated from the multiply twinned seeds which are the most thermodynamically favorable seeds [2, 25, 63]. These can grow into the crystal structures which are icosahedra, truncated cubes and quasi-spheres. The multiply twinned crystals are known that able to develop under high concentration of Ag^+ [63]. From our experiments, it can be noticed that the morphology of the recovered silver was transformed from microplates to microparticles (Figures 5.3A12, 5.3A15 and 5.3A11)

under the increasing of Ag^+ concentration (from 0.1–0.58 M). This observation is in good agreement with thermodynamically favorable mechanism [2, 25, 63].
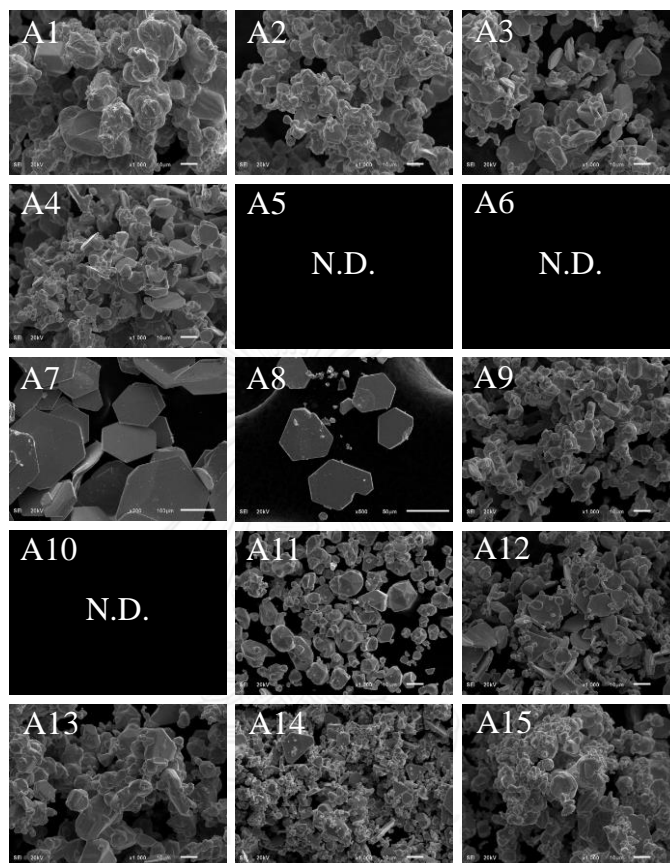
Figure 5.3 SEM micrographs of recovered silver microcrystals obtained from recovery process which A1-A15 represents the following experimental condition 1-15 in Table 5.2, respectively. N.D. represents not detected due to 0% recovery.

The influence of solution pH on the morphology of the recovered silver was investigated by varying over the range of pH 7.9–13.1 while concentration of Ag^+ and mole ratio of $H_2O_2:Ag^+$ were fixed at 0.34 M and 2.75, respectively. It can be seen that there is no observation on the recovered silver using low solution pH (Figure 5.3A10) due to the low reduction efficiency of H_2O_2. The microparticles were initially

generated (Figure 5.3A15) when solution pH was increased to 9.0. It was found that a relative high solution pH induces a formation of big microparticles as shown in Figure 5.3A9 (pH = 13.1).

The influence of mole ratio H_2O_2:Ag^+ was performed by varying over the range of 0.59–4.92 while solution pH and concentration of Ag^+ were 10.5 and 0.34 M, respectively. At mole ratio of H_2O_2:Ag^+ lower than 2.75, the microplate structures were observed as the major product. However, the morphology of the recovered silver microstructures was transformed from microplates to microparticles (Figures 5.3A14, 5.3A15 and 5.3A13) when the mole ratio H_2O_2:Ag^+ was increased higher than 2.75. This suggests that H_2O_2 can be acted as reducing agent and also an efficient shape controlling agents [10, 56-58].

The element compositions and purity of the recovered silver randomly selected from the experiment conditions (1, 3, 13 and 15) were analyzed using EDS and XRD techniques, respectively. Figure 5.4A with chemical compositions (Table 5.3) show that only silver content (>99.5%) was determined, while a trace amount of chlorine related to a formation of thin AgCl film on the silver microstructure surface was also detected [47]. Moreover, the XRD patterns of silver microstructures in Figure 5.4C show characteristic diffraction peaks of (111), (200), (220), and (311) planes indexed to the fcc structure of metallic silver (JCPDS No. 65-2871) without any impurity peaks. This suggests that the silver microstructures recovered from all selected conditions are highly pure metallic silver without any contaminated chemical elements. According to the high purity of the recovered product, it offers a great opportunity to directly reuse the recovery silvers in wide applications such as silver

compositions in electronic devices and raw material to produce silver jewelry without any additional refinements [52, 170].

Table 5.3 Elemental compositions (Ag and Cl) of the recovered silver microcrystals from the selected experimental condition: 1, 3, 13, and 15 measured by EDS technique.

Recovered silver from experimental conditions	%Atom	
	Ag	Cl
1	99.98	0.02
3	100	N.D.
13	100	N.D.
15	99.76	0.24
3 with 0.5% w/v PVP	99.64	0.36

N.D. represents not detected due to lower than detection limit

As we have stated earlier, the morphology of the recovered silver can be controlled by adding a capping agent or surfactant during in the recovery process. The recovered silver microstructures of experimental condition number 3 with and without 0.5% w/v PVP as a stabilizer was shown in Figures 5.4A and 5.4B, respectively. EDS spectra and EDS maps show that the precipitated silver microstructures were recovered with very high purity (>99.5%). Without any stabilizer, the final product expresses the mixtures of anisotropic microstructures. On the other hand, only silver microplates were observed as a favorable product when stabilizer (PVP in the case)
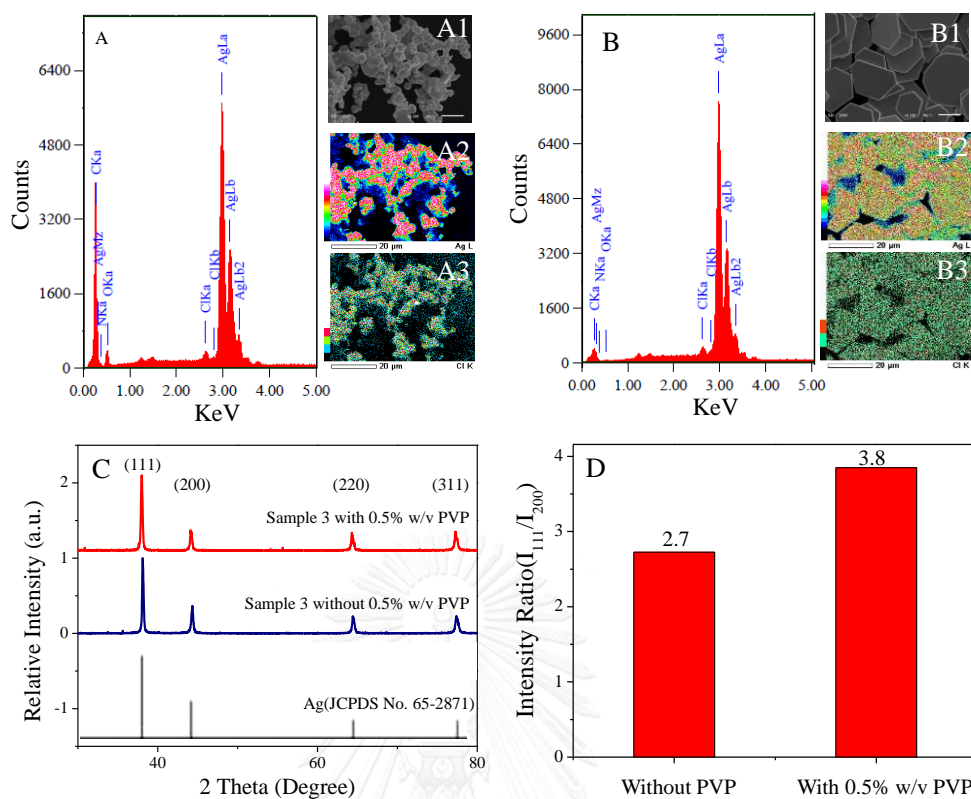
Figure 5.4 (A) EDS spectra of silver microcrystals with (A1) SEM micrograph, (A2) EDS map of Ag, and (A3) Cl of sample collected from the experimental condition 3 without 0.5% PVP. (B) EDS spectra of silver microcrystals with (B1) SEM micrograph, (B2) EDS map of Ag, and (B3) EDS map of Cl of sample collected from the experimental condition 3 with 0.5% PVP. (C) the purity of these samples were investigated using XRD technique and (D) intensity ratios of (111) and (200) peaks were demonstrated.

was introduced in the recovery process as shown in Figure 5.5. SEM images of the recovered product was in good agreement with XRD pattern shown in Figure 5.4C Generally, the asymmetric microplates bound by Ag{111} planes with alternated Ag{100} and Ag{111} lateral sides were formed.[47, 75, 76] The intensity ratio

between Ag(111) and Ag(200) of silver microplates is higher than silver microparticles (3.8 and 2.7 respectively) due to the domination of Ag{111} facets from microplate structures (Figure 5.4D).
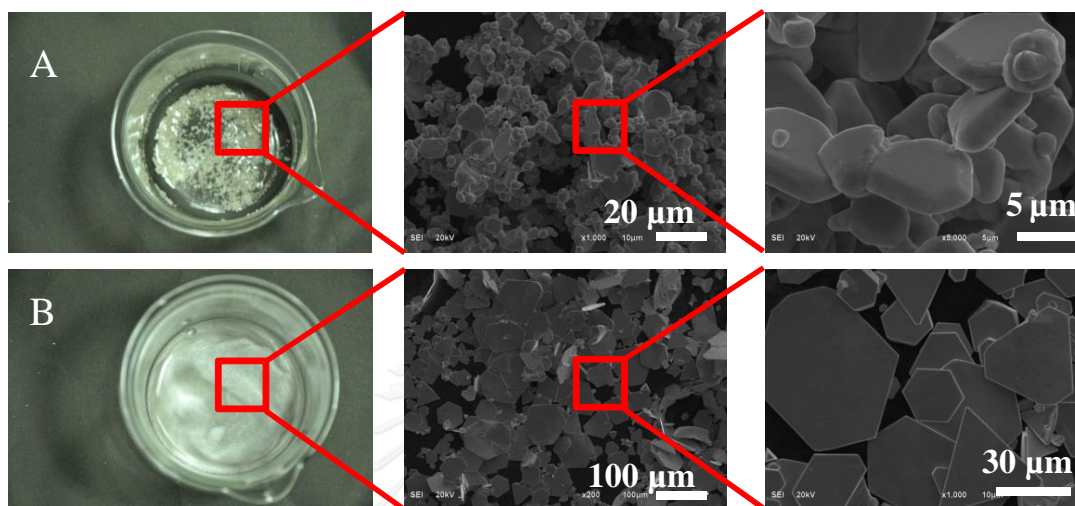
Figure 5.5 Morphologies of silver microstructures. The samples were prepared using the same condition as experimental condition 3 (A) without and (B) with 0.5% w/v PVP.

The roles of etchant species and stabilizer were discussed to demonstrate the growth pathway of plate structure induced by PVP. Our recovery system consisted of many etchants such as Cl^-/O_2, NH_4OH/H_2O_2, and H_2O_2. The functions of etchant to oxidatively etch an unstable structure was thoroughly explained in our previous work [47]. It is well-known that a species of Cl^-/O_2 can dissolve singly and multiply twinned seeds [2, 35-37], NH_4OH/H_2O_2 etches single crystal seed containing Ag{100} facets [38, 39], while H_2O_2 etches all structures with different rates [27]. When PVP was added as a stabilizer, structural selection process was introduced. PVP can be formed complex with Ag^+ [50, 60, 70, 83-86] and was preferentially adsorbed

on Ag{100} while NH$_3$ [4], Cl$^-$ [40-44] and AgCl [44-46] were preferentially adsorbed on Ag{111}. These phenomena promoted the growth on only Ag{100} and protected Ag{111} form etching environments. The selective dissolution of specific crystallographic facets and surface passivation of Ag{111}, however, enables the survival of high purity of plate structure in such an oxidative environment.

5.3.3 Central Composite Design (CCD)

A regression model including linear, interactive and quadratic parameters correlating to the recovery efficiency was calculated using the multiple linear regressions (MLR). From the ANOVA test (Table 5.4), it was found that only parameters of solution pH and mole ratio of H$_2$O$_2$:Ag$^+$ affected the %recovery and they were strongly correlated. Solution pH plays an important role in the recovery process as it control the reducing power of H$_2$O$_2$. The reducing efficiency of H$_2$O$_2$ will increase with an increasing of the solution pH [58, 59, 68]. However, the decomposition of H$_2$O$_2$ is accelerated under the extremely high alkaline conditions (Equation 5.5) [67] and silver metal is also a good catalyst for the decomposition of H$_2$O$_2$ shown in (Equation 5.6) [53].

$$2H_2O_2 \xrightarrow{\text{OH}^-} 2H_2O + O_2 \quad \text{(Eq. 5.5)}$$

$$2H_2O_2 \xrightarrow{\text{Ag}} 2H_2O + O_2 \quad \text{(Eq. 5.6)}$$

As shown in Equation 5.3, the adequate amount of H$_2$O$_2$ is required in order to reduce all silver-waste ions into metallic silver. Therefore, the required amount of H$_2$O$_2$ is directly proportional to the concentration of Ag$^+$. The higher Ag$^+$ concentration, the larger amount of H$_2$O$_2$ is obligated. Because of the relation of the acquired H$_2$O$_2$ and Ag$^+$, the mole ratio of H$_2$O$_2$:Ag$^+$ will be considered instead of using only H$_2$O$_2$ concentration. With the low mole ratio of H$_2$O$_2$:Ag$^+$, the reducing

agent is insufficient to completely reduce $[Ag(NH_3)_2]^+$. We already mentioned in the previous section that H_2O_2 and alkaline hydrogen peroxide (NH_4OH/H_2O_2) can function as etchant. If the large amount of H_2O_2 is presented in the system, it will induce the oxidative etching of the recovered metallic silver into Ag^+ as shown in Equations 7–8 [27, 38, 39]. This results the decreasing of the %recovery.

$$2Ag + H_2O_2 \longrightarrow 2Ag^+ + 2OH^- \qquad \text{(Eq. 5.7)}$$

$$2Ag + 4NH_3 + H_2O_2 \longrightarrow 2[Ag(NH_3)_2]^+ + 2OH^- \qquad \text{(Eq. 5.8)}$$
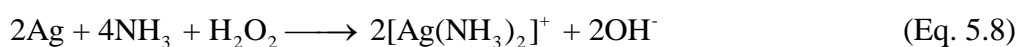
Table 5.4 ANOVA of the quadratic regression model for silver recovery to determine the significance of the effects in the system.

Parameters	Sum of squares	DF[a]	Mean square	F-value	p-value
Model	54,823.94	9	6,091.55	15.08	<0.0001[b]
X_1	49,188.12	1	49,188.12	121.75	<0.0001[b]
X_2	808.97	1	808.97	2.00	0.1652[c]
X_3	3,687.28	1	3,687.28	9.13	0.0045[b]
X_1^2	7,149.40	1	7,149.40	17.70	0.0002[b]
X_2^2	380.62	1	380.62	0.94	0.3379[c]
X_3^2	8,581.35	1	8,581.35	21.24	<0.0001[b]
X_1X_2	73.62	1	73.62	0.18	0.6719[c]
X_1X_3	113.13	1	113.13	0.28	0.5998[c]
X_2X_3	17.53	1	17.53	0.04	0.8361[c]
Residual	15,352.30	38	404.01		
Lack of fit	15,314.40	5	3,062.88	2,666.86	<0.0001[b]
pure error	37.90	33	1.15		
Total	70,176.24	47			
R^2	0.9250				

[a] Degree of freedom, [b] Significant at $p < 0.01$, [c] Not significant at $p > 0.01$

To obtain the applicable conditions for silver recovery, the response surface was generated. To visualize all interactions in the same surface plot, we attempted to set the 3D-plot as shown in Figure 5.6. The 3D-surface plot contains three-axis corresponding to parameters (X_1, X_2 and X_3) and the solid dots represents the conditions giving >95% recovery. To elucidate the effect of recovery conditions, the solids dots on the 3D-surface plot was projected on 3 different planes which are X_1-X_2, X_1-X_3 and X_2-X_3 plane. From the projections, it can be concluded that the solution pH and the mole ratio of H_2O_2:Ag^+ should be in the range of 11.4–13.1 (Figures 5.6B and 5.6C) and 2.37–4.37 (Figures 5.6C and 5.6D), respectively. The role of solution pH can be explained by the reduction activity of H_2O_2 increased in the alkaline condition [47, 58, 59, 68]. The mole ratio of H_2O_2:Ag^+ should in balance to be sufficient for completely reducing $[Ag(NH_3)_2]^+$ to metallic silver. Our experiments and the obtained model were performed using DI water as a solvent to avoid the effects of other ions. To reduce the cost of recovery process, the alternative experiments were redone using tab water as a solvent. The results showed that the %recoveries using DI water and tab water are not significantly different as shown in Figure 5.7. Therefore, the developed silver recovery process was not affected by the contamination of Cl^- in tab water. This process is capable to use tab water as a solvent in the entire process to reduce cost of operation.
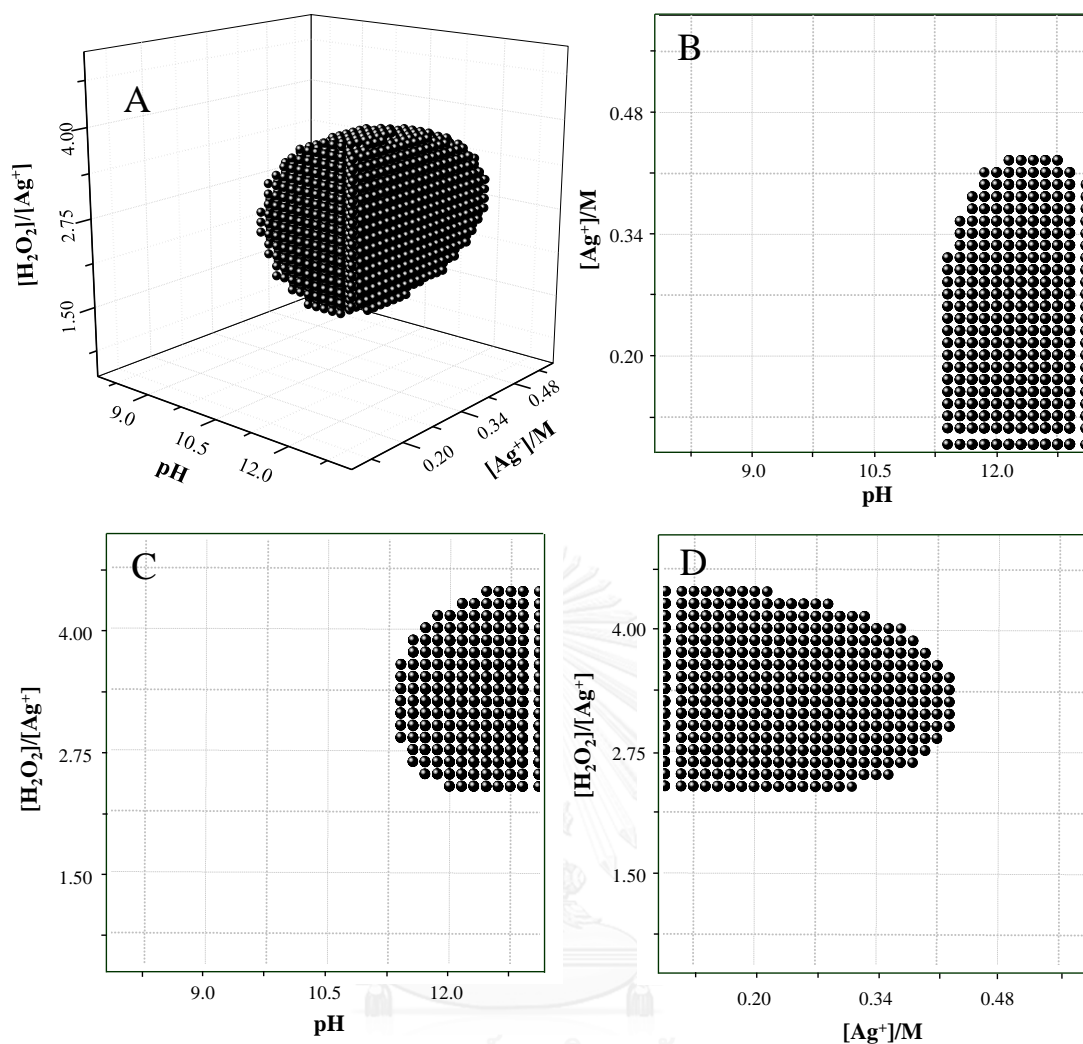
Figure 5.6 3D of the Responsive surfaces calculated using the regression model:

$$\%\text{Recovery} = 76.57 + 34.22X_1 - 4.39X_2 + 9.37X_3 - 13.17X_1^2 - 3.04X_2^2 - 14.42X_3^2$$

$$- 1.75X_1X_2 + 2.17X_1X_3 - 0.85X_2X_3$$

(A) 3D response image of the effect of X_1, X_2 and X_3 on the %recovery of silver using H_2O_2 as a reducing agent. The data was shown only the conditions which give %recovery greater than 95%. The image was projected to (B) X_1-X_2 plane, (C) X_1-X_3 plane, and (D) X_2-X_3 plane.
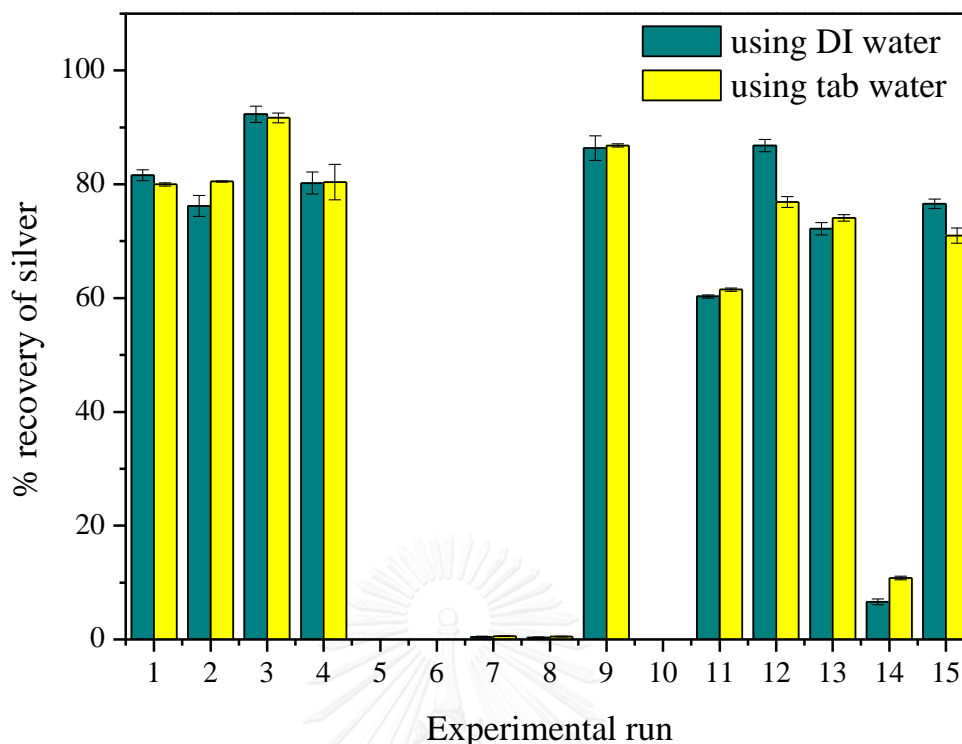
Figure 5.7 SEM micrographs of silver microstructures obtained from recovery process using tab water as a solvent. Sample labels correspond to the samples as shown in Table 5.2. N.D. represents not detected due to 0% recovery.

5.3.4 Applications

The condition at pH = 12.6, $[Ag^+]$ = 0.144 M, and mole ratio of H_2O_2:Ag^+ = 4.03 which give the highest predicted %recovery using the model was chosen. This condition was applied to get the completed recovery for silver-contained waste from research chemical laboratory (Figure 5.8) compared with the stock solution (saturated AgCl in 5.3 M NH_4OH). Firstly, waste was digested to extract Ag^+ by leaching with 1 M HNO_3. Undissolved particles were separated from the solution by using filtration paper, while the extracted Ag^+ were separated from the solution by precipitating in form of AgCl using NaCl solution. To remove $PbCl_2$ and Hg_2Cl_2

which can be co-precipitated with AgCl, 0.5 M HNO_3 was added to remove these impurities [171]. Then, pure precipitated AgCl was cleaned with tab water and then dissolved in NH_4OH solution until the clear solution was observed. By end of this process, the saturated solution with Ag^+ concentration of 0.614 M (Table 5.1) was expected. To reach the optimal condition, pH of the saturated solution was adjusted using NaOH and the volume was adjusted by adding of tab water to control final Ag^+ concentration. The morphology of product can be tuned by non-adding/adding a stabilizer e.g. PVP. When H_2O_2 is added, sliver microstructures were immediately generated. The products were washed several times with tab water and one time with 0.1 M NH_4OH solution to eliminate AgCl film on the silver microstructure surface. The %recovery was determined as 91.27%.
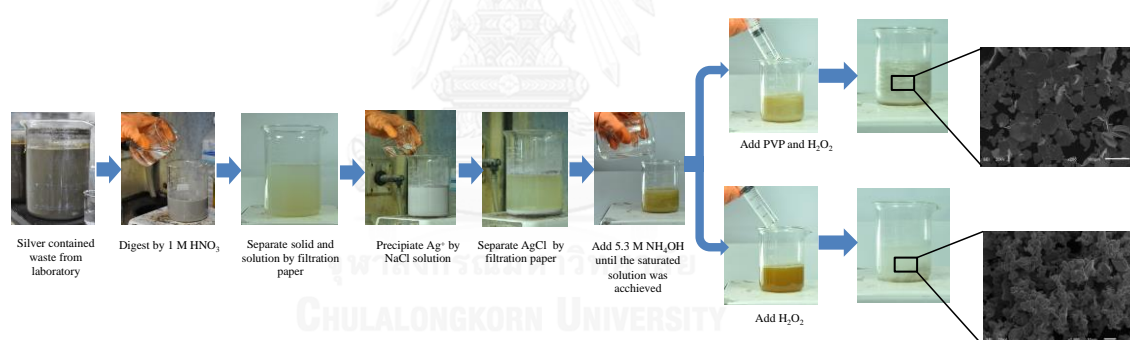
Figure 5.8 Protocol for silver recovery of silver contained waste from chemical research laboratory.

According to the high purity and specific morphology of the recovered product, the recovered silver microcrystals were applied as a raw material to produce silver clay for silver jewelry fabrication. Silver microcrystals were grinded and mixed with binders. The mixture was put in oven (~100° C for 2 hours) to get rid of humidity. The prepared silver clay exhibits soft features like clay that can be

fabricated the jewelry body by various techniques (molding, sculpturing, stamping, injecting and hand-making). This produced silver clay open a new window for the artists and designers to create an artwork piece with high complication. In the study, the synthesized silver clay are shaped by molding, stamping, and injecting and then sintered at 800° C for 30 minutes to obtain the jewelry product with a fine texture similar to be made from bulk silver by conventional technique. This is not possible to use silver with particle size larger than 10 micrometers as it requires very high temperature (>1000°C) for sintering process. SEM technique was used to determine the morphology of the sintering silver. The sintering profiles of our product were compared with the profiles obtained from using commercial silver clays (PMC3, Japan and SHANNTA, Thailand) as shown in Figure 5.9. From SEM images, it was found that silver microstructures were completely sintered. The sintering profiles were similar to the others except the number of pore and pore size. The diameter shrinkage of our product was comparable with the commercial products as shown in Table 5.5. In the final step, the created jewelry from various processes was polished to get shiny jewelry as shown in Figure 5.10.
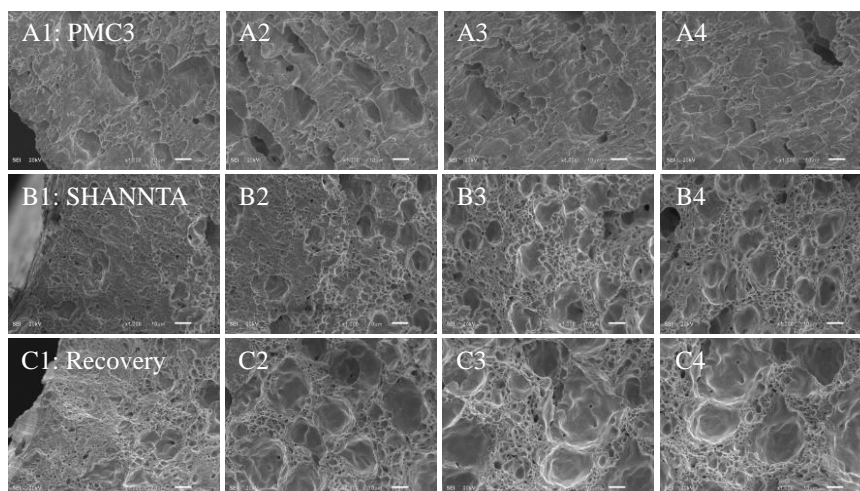
Figure 5.9 Comparison of sintering profile of silver clay from commercial products (A) PMC, the product from Japan, (B) SHANTA, the product from Thailand compared with (C) recovered silver clay. SEM micrographs were measured from surface (label by 1) to inner region (label by 4). All scale bars are 10 µm.
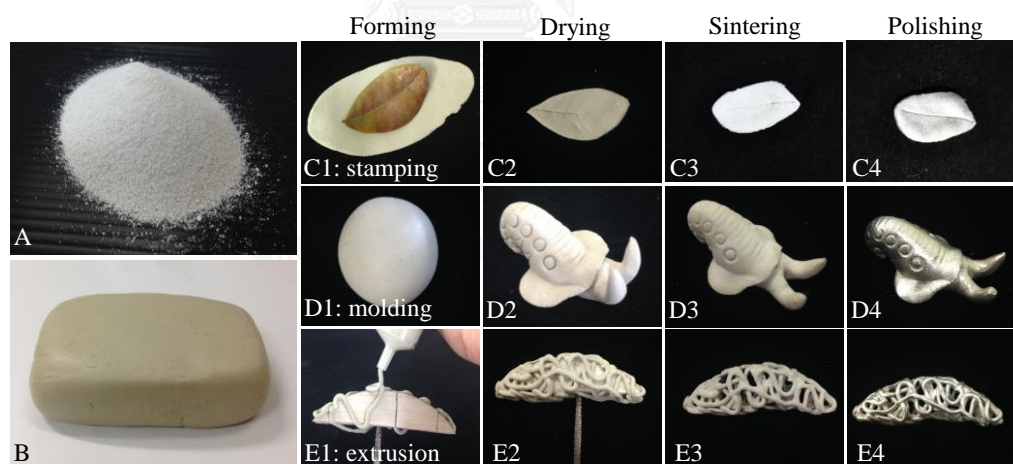
Figure 5.10 (A) Recovered silver microparticles were grinded in order to make the fine particles (B) silver clay was obtained from the mixing of recovered silver microcrystals with organic binder. The body of silver jewelry can be formed using different technique (C) stamping, (D) molding and (E) extrusion from syringe. To get the shiny silver jewelry, it will be dried to get rid of humidity, sintered at ~800 $^{\circ}$C to remove organic binder and polished to get a shiny surface.

Table 5.5 Percentage of diameter shrinkage of hand-making silver jewelry from commercial silver clays and silver clay from recovered silver.

Sample	Diameter shrinkage (%)
PMC3[a]	18
SHANNTA[b]	16
Silver clay from recovery process	18

[a] commercialized product form Japan

[b] commercialized product from Thailand

Herein, our recovery process offers the simple, rapid, highly and environmental friendly protocol to recover silver from silver- contained wastes. In addition, the recovered silver microcrystals are in high purity with microscale-size. This offers a good opportunity to be used as a raw material to produce silver clay for hand-making jewelry. The silver compositions can be sintered under house-oven temperature ($\sim$800° C). Furthermore, the physical properties are as good as a jewelry made from commercial silver-clay products.

5.4 CONCLUSIONS

We have developed a simple, rapid, highly efficient, and environmental friendly technique for a large scale recovery of silver wastes. The silver wastes in solid, slurry and liquid form could be converted to a highly pure and ready to use silver microcrystal. The reducing capability of H_2O_2 was explored for reducing silver ammine complex derived from AgCl. The morphology (*i.e.,* plates, icosahedra,

truncated cubes and quasi-spheres) of the highly pure (up to 99.99%) silver microcrystal can be selectively controlled by an addition of stabilizer, for example uniform silver microplates were solely obtained with PVP stabilizer. Our developed technique is highly economical as tab water with high Cl^- content can be employed. From the 3D response surface plot, the optimized conditions under the influences of pH, concentration of Ag^+ and the mole ratio of $H_2O_2:Ag^+$ were determined at the range of pH = 11.4–13.1, concentration of $Ag^+<0.42$ M, and mole ratio of $H_2O_2:Ag^+$ = 2.37–4.37. Without further purification and treatment, a direct usage of the recovered silver microcrystals as a raw material for wearable silver jewelry was explored as their size and morphology attend a high standard of silver clay specifications. The physical properties (sintering profile, shrinkage and surface property) of the silver jewelry made from the recovered silver microcrystals are comparable with those of the commercial products (PMC3, SHANNTA).

CHAPTER VI

CONCLUSION

We have successfully developed the morphology controlled chemical synthesis protocols of silver micro/nanostructures. The growth mechanisms of silver microplates, AgCl microcrystal and nanoporous silver microstructures were proposed. The research findings can be applied as large scale silver recovery from industry and laboratory wastes, catalysts, template for galvanic replacement reaction and silver clay. As the research topic in this work was categorized into 4 parts, this work could be concluded as follows.

6.1 RAPID FABRICATION OF SILVER MICROPLATES UNDER AN OXIDATIVE ETCHING ENVIRONMENT CONSISTING OF O_2/Cl^-, NH_4OH/H_2O_2, AND H_2O_2

In this work, we report a simple yet rapid protocol for a large scale synthesis of silver microplates (AgMPls) from silver ammine complex ($[Ag(NH_3)_2]^+$) under an etching environment containing O_2/Cl^-, NH_4OH/H_2O_2, and H_2O_2 capable of dissolving silver crystals except plate structures. H_2O_2 is employed as the sole reducing agent. Chloride ions are essential for creating etching environment capable of selective dissolution of single and multiply twinned crystals, while leaving plate structures unaffected. Without chloride ions, H_2O_2 reduces $[Ag(NH_3)_2]^+$ complex to silver microparticles containing truncated cubes, icosahedra, pentagonal rods, and

plate microstructures with icosahedra as the major product. The developed protocol enables an environmental friendly fabrication of highly pure AgMPls and AgMPs directly from AgCl precipitate.

6.2 3D AgCl MICROSTRUCTURES SELECTIVELY FABRICATED *VIA* A Cl⁻-INDUCED PRECIPITATION FROM $[Ag(NH_3)_2]^+$

Various AgCl microstructures including octapods, octapods with fishbone pods, hexapods, hexapods with 4-blade arrowhead pods, concave octahedrons, and octahedrons are selectively precipitated from $[Ag(NH_3)_2]^+$ solution by an addition of Cl⁻. The AgCl microstructures were rapidly formed and precipitated within 5 min. In a Cl⁻-rich environment, the octapod grew from cubic seeds as the growth along <111> directions was favorable. The hexapod, on the other hand, grew from octahedral seeds in an NH_4OH-rich environment as the growth along <100> directions was dominated. By manipulating the seed morphology and the growth environment, complex AgCl microstructures of thermodynamically unfavorable structures (hexapods and octahedrons) can be selectively fabricated. By a partial photo-reduction of the surface AgCl into isolated AgNPs, the fabricated AgCl microstructures were turned into an efficient Ag@AgCl visible-light photocatalyst as a completed decomposition of methyl orange was achieved within 20 min. This work not only explores a method to control the preferential growth along <100> and <111> directions of AgCl microstructures, but also provides an in-depth understanding on the crystal growth mechanisms and how to manipulate them efficiently.

6.3 3D NANOPOROUS Ag MICROSTRUCTURES FABRICATED FROM AgCl MICROCRYSTAL TEMPLATES *VIA* CONCERTED OXIDATIVE ETCHING/RE-DEPOSITION AND GALVANIC REPLACEMENT

3D nanoporous Ag microstructures (np-AgMSs) were successfully fabricated from AgCl microcrystal templates by galvanic replacement approach with sacrificial Zn metal. This simple, rapid, and stabilizer-free protocol preserves the initial morphologies of AgCl microcrystal templates. Chloride ion is proven an essential ingredient in electrolyte as it facilitates the oxidation reaction that liberation of electron from the sacrificial Zn metal. The formation mechanism of np-AgMSs is proposed *via* the reduction of the mobile Ag^+ dissolved from AgCl at the AgCl/metal interfaces. The concerting reactions between oxidative etching of np-AgMSs (by Cl^- and Cl^-/O_2) and re-deposition of Ag atoms convert large silver grains to small silver grains. The grain size of np-AgMSs can be tuned by adjusting the concentration of Cl^-. The np-AgMSs are efficient catalyst for the reduction of *p*-nitrophenol by $NaBH_4$.

6.4 ECO-FRIENDLY PROCESS FOR RECOVERY OF SILVER WASTE BY H_2O_2-INDUCED FORMATION OF SILVER MICROCRYSTAL FROM AgCl PRECIPITATES

In this study, a simple, rapid, highly efficient, and environmentally friendly process for converting industrial and laboratory wastes into highly pure silver microcrystals (>99.99%) was developed. Various forms of silver wastes (solid, slurry, solution, stabilized nanoparticles) were leached and precipitated into AgCl before dissolving into water soluble silver ammine complex. We use H_2O_2 to reduce silver

ammine complex into microcrystalline silver. Microcrystals of various morphologies (*i.e.*, plates, icosahedra, truncated cubes and quasi-spheres) could be selectively produced by an addition of PVP. One particular advantage of this technique is its flexibility where tab water with high Cl^- content can be used without losing of efficiency. The central composite design (CCD) investigation suggested that pH and the mole ratio of $H_2O_2:Ag^+$ strongly influence to the recovery efficiency. The optimal recovery condition could be precisely selected *via* response surface methodology (RSM). The predicted condition was employed for a trial recovery of silver ammine complex prepared from a collection of silver waste during 3-years research on industrial silver nanoparticle production. A 50-L solution of silver ammine complex with silver content of >700 grams could be recovered with 91.27% efficiency. A set of wearable silver jewelries was successfully fabricated from homemade silver clay prepared directly from the recovered silver microcrystals.

REFERENCES

1. Xia, Y., Xiong, Y., Lim, B., and Skrabalak, S.E., Shape-controlled synthesis of metal nanocrystals: Simple chemistry meets complex physics? *Angewandte Chemie International Edition*, **2009**. *48*, 60-103.

2. Wiley, B., Herricks, T., Sun, Y., and Xia, Y., Polyol synthesis of silver nanoparticles: Use of chloride and oxygen to promote the formation of single-crystal, truncated cubes and tetrahedrons. *Nano Letters*, **2004**. *4*, 1733-1739.

3. Kim, F., Song, J.H., and Yang, P., Photochemical synthesis of gold nanorods. *Journal of the American Chemical Society*, **2002**. *124*, 14316-14317.

4. Du, J., Han, B., Liu, Z., Liu, Y., and Kang, D.J., Control synthesis of silver nanosheets, chainlike sheets, and microwires *via* a simple solvent−thermal method. *Crystal Growth & Design*, **2007**. *7*, 900-904.

5. Zhang, S.-H., Jiang, Z.-Y., Xie, Z.-X., Xu, X., Huang, R.-B., and Zheng, L.-S., Growth of silver nanowires from solutions: A cyclic penta-twinned-crystal growth mechanism. *The Journal of Physical Chemistry B*, **2005**. *109*, 9416-9421.

6. Tang, B., Xu, S., An, J., Zhao, B., and Xu, W., Photoinduced shape conversion and reconstruction of silver nanoprisms. *The Journal of Physical Chemistry C*, **2009**. *113*, 7025-7030.

7. Yang, J., Zhang, Q., Lee, J.Y., and Too, H.-P., Dissolution–recrystallization mechanism for the conversion of silver nanospheres to triangular nanoplates. *Journal of Colloid and Interface Science*, **2007**. *308*, 157-161.

8.   Zaheer, Z. and Rafiuddin, Crystal growth of different morphologies (nanospheres, nanoribbons and nanoplates) of silver nanoparticles. *Colloids and Surfaces A: Physicochemical and Engineering Aspects*, **2012**. *393*, 1-5.

9.   Deng, Z., Mansuipur, M., and Muscat, A.J., New method to single-crystal micrometer-sized ultra-thin silver nanosheets: synthesis and characterization. *The Journal of Physical Chemistry C*, **2008**. *113*, 867-873.

10.   Chen, H., Kern, E., Ziegler, C., and Eychmüller, A., Ultrasonically assisted synthesis of 3D hierarchical silver microstructures. *The Journal of Physical Chemistry C*, **2009**. *113*, 19258-19262.

11.   Dai, L., Chi, Q., Zhao, Y., Liu, H., Zhou, Z., Li, J., and Huang, T., Controlled synthesis of novel octapod platinum nanocrystals under microwave irradiation. *Materials Research Bulletin*, **2014**. *49*, 413-419.

12.   Maksimuk, S., Teng, X., and Yang, H., Roles of twin defects in the formation of platinum multipod nanocrystals. *The Journal of Physical Chemistry C*, **2007**. *111*, 14312-14319.

13.   Ma, L., Wang, C., Gong, M., Liao, L., Long, R., Wang, J., Wu, D., Zhong, W., Kim, M.J., Chen, Y., Xie, Y., and Xiong, Y., Control over the branched structures of platinum nanocrystals for electrocatalytic applications. *ACS Nano*, **2012**. *6*, 9797-9806.

14.   LaMer, V.K. and Dinegar, R.H., Theory, production and mechanism of formation of monodispersed hydrosols. *Journal of the American Chemical Society*, **1950**. *72*, 4847-4854.

15.   Gai, P.L. and Harmer, M.A., Surface atomic defect structures and growth of gold nanorods. *Nano Letters*, **2002**. *2*, 771-774.

16.   Burda, C., Chen, X., Narayanan, R., and El-Sayed, M.A., Chemistry and properties of nanocrystals of different shapes. *Chemical Reviews*, **2005**. *105*, 1025-1102.

17.   Morin, S.A., Forticaux, A., Bierman, M.J., and Jin, S., Screw dislocation-driven growth of two-dimensional nanoplates. *Nano Letters*, **2011**. *11*, 4449-4455.

18.   Meng, F., Morin, S.A., Forticaux, A., and Jin, S., Screw dislocation driven growth of nanomaterials. *Accounts of Chemical Research*, **2013**. *46*, 1616-1626.

19.   Wiley, B.J., Xiong, Y., Li, Z.-Y., Yin, Y., and Xia, Y., Right bipyramids of silver: A new shape derived from single twinned seeds. *Nano Letters*, **2006**. *6*, 765-768.

20.   Wiley, B.J., Chen, Y., McLellan, J.M., Xiong, Y., Li, Z.-Y., Ginger, D., and Xia, Y., Synthesis and optical properties of silver nanobars and nanorice. *Nano Letters*, **2007**. *7*, 1032-1036.

21.   Xiong, Y., Chen, J., Wiley, B., Xia, Y., Aloni, S., and Yin, Y., Understanding the role of oxidative etching in the polyol synthesis of Pd nanoparticles with uniform shape and size. *Journal of the American Chemical Society*, **2005**. *127*, 7332-7333.

22.   Xiong, Y., Wiley, B., Chen, J., Li, Z.-Y., Yin, Y., and Xia, Y., Corrosion-based synthesis of single-crystal Pd nanoboxes and nanocages and their surface plasmon properties. *Angewandte Chemie*, **2005**. *117*, 8127-8131.

23.   Zettsu, N., McLellan, J.M., Wiley, B., Yin, Y., Li, Z.-Y., and Xia, Y., Synthesis, stability, and surface plasmonic properties of rhodium multipods,

and their use as substrates for surface-enhanced Raman scattering. *Angewandte Chemie*, **2006**. *118*, 1310-1314.

24. Sun, Y., Mayers, B., Herricks, T., and Xia, Y., Polyol synthesis of uniform silver nanowires: a plausible growth mechanism and the supporting evidence. *Nano Letters*, **2003**. *3*, 955-960.

25. Xiong, Y. and Xia, Y., Shape-controlled synthesis of metal nanostructures: The case of palladium. *Advanced Materials*, **2007**. *19*, 3385-3391.

26. Xiong, Y., McLellan, J.M., Yin, Y., and Xia, Y., Synthesis of palladium icosahedra with twinned structure by blocking oxidative etching with citric acid or citrate Ions. *Angewandte Chemie International Edition*, **2007**. *46*, 790-794.

27. Tsuji, M., Gomi, S., Maeda, Y., Matsunaga, M., Hikino, S., Uto, K., Tsuji, T., and Kawazumi, H., Rapid transformation from spherical nanoparticles, nanorods, cubes, or bipyramids to triangular prisms of silver with PVP, citrate, and H_2O_2. *Langmuir*, **2012**. *28*, 8845-8861.

28. Carrasquillo, A., Jeng, J.-J., Barriga, R.J., Temesghen, W.F., and Soriaga, M.P., Electrode-surface coordination chemistry: ligand substitution and competitive coordination of halides at well-defined Pd(100) and Pd(111) single crystals. *Inorganica Chimica Acta*, **1997**. *255*, 249-254.

29. Schimpf, J.A., Abreu, J.B., and Soriaga, M.P., Electrochemical regeneration of clean and ordered Pd(100) surfaces by iodine adsorption-desorption: evidence from low-energy electron diffraction. *Journal of Electroanalytical Chemistry*, **1994**. *364*, 247-249.

30. Huang, H.H., Ni, X.P., Loy, G.L., Chew, C.H., Tan, K.L., Loh, F.C., Deng, J.F., and Xu, G.Q., Photochemical formation of silver nanoparticles in poly(N-vinylpyrrolidone). *Langmuir*, **1996**. *12*, 909-912.

31. Zhang, Z., Zhao, B., and Hu, L., PVP protective mechanism of ultrafine silver powder synthesized by chemical reduction processes. *Journal of Solid State Chemistry*, **1996**. *121*, 105-110.

32. Bonet, F., Tekaia-Elhsissen, K., and Sarathy, K.V., Study of interaction of ethylene glycol/PVP phase on noble metal powders prepared by polyol process. *Bulletin of Materials Science*, **2000**. *23*, 165-168.

33. Gao, Y., Jiang, P., Liu, D.F., Yuan, H.J., Yan, X.Q., Zhou, Z.P., Wang, J.X., Song, L., Liu, L.F., Zhou, W.Y., Wang, G., Wang, C.Y., Xie, S.S., Zhang, J.M., and Shen, D.Y., Evidence for the monolayer assembly of poly(vinylpyrrolidone) on the surfaces of silver nanowires. *The Journal of Physical Chemistry B*, **2004**. *108*, 12877-12881.

34. Xia, X., Zeng, J., Zhang, Q., Moran, C.H., and Xia, Y., Recent developments in shape-controlled synthesis of silver nanocrystals. *The Journal of Physical Chemistry C*, **2012**. *116*, 21647-21656.

35. Im, S.H., Lee, Y.T., Wiley, B., and Xia, Y., Large-scale synthesis of silver nanocubes: The role of HCl in promoting cube perfection and monodispersity. *Angewandte Chemie*, **2005**. *117*, 2192-2195.

36. Tang, X., Tsuji, M., Jiang, P., Nishio, M., Jang, S.-M., and Yoon, S.-H., Rapid and high-yield synthesis of silver nanowires using air-assisted polyol method with chloride ions. *Colloids and Surfaces A: Physicochemical and Engineering Aspects*, **2009**. *338*, 33-39.

37.   Xu, S., Tang, B., Zheng, X., Zhou, J., An, J., Ning, X., and Xu, W., The facet selectivity of inorganic ions on silver nanocrystals in etching reactions. *Nanotechnology*, **2009**. *20*, 1-7.

38.   Cobley, C.M., Rycenga, M., Zhou, F., Li, Z.-Y., and Xia, Y., Controlled etching as a route to high quality silver nanospheres for optical studies. *The Journal of Physical Chemistry C*, **2009**. *113*, 16975-16982.

39.   Mulvihill, M.J., Ling, X.Y., Henzie, J., and Yang, P., Anisotropic etching of silver nanoparticles for plasmonic structures capable of single-particle SERS. *Journal of the American Chemical Society*, **2009**. *132*, 268-274.

40.   Aloisi, G., Funtikov, A.M., and Will, T., Chloride adsorption on Ag(111) studied by in-situ scanning tunnelling microscopy. *Journal of Electroanalytical Chemistry*, **1994**. *370*, 297-300.

41.   Beltramo, G. and Santos, E., Characterisation of chloride and bromide specific adsorption process on silver single crystal surfaces by impedance spectroscopy: Part I. An extended model to obtain the charge density from impedance spectra applied to Ag(111) at low concentrations of halides. *Journal of Electroanalytical Chemistry*, **2003**. *556*, 127-136.

42.   Foresti, M.L., Innocenti, M., Loglio, F., Becucci, L., and Guidelli, R., Chloride and iodide electrosorption on Ag(111). *Journal of Electroanalytical Chemistry*, **2010**. *649*, 89-94.

43.   Jović, B.M., Jović, V.D., and Dražić, D.M., Kinetics of chloride ion adsorption and the mechanism of AgCl layer formation on the (111), (100) and (110) faces of silver. *Journal of Electroanalytical Chemistry*, **1995**. *399*, 197-206.

44. Temsamani, K.R. and Lu Cheng, K., Studies of chloride adsorption on the Ag/AgCl electrode. *Sensors and Actuators B: Chemical*, **2001**. *76*, 551-555.

45. Andryushechkin, B.V., Eltsov, K.N., and Shevlyuga, V.M., Atomic structure of silver chloride formed on Ag(111) surface upon low temperature chlorination. *Surface Science*, **1999**. *433–435*, 109-113.

46. Stevenson, K.J., Gao, X., W. Hatchett, D., and White, H.S., Voltammetric measurement of anion adsorption on Ag(111). *Journal of Electroanalytical Chemistry*, **1998**. *447*, 43-51.

47. Gatemala, H., Pienpinijtham, P., Thammacharoen, C., and Ekgasit, S., Rapid fabrication of silver microplates under an oxidative etching environment consisting of O_2/Cl^-, NH_4OH/H_2O_2, and H_2O_2. *CrystEngComm*, **2015**. *17*, 5530-5537.

48. Gatemala, H., Thammacharoen, C., and Ekgasit, S., 3D AgCl microstructures selectively fabricated *via* Cl^--induced precipitation from $[Ag(NH_3)_2]^+$. *CrystEngComm*, **2014**. *16*, 6688-6696.

49. Khan, Z., Hussain, J.I., Kumar, S., and Hashmi, A.A., Silver nanoplates and nanowires by a simple chemical reduction method. *Colloids and Surfaces B: Biointerfaces*, **2011**. *86*, 87-92.

50. Luo, X., Li, Z., Yuan, C., and Chen, Y., Polyol synthesis of silver nanoplates: The crystal growth mechanism based on a rivalrous adsorption. *Materials Chemistry and Physics*, **2011**. *128*, 77-82.

51. Xia, Y. and Halas, N.J., Shape-controlled synthesis and surface plasmonic properties of metallic nanostructures. *MRS Bulletin*, **2005**. *30*, 338-348.

52. Catchpole, K.R. and Polman, A., Design principles for particle plasmon enhanced solar cells. *Applied Physics Letters*, **2008**. *93*, 191113-191113-3.

53. Wentworth, R.L., *The mechanism of the catalytic decomposition of hydrogen peroxide by silver*. 1951: M.I.T. Division of Industrial Cooperation.

54. Maggs, F.T. and Sutton, D., Some aspects of the catalytic decomposition of concentrated hydrogen peroxide by silver. Part 1.-The solubility and rate of solution of silver. *Transactions of the Faraday Society*, **1958**. *54*, 1861-1870.

55. Bagg, J., The catalytic decomposition of hydrogen peroxide solutions by single crystals of silver. *Australian Journal of Chemistry*, **1962**. *15*, 201-210.

56. Zhang, Q., Li, N., Goebl, J., Lu, Z., and Yin, Y., A systematic study of the synthesis of silver nanoplates: Is citrate a "magic" reagent? *Journal of the American Chemical Society*, **2011**. *133*, 18931-18939.

57. Li, N., Zhang, Q., Quinlivan, S., Goebl, J., Gan, Y., and Yin, Y., H_2O_2-aided seed-mediated synthesis of silver nanoplates with improved yield and efficiency. *ChemPhysChem*, **2012**. *13*, 2526-2530.

58. Parnklang, T., Lertvachirapaiboon, C., Pienpinijtham, P., Wongravee, K., Thammacharoen, C., and Ekgasit, S., H_2O_2-triggered shape transformation of silver nanospheres to nanoprisms with controllable longitudinal LSPR wavelengths. *RSC Advances*, **2013**. *3*, 12886-12894.

59. Nootchanat, S., Thammacharoen, C., Lohwongwatana, B., and Ekgasit, S., Formation of large H_2O_2-reduced gold nanosheets *via* starch-induced two-dimensional oriented attachment. *RSC Advances*, **2013**. *3*, 3707-3716.

60. Chen, H., Simon, F., and Eychmüller, A., Large-scale synthesis of micrometer-sized silver nanosheets. *The Journal of Physical Chemistry C*, **2010**. *114*, 4495-4501.

61. Cui, G., Qi, S., Wang, X., Tian, G., Sun, G., Liu, W., Yan, X., Wu, D., Wu, Z., and Zhang, L., Interfacial growth of controllable morphology of silver patterns on plastic substrates. *The Journal of Physical Chemistry B*, **2012**. *116*, 12349-12356.

62. David, R.L., ed. *CRC Handbook of Chemistry and Physics*. 90th Edition (CD-ROM Version 2010) ed. 2010, CRC Press: Boca Raton, Florida.

63. Ajayan, P.M. and Marks, L.D., Quasimelting and phases of small particles. *Physical Review Letters*, **1988**. *60*, 585-587.

64. Nasanen, R., Equilibrium in ammonical solution of silver nitrate. *Acta Chemica Scadinavica*, **1947**. *1*, 763-769.

65. Ho, C.-M., Yau, S.K.-W., Lok, C.-N., So, M.-H., and Che, C.-M., Oxidative dissolution of silver nanoparticles by biologically relevant oxidants: A kinetic and mechanistic study. *Chemistry – An Asian Journal*, **2010**. *5*, 285-293.

66. Lee, Y.-I., Kim, S., Jung, S.-B., Myung, N.V., and Choa, Y.-H., Enhanced electrical and mechanical properties of silver nanoplatelet-based conductive features direct printed on a flexible substrate. *ACS Applied Materials & Interfaces*, **2013**. *5*, 5908-5913.

67. Duke, F.R. and Haas, T.W., The homogeneous base-catalyzed decomposition of hydrogen peroxide. *The Journal of Physical Chemistry*, **1961**. *65*, 304-306.

68.   Panda, B.R. and Chattopadhyay, A., Synthesis of Au nanoparticles at "all" pH by H_2O_2 reduction of $HAuCl_4$. *Journal of Nanoscience and Nanotechnology*, **2007**. *7*, 1911-1915.

69.   Jana, D. and De, G., Spontaneous generation and shape conversion of silver nanoparticles in alumina sol, and shaped silver nanoparticle incorporated alumina films. *Journal of Materials Chemistry*, **2011**. *21*, 6072-6078.

70.   Xia, X., Zeng, J., Oetjen, L.K., Li, Q., and Xia, Y., Quantitative analysis of the role played by poly(vinylpyrrolidone) in seed-mediated growth of Ag nanocrystals. *Journal of the American Chemical Society*, **2011**. *134*, 1793-1801.

71.   Chuang, J.C., Haldar, R.K., Merianos, J.J., Shih, J.S., and Smith, T.E., *Strongly swellable, moderately crosslinked polyvinylpyrrolidone*. 1993, WIPO Patent

72.   Kunda, W., *Process for the production of elemental silver from silver chloride or silver sulphate*. 1981, U.S. Patent.

73.   Merianos, J.J., *Anhydrous complexes of PVP and hydrogen peroxide*. 1991, U.S. Patent.

74.   Panarin, E.F., Kalninsh, K.K., and Pestov, D.V., Complexation of hydrogen peroxide with polyvinylpyrrolidone: ab initio calculations. *European Polymer Journal*, **2001**. *37*, 375-379.

75.   Aherne, D., Ledwith, D.M., Gara, M., and Kelly, J.M., Optical properties and growth aspects of silver nanoprisms produced by a highly reproducible and rapid synthesis at room temperature. *Advanced Functional Materials*, **2008**. *18*, 2005-2016.

76. Goebl, J., Zhang, Q., He, L., and Yin, Y., Monitoring the shape evolution of silver nanoplates: A marker study. *Angewandte Chemie International Edition*, **2012**. *51*, 552-555.

77. Bowker, M., An XPS investigation of the chloridation of Ag(110). *Journal of Electron Spectroscopy and Related Phenomena*, **1986**. *37*, 319-327.

78. Briggs, D., Marbrow, R.A., and Lambert, R.M., An XPS and ups study of chloride chemisorption on Ag(110). *Chemical Physics Letters*, **1978**. *53*, 462-464.

79. Sharma, J., DiBona, P., and Wiegand, D.A., XPS studies of the photodecomposition of AgCl. *Applications of Surface Science*, **1982**. *11–12*, 420-424.

80. Strydom, C.A., van Staden, J.F., and Strydom, H.J., An XPS investigation of silver chloride coated ion-selective electrodes. *Journal of Electroanalytical Chemistry and Interfacial Electrochemistry*, **1990**. *277*, 165-177.

81. Hecht, D. and Strehblow, H.H., XPS investigations of the electrochemical double layer on silver in alkaline chloride solutions. *Journal of Electroanalytical Chemistry*, **1997**. *440*, 211-217.

82. Prieto, P., Nistor, V., Nouneh, K., Oyama, M., Abd-Lefdil, M., and Díaz, R., XPS study of silver, nickel and bimetallic silver–nickel nanoparticles prepared by seed-mediated growth. *Applied Surface Science*, **2012**. *258*, 8807-8813.

83. Chen, A., Kamata, K., Nakagawa, M., Iyoda, T., Haiqiao, and Li, X., Formation process of silver−polypyrrole coaxial nanocables synthesized by redox reaction between $AgNO_3$ and pyrrole in the presence of

poly(vinylpyrrolidone). *The Journal of Physical Chemistry B*, **2005**. *109*, 18283-18288.

84. Mdluli, P.S., Sosibo, N.M., Mashazi, P.N., Nyokong, T., Tshikhudo, R.T., Skepu, A., and van der Lingen, E., Selective adsorption of PVP on the surface of silver nanoparticles: A molecular dynamics study. *Journal of Molecular Structure*, **2011**. *1004*, 131-137.

85. Rycenga, M., Cobley, C.M., Zeng, J., Li, W., Moran, C.H., Zhang, Q., Qin, D., and Xia, Y., Controlling the synthesis and assembly of silver nanostructures for plasmonic applications. *Chemical Reviews*, **2011**. *111*, 3669-3712.

86. Wang, H., Qiao, X., Chen, J., Wang, X., and Ding, S., Mechanisms of PVP in the preparation of silver nanoparticles. *Materials Chemistry and Physics*, **2005**. *94*, 449-453.

87. Chen, W.-T., Ma, C.-C., Lee, M.-H., Chu, Y.-C., Tsai, L.-C., and Shu, C.-M., Silver recovery and chemical oxygen demand (COD) removal from waste fixer solutions. *Applied Energy*, **2012**. *100*, 187-192.

88. Aktas, S., Silver recovery from spent silver oxide button cells. *Hydrometallurgy*, **2010**. *104*, 106-111.

89. Lee, C.W. and Fung, K.W., Recovery of silver and mercury from dental amalgam waste. *Resource Recovery and Conservation*, **1981**. *5*, 363-371.

90. Pethkar, A.V., Kulkarni, S.K., and Paknikar, K.M., Comparative studies on metal biosorption by two strains of Cladosporium cladosporioides. *Bioresource Technology*, **2001**. *80*, 211-215.

91. Sathaiyan, N., Nandakumar, V., and Ramachandran, P., Hydrometallurgical recovery of silver from waste silver oxide button cells. *Journal of Power Sources*, **2006**. *161*, 1463-1468.

92. Cheong, S., Watt, J., Ingham, B., Toney, M.F., and Tilley, R.D., In-situ and ex-situ studies of platinum nanocrystals: Growth and evolution in solution. *Journal of the American Chemical Society*, **2009**. *131*, 14590-14595.

93. Chen, J., Herricks, T., and Xia, Y., Polyol synthesis of platinum nanostructures: Control of morphology through the manipulation of reduction kinetics. *Angewandte Chemie*, **2005**. *117*, 2645-2648.

94. Jin, M., Zhang, H., Xie, Z., and Xia, Y., Palladium concave nanocubes with high-index facets and their enhanced catalytic properties. *Angewandte Chemie International Edition*, **2011**. *50*, 7850-7854.

95. Yu, T., Kim, D.Y., Zhang, H., and Xia, Y., Platinum concave nanocubes with high-index facets and their enhanced activity for oxygen reduction reaction. *Angewandte Chemie International Edition*, **2011**. *50*, 2773-2777.

96. Dong, R., Tian, B., Zeng, C., Li, T., Wang, T., and Zhang, J., Ecofriendly synthesis and photocatalytic activity of uniform cubic Ag@AgCl plasmonic photocatalyst. *The Journal of Physical Chemistry C*, **2012**. *117*, 213-220.

97. Wang, P., Huang, B., Qin, X., Zhang, X., Dai, Y., Wei, J., and Whangbo, M.-H., Ag@AgCl: A highly efficient and stable photocatalyst active under visible light. *Angewandte Chemie International Edition*, **2008**. *47*, 7931-7933.

98. Wang, P., Huang, B., Zhang, Q., Zhang, X., Qin, X., Dai, Y., Zhan, J., Yu, J., Liu, H., and Lou, Z., Highly efficient visible light plasmonic photocatalyst Ag@Ag(Br,I). *Chemistry – A European Journal*, **2010**. *16*, 10042-10047.

99.   Wang, P., Huang, B., Zhang, X., Qin, X., Jin, H., Dai, Y., Wang, Z., Wei, J., Zhan, J., Wang, S., Wang, J., and Whangbo, M.-H., Highly efficient Visible-light plasmonic photocatalyst Ag@AgBr. *Chemistry – A European Journal*, **2009**. *15*, 1821-1824.

100.   Zhang, Q., Ge, J., Pham, T., Goebl, J., Hu, Y., Lu, Z., and Yin, Y., Reconstruction of silver nanoplates by UV irradiation: Tailored optical properties and enhanced stability. *Angewandte Chemie International Edition*, **2009**. *48*, 3516-3519.

101.   Cheng, L., Ma, C., Yang, G., You, H., and Fang, J., Hierarchical silver mesoparticles with tunable surface topographies for highly sensitive surface-enhanced Raman spectroscopy. *Journal of Materials Chemistry A*, **2014**. *2*, 4534-4542.

102.   Kimijima, K.i. and Sugimoto, T., Growth mechanism of AgCl nanoparticles in a reverse micelle system. *The Journal of Physical Chemistry B*, **2004**. *108*, 3735-3738.

103.   Zhu, M., Chen, P., and Liu, M., High-performance visible-light-driven plasmonic photocatalysts Ag/AgCl with controlled size and shape using graphene oxide as capping agent and catalyst promoter. *Langmuir*, **2013**. *29*, 9259-9268.

104.   An, C., Peng, S., and Sun, Y., Facile synthesis of sunlight-driven AgCl:Ag plasmonic nanophotocatalyst. *Advanced Materials*, **2010**. *22*, 2570-2574.

105.   Chen, D., Yoo, S.H., Huang, Q., Ali, G., and Cho, S.O., Sonochemical synthesis of Ag/AgCl nanocubes and their efficient visible-light-driven

photocatalytic performance. *Chemistry – A European Journal*, **2012**. *18*, 5192-5200.

106.   Lou, Z., Huang, B., Wang, Z., Qin, X., Zhang, X., Liu, Y., Zhang, R., Dai, Y., and Whangbo, M.-H., Interface kinetic diffusion reaction leading to fast and continuous generation of AgCl nanocubes in NaCl solution. *Dalton Transactions*, **2013**. *42*, 15219-15225.

107.   Tang, Y., Jiang, Z., Xing, G., Li, A., Kanhere, P.D., Zhang, Y., Sum, T.C., Li, S., Chen, X., Dong, Z., and Chen, Z., Efficient Ag@AgCl cubic cage photocatalysts profit from ultrafast plasmon-induced electron transfer processes. *Advanced Functional Materials*, **2013**. *23*, 2932-2940.

108.   Lou, Z., Huang, B., Ma, X., Zhang, X., Qin, X., Wang, Z., Dai, Y., and Liu, Y., A 3D AgCl hierarchical superstructure synthesized by a wet chemical oxidation method. *Chemistry – A European Journal*, **2012**. *18*, 16090-16096.

109.   Lou, Z., Huang, B., Qin, X., Zhang, X., Cheng, H., Liu, Y., Wang, S., Wang, J., and Dai, Y., One-step synthesis of AgCl concave cubes by preferential overgrowth along <111> and <110> directions. *Chemical Communications*, **2012**. *48*, 3488-3490.

110.   Maudos, I., Chimenos, J.M., Segarra, M., and Espiell, F., Kinetic study of silver chloride dissolution in complexating media. *Hydrometallurgy*, **1996**. *40*, 153-167.

111.   Zhang, H., Jin, M., Xiong, Y., Lim, B., and Xia, Y., Shape-controlled synthesis of Pd nanocrystals and their catalytic applications. *Accounts of Chemical Research*, **2012**. *46*, 1783-1794.

112. Ma, X., Dai, Y., Lu, J., Guo, M., and Huang, B., Tuning of the surface-exposing and photocatalytic activity for AgX (X = Cl and Br): A theoretical study. *The Journal of Physical Chemistry C*, **2012**. *116*, 19372-19378.

113. Liu, X., Zhang, F., Huang, R., Pan, C., and Zhu, J., Capping modes in PVP-directed silver nanocrystal growth: multi-twinned nanorods versus single-crystalline nano-hexapods. *Crystal Growth & Design*, **2008**. *8*, 1916-1923.

114. Formo, E.V., Fu, W., Rondinone, A.J., and Dai, S., Utilizing AgCl:Ag and AgCl mesostructures as solid precursors in the formation of highly textured silver nanomaterials *via* electron-beam induced decomposition. *RSC Advances*, **2012**. *2*, 9359-9361.

115. Luo, X., Lian, S., Wang, L., Yang, S., Yang, Z., Ding, B., and Song, X., Volume shrinkage induced formation of porous Ag sub-microcubes *via* solid-liquid reaction for SERS. *CrystEngComm*, **2013**. *15*, 2588-2591.

116. Chen, J., Wiley, B., McLellan, J., Xiong, Y., Li, Z.-Y., and Xia, Y., Optical properties of Pd−Ag and Pt−Ag nanoboxes synthesized *via* galvanic replacement reactions. *Nano Letters*, **2005**. *5*, 2058-2062.

117. Lu, X., Tuan, H.-Y., Chen, J., Li, Z.-Y., Korgel, B.A., and Xia, Y., Mechanistic studies on the galvanic replacement reaction between multiply twinned particles of Ag and HAuCl4 in an organic medium. *Journal of the American Chemical Society*, **2007**. *129*, 1733-1742.

118. Hong, X., Wang, D., Cai, S., Rong, H., and Li, Y., Single-crystalline octahedral Au−Ag nanoframes. *Journal of the American Chemical Society*, **2012**. *134*, 18165-18168.

119. Zhang, Q., Lee, Y.H., Phang, I.Y., Pedireddy, S., Tjiu, W.W., and Ling, X.Y., Bimetallic platonic Janus nanocrystals. *Langmuir*, **2013**. *29*, 12844-12851.

120. Li, J., Yang, W., Ning, J., Zhong, Y., and Hu, Y., Rapid formation of AgnX(X = S, Cl, PO4, C2O4) nanotubes via an acid-etching anion exchange reaction. *Nanoscale*, **2014**.

121. Chen, D., Liu, M., Chen, Q., Ge, L., Fan, B., Wang, H., Lu, H., Yang, D., Zhang, R., Yan, Q., Shao, G., Sun, J., and Gao, L., Large-scale synthesis and enhanced visible-light-driven photocatalytic performance of hierarchical Ag/AgCl nanocrystals derived from freeze-dried PVP–Ag$^+$ hybrid precursors with porosity. *Applied Catalysis B: Environmental*, **2014**. *144*, 394-407.

122. Ai, L., Zhang, C., and Jiang, J., Hierarchical porous AgCl@Ag hollow architectures: Self-templating synthesis and highly enhanced visible light photocatalytic activity. *Applied Catalysis B: Environmental*, **2013**. *142–143*, 744-751.

123. Jiang, J. and Zhang, L., Rapid microwave-assisted nonaqueous synthesis and growth mechanism of AgCl/Ag, and its daylight-driven plasmonic photocatalysis. *Chemistry – A European Journal*, **2011**. *17*, 3710-3717.

124. Hieda, M., Garcia, R., Dixon, M., Daniel, T., Allara, D., and Chan, M.H.W., Ultrasensitive quartz crystal microbalance with porous gold electrodes. *Applied Physics Letters*, **2004**. *84*, 628-630.

125. Stein, A., Sphere templating methods for periodic porous solids. *Microporous and Mesoporous Materials*, **2001**. *44–45*, 227-239.

126. Jin, H.-J., Wang, X.-L., Parida, S., Wang, K., Seo, M., and Weissmüller, J., Nanoporous Au−Pt alloys as large strain electrochemical actuators. *Nano Letters*, **2010**. *10*, 187-194.

127. Xu, C., Xu, X., Su, J., and Ding, Y., Research on unsupported nanoporous gold catalyst for CO oxidation. *Journal of Catalysis*, **2007**. *252*, 243-248.

128. Zeis, R., Lei, T., Sieradzki, K., Snyder, J., and Erlebacher, J., Catalytic reduction of oxygen and hydrogen peroxide by nanoporous gold. *Journal of Catalysis*, **2008**. *253*, 132-138.

129. Wang, X., Wang, W., Qi, Z., Zhao, C., Ji, H., and Zhang, Z., High catalytic activity of ultrafine nanoporous palladium for electro-oxidation of methanol, ethanol, and formic acid. *Electrochemistry Communications*, **2009**. *11*, 1896-1899.

130. van Noort, D. and Mandenius, C.-F., Porous gold surfaces for biosensor applications. *Biosensors and Bioelectronics*, **2000**. *15*, 203-209.

131. Rintoul, M.D., Torquato, S., Yeong, C., Keane, D.T., Erramilli, S., Jun, Y.N., Dabbs, D.M., and Aksay, I.A., Structure and transport properties of a porous magnetic gel *via* x-ray microtomography. *Physical Review E*, **1996**. *54*, 2663-2669.

132. Baker, C., Pradhan, A., Pakstis, L., Pochan, D., and Shah, S., Synthesis and antibacterial properties of silver nanoparticles. *Journal of Nanoscience and Nanotechnology*, **2005**. *5*, 244-9.

133. Hussain, J.I., Talib, A., Kumar, S., Al-Thabaiti, S.A., Hashmi, A.A., and Khan, Z., Time dependence of nucleation and growth of silver nanoparticles.

Colloids and Surfaces A: Physicochemical and Engineering Aspects, **2011**. *381*, 23-30.

134. Tagad, C.K., Dugasani, S.R., Aiyer, R., Park, S., Kulkarni, A., and Sabharwal, S., Green synthesis of silver nanoparticles and their application for the development of optical fiber based hydrogen peroxide sensor. *Sensors and Actuators B: Chemical*, **2013**. *183*, 144-149.

135. Parnklang, T., Lamlua, B., Gatemala, H., Thammacharoen, C., Kuimalee, S., Lohwongwatana, B., and Ekgasit, S., Shape transformation of silver nanospheres to silver nanoplates induced by redox reaction of hydrogen peroxide. *Materials Chemistry and Physics*, **2015**. *153*, 127-134.

136. An, J., Tang, B., Ning, X., Zhou, J., Zhao, B., Xu, W., Corredor, C., and Lombardi, J.R., Photoinduced shape evolution: From triangular to hexagonal silver nanoplates. *The Journal of Physical Chemistry C*, **2007**. *111*, 18055-18059.

137. Detsi, E., Vukovic, Z., Punzhin, S., Bronsveld, P.M., Onck, P.R., and Hosson, J.T.M.D., Fine-tuning the feature size of nanoporous silver. *CrystEngComm*, **2012**. *14*, 5402-5406.

138. Li, Y. and Ding, Y., Porous AgCl/Ag nanocomposites with enhanced visible light photocatalytic properties. *The Journal of Physical Chemistry C*, **2010**. *114*, 3175-3179.

139. Bokhonov, B.B. and Dudina, D.V., Recrystallisation-accompanied phase separation in Ag-Fe and Ag-Ni nanocomposites: a route to structure tailoring of nanoporous silver. *RSC Advances*, **2013**. *3*, 12655-12661.

140. Zhang, C., Sun, J., Xu, J., Wang, X., Ji, H., Zhao, C., and Zhang, Z., Formation and microstructure of nanoporous silver by dealloying rapidly solidified Zn–Ag alloys. *Electrochimica Acta*, **2012**. *63*, 302-311.

141. Jin, R.-H. and Yuan, J.-J., Fabrication of silver porous frameworks using poly(ethyleneimine) hydrogel as a soft sacrificial template. *Journal of Materials Chemistry*, **2005**. *15*, 4513-4517.

142. Lu, H., Fabrication and characterization of porous silver powder prepared by spray drying and calcining technology. *Powder Technology*, **2010**. *203*, 176-179.

143. Zheng, R., Guo, X., and Fu, H., One-step, template-free route to silver porous hollow spheres and their optical property. *Applied Surface Science*, **2011**. *257*, 2367-2370.

144. Fang, C., Ellis, A.V., and Voelcker, N.H., Electrochemically prepared porous silver and its application in surface-enhanced Raman scattering. *Journal of Electroanalytical Chemistry*, **2011**. *659*, 151-160.

145. Shahbazi, P. and Kiani, A., Nanoporous Ag and Pd foam: Redox induced fabrication using electrochemically deposited nanoporous Cu foam with no need to any additive. *Electrochimica Acta*, **2011**. *56*, 9520-9529.

146. Cherevko, S., Xing, X., and Chung, C.-H., Electrodeposition of three-dimensional porous silver foams. *Electrochemistry Communications*, **2010**. *12*, 467-470.

147. Yeh, F.-H., Tai, C.-C., Huang, J.-F., and Sun, I.W., Formation of porous silver by electrochemical alloying/dealloying in a water-insensitive zinc chloride-1-

ethyl-3-methyl imidazolium chloride ionic liquid. *The Journal of Physical Chemistry B*, **2006**. *110*, 5215-5222.

148. Wongravee, K., Gatemala, H., Thammacharoen, C., Ekgasit, S., Vantasin, S., Tanabe, I., and Ozaki, Y., Nanoporous silver microstructure for single particle surface-enhanced Raman scattering spectroscopy. *RSC Advances*, **2015**. *5*, 1391-1397.

149. Song, S. and Chen, Z., Effect of UV illumination on the NaCl-induced atmospheric corrosion of pure zinc. *Journal of The Electrochemical Society*, **2014**. *161*, C288-C293.

150. Cachet, C. and Wiart, R., The kinetics of zinc dissolution in chloride electrolytes: Impedance measurements and electrode morphology. *Journal of Electroanalytical Chemistry and Interfacial Electrochemistry*, **1980**. *111*, 235-246.

151. Rosalbino, F., Scavino, G., Macciò, D., and Saccone, A., Influence of the alloying component on the corrosion behaviour of zinc in neutral aerated sodium chloride solution. *Corrosion Science*, **2014**. *89*, 286-294.

152. Zembura, Z. and Burzynska, L., The corrosion of zinc in de-aerated 0.1 M NaCl in the pH range from 1.6 to 13.3. *Corrosion Science*, **1977**. *17*, 871-878.

153. Mouanga, M., Berçot, P., and Rauch, J.Y., Comparison of corrosion behaviour of zinc in NaCl and in NaOH solutions. Part I: Corrosion layer characterization. *Corrosion Science*, **2010**. *52*, 3984-3992.

154. An, J., Tang, B., Zheng, X., Zhou, J., Dong, F., Xu, S., Wang, Y., Zhao, B., and Xu, W., Sculpturing effect of chloride ions in shape transformation from

triangular to discal silver nanoplates. *The Journal of Physical Chemistry C*, **2008**. *112*, 15176-15182.

155. Tsuji, T., Okazaki, Y., and Tsuji, M., Photo-induced morphological conversions of silver nanoparticles prepared using laser ablation in water—Enhanced morphological conversions using halogen etching. *Journal of Photochemistry and Photobiology A: Chemistry*, **2008**. *194*, 247-253.

156. Zhao, P., Feng, X., Huang, D., Yang, G., and Astruc, D., Basic concepts and recent advances in nitrophenol reduction by gold- and other transition metal nanoparticles. *Coordination Chemistry Reviews*, **2015**. *287*, 114-136.

157. Mao, Y., Wei, J., Wang, C., Feng, Y., Yang, H., and Meng, X., Growth and characterization of sponge-like silver with high catalytic activity for the reduction of p-nitrophenol. *Materials Letters*, **2015**. *154*, 47-50.

158. Guo, M., He, J., Li, Y., Ma, S., and Sun, X., One-step synthesis of hollow porous gold nanoparticles with tunable particle size for the reduction of 4-nitrophenol. *Journal of Hazardous Materials*, **2016**. *310*, 89-97.

159. Corma, A., Concepción, P., and Serna, P., A different reaction pathway for the reduction of aromatic nitro compounds on gold catalysts. *Angewandte Chemie International Edition*, **2007**. *46*, 7266-7269.

160. Wunder, S., Polzer, F., Lu, Y., Mei, Y., and Ballauff, M., Kinetic analysis of catalytic reduction of 4-nitrophenol by metallic nanoparticles immobilized in spherical polyelectrolyte brushes. *The Journal of Physical Chemistry C*, **2010**. *114*, 8814-8820.

161. Pradhan, N., Pal, A., and Pal, T., Silver nanoparticle catalyzed reduction of aromatic nitro compounds. *Colloids and Surfaces A: Physicochemical and Engineering Aspects*, **2002**. *196*, 247-257.

162. GFMS, *World silver survey 2015: A summary*. 2015, The Silver Institute: Washington, D.C. p. 12.

163. Katrivanos, F.C., *Silver*. 2015, U.S. Geological Survey: Virginia. p. 15.

164. Asharani, P.V., Wu, Y.L., Gong, Z., and Valiyaveettil, S., Toxicity of silver nanoparticles in zebrafish models. *Nanotechnology*, **2008**. *19*, 255102-225110.

165. Guadagnolo, C.M., Brauner, C.J., and Wood, C.M., Effects of an acute silver challenge on survival, silver distribution and ionoregulation within developing rainbow trout eggs (Oncorhynchus mykiss). *Aquatic Toxicology*, **2000**. *51*, 195-211.

166. Wongravee, K., Parnklang, T., Pienpinijtham, P., Lertvachirapaiboon, C., Ozaki, Y., Thammacharoen, C., and Ekgasit, S., Chemometric analysis of spectroscopic data on shape evolution of silver nanoparticles induced by hydrogen peroxide. *Physical Chemistry Chemical Physics*, **2013**. *15*, 4183-4189.

167. Jiang, T., Yang, Y., Huang, Z., Zhang, B., and Qiu, G., Leaching kinetics of pyrolusite from manganese–silver ores in the presence of hydrogen peroxide. *Hydrometallurgy*, **2004**. *72*, 129-138.

168. Bas, A.D., Yazici, E.Y., and Deveci, H., Recovery of silver from X-ray film processing effluents by hydrogen peroxide treatment. *Hydrometallurgy*, **2012**. *121–124*, 22-27.

169. Mahdizadeh, F., Eskandarian, M., Zabarjadi, J., Ehsani, A., and Afshar, A., Silver recovery from radiographic film processing effluents by hydrogen peroxide: Modeling and optimization using response surface methodology. *Korean Journal of Chemical Engineering*, **2014**. *31*, 74-80.

170. Thongnopkun, P., Jamkratoke, M., and Ekgasit, S., Thermal behavior of nano-silver clay in the application of handmade jewelry. *Materials Science and Engineering: A*, **2012**. *556*, 849-854.

171. Naseri Joda, N. and Rashchi, F., Recovery of ultra fine grained silver and copper from PC board scraps. *Separation and Purification Technology*, **2012**. *92*, 36-42.
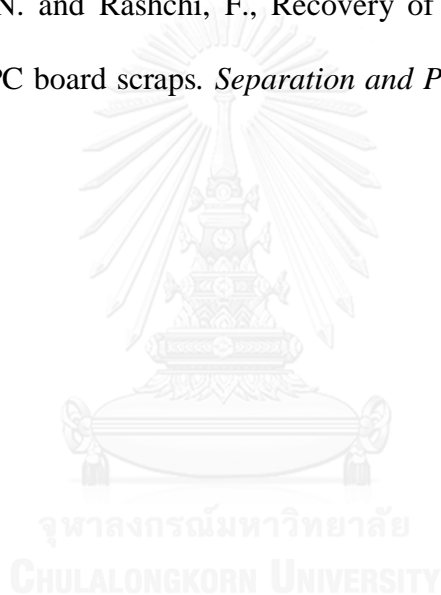
APPENDIX

RESEARCH ACHIEVEMENTS

We have successfully developed the morphologically controlled synthesis protocols of silver micro/nanostructures using chemical approach. Our works were achieved many awards from the nation, scientific society and international organization. In addition our works were published in peer-review journal. The list of research achievements is shown below.

Conferences

- Fabrication and characterization of porous silver microstructures prepared by galvanic replacement, 29th MST Annual Conference, 30 January - 1 February 2012, Cha-am, Thailand

- Construction of porous silver microstructures *via* galvanic replacement, The Science Forum 2012, 19 – 20 April 2012, Bangkok, Thailand

- Shape-controlled synthesis of silver microplates *via* reduction of $[Ag(NH_3)_2]^+Cl^-$ using hydrogen peroxide as a reducing agent, 30th MST Annual Conference, 23 – 25 January 2013, Chanthaburi, Thailand

- Fabrication and characterization of Ag{111} facet dominated silver microplates using H_2O_2 as a reducing agent, The Science Forum 2013, 14 – 25 March 2013, Bangkok, Thailand

- Complex 3D AgCl microstructures (octapods and hexapods) synthesized by selective precipitation approach, Pure and Applied Chemistry International Conference 2014, 8 - 10 January 2014, Khon Kaen, Thailand

- Surface enhanced IR absorption spectro-electrochemistry of immobilized [NiFe] hydrogenase on graphene Oxide/Au hybrid electrodes, THE INTERNATIONAL CHEMICAL CONGRESS OF PACIFIC BASIN SOCIETIES 2015, 15 – 20 December 2015, Honolulu, Hawaii, USA

- Experimental design study of economical process for silver recovery using hydrogen peroxide as a reducing agent, Pure and Applied Chemistry International Conference 2016, 9 - 11 February 2016, Bangkok, Thailand

Honors and Awards

National

- The best oral presentation award, session: Apply science and technology, The Science Forum 2012, 19 – 20 April 2012, Bangkok, Thailand

- The best oral presentation award, session: Apply science and technology, The Science Forum 2013, 14 – 25 March 2013, Bangkok, Thailand

- First prize of oral presentation, session: Materials science, 30th MST Annual Conference, 23 – 25 January 2013, Chanthaburi, Thailand

- The second prize of graduate student in the 5th Thailand nanotechnology innovation contest 2014 organized by King Mongkut's Institute of Technology Ladkrabang. Title: Thai silver clay for unique silver jewelry application

- The consolation prize in the Innovation contest 2015 organized by National Research Council of Thailand (NRCT). Title: SHANNTA Silver Clay: The only Thai Brand Silver Clay for Design and Fabrication of Silver Jewelry

- The best oral presentation award, session: Environmental Chemistry, Pure and Applied Chemistry International Conference 2016, 9 - 11 February 2016, Bangkok, Thailand

International

- The winner of student poster competition, THE INTERNATIONAL CHEMICAL CONGRESS OF PACIFIC BASIN SOCIETIES 2015, 15 – 20 December 2015, Honolulu, Hawaii, USA

Publications

- <u>Gatemala, H.</u>; Thammacharoen, C.; Ekgasit, S., 3D AgCl microstructures selectively fabricated *via* Cl^--induced precipitation from $[Ag(NH_3)_2]^+$. *CrystEngComm* **2014**, *16 (29)*, 6688-6696.

- <u>Gatemala, H.</u>; Pienpinijtham, P.; Thammacharoen, C.; Ekgasit, S., Rapid fabrication of silver microplates under an oxidative etching environment consisting of O_2/Cl^-, NH_4OH/H_2O_2, and H_2O_2. *CrystEngComm* **2015,** *17* (29), 5530-5537.

- Wongravee, K.; <u>Gatemala, H.</u>; Thammacharoen, C.; Ekgasit, S.; Vantasin, S.; Tanabe, I.; Ozaki, Y., Nanoporous silver microstructure for single particle surface-enhanced Raman scattering spectroscopy. *RSC Advances* **2015,** *5* (2), 1391-1397.

- Parnklang, T.; Lamlua, B.; <u>Gatemala, H.</u>; Thammacharoen, C.; Kuimalee, S.; Lohwongwatana, B.; Ekgasit, S., Shape transformation of silver nanospheres

to silver nanoplates induced by redox reaction of hydrogen peroxide. *Materials Chemistry and Physics* **2015,** *153*, 127-134.

- Vantasin, S.; Ji, W.; Tanaka, Y.; Kitahama, Y.; Wang, M.; Wongravee, K.; <u>Gatemala, H.</u>; Ekgasit, S.; Ozaki, Y., 3D SERS imaging using chemically synthesized highly symmetric nanoporous silver microparticles. *Angewandte Chemie International Edition*, **2016**, DOI: 10.1002/anie.201603758.

VITA

Name: Mr. Harnchana Gatemala

Contact Address: Sensor Research Unit, Department of Chemistry,

Faculty of Science, Chulalongkorn University,

Bangkok, 10330, Thailand

E-mail: harnchana.gate@gmail.com

Personal: Born 16 September 1984, Mahasarakham, Thailand

Education

2006 B. Sc. Chemistry (First Class Honors)

Khon Kaen University, Khon Kaen, Thailand

2011 M. Sc. Chemistry

Suranaree University of Technology, Nakhon Ratchasima, Thailand

Research interests/expertise

• Morphology controlled synthesis of metal (Au, Ag, Cu, Pt, Pd) micro/nanostructures

• Industrial application of metal micro/nanostructures

• Enzyme-based electrode for hydrogen fuel cell

• Computer programming (FORTRAN and C/C++ language) and computational methods (Molecular Dynamic (MD) simulation and Monte Carlo (MC) technique)

Industrial application of metal micro/nanostructures

• Silver and copper clay (standard type, paper type, syringe type and paste type)

• Conductive ink by silver microplates

• Black silver for antibacterial application